POLITECNICO DI MILANO

Department of Civil and Environmental Engineering

Doctoral Programme in Environmental and Infrastructure Engineering

Granular shear flows: constitutive modeling and numerical simulations

Doctoral Dissertation of:
Dalila Vescovi

Supervisors:
Dr. Diego Berzi
Prof. Claudio Giulio di Prisco

Tutor:
Prof. Enrico Larcan

The Chair of the Doctoral Program:
Prof. Alberto Guadagnini

Cycle XXVI

Abstract

In the recent past, the flow of granular materials has been the subject of many scientific works; this is due to the large number of natural phenomena (i.e., landslides and debris flows) and industrial processes involving solid particles flowing. The collective mechanical behavior of a granular system is governed by the properties of the individual particles and the interactions among the grains. At the microscale level, the particles interact through two dissipative mechanisms: enduring contacts among grains which are involved in force chains, and inelastic collisions. When the first mechanism prevails, the material behaves like a solid (quasi-static regime). On the other hand, when the particles interact only through collisions, the material response can be assimilated to that of a gas (collisional regime). When the grains interact both through force chains and through collisions, the material is in the transition phase between the two extreme behaviors.

The aim of this work is to propose a theoretical, constitutive model for granular flows, able to deal with the phase transition, where both enduring contacts among particles involved in force chains and collisions are considered. In particular, the steady state condition of a granular material under shear is analyzed.
The energy and the total stress are assumed to be the linear sum of a quasi-static and a collisional component, accounting, respectively, for the force chains and the collisions. The quasi-static and the collisional contribution are modeled in the context of the critical state theory of soil mechanics and the kinetic theory of granular gases, respectively.
In the critical state theory, the granular material approaches a certain attractor state, independent of the initial arrangement, characterized by the capability of developing unlimited shear strains without any change in the concentration. In this context, the dominant role is played by the friction, which is supposed to support force chains. Also, the quasi-static component of the stress vanishes when the particle concentration is less than the random loose packing, which represents the lower limit for the existence of a disordered granular packing.
In the kinetic theory, the particles are assumed to interact through instantaneous, binary and uncorrelated collisions. A new state variable of the system is introduced, the granular temperature, which accounts for the velocity fluctuations. The model has been extended to account for the decrease in the energy dissipation due to the existence of correlated motion among the particles and to deal with non-instantaneous collisions.

The proposed theory is applied to two configurations: simple shear flows and Couette flows. Simple shear flows are characterized by homogeneous shearing: all the variables are constant along the flow field, except for the horizontal velocity which is linearly distributed. In such a simple case, at the steady state, under the usual assumptions of constant shear and normal stresses, the flux of energy is neglected, and an analytical solution can be obtained. According to this approach, the critical state can be interpreted as a particular steady state for which the granular temperature vanishes, as well as the shear rate. Also, a qualitative phase diagram has been drawn in the normal stress-concentration plane. The theory has been proved to be capable of reproducing, qualitatively and quantitatively, numerical simulations on spheres taken from the literature, when the concentration is low and the rensponse of the material is dominated by collisions, in both the cases of frictionless and frictional particles. Furthermore, when deformations are very slow and the force chains play a relevant role, the model is able to qualitatively predict the characteristic

features of simple shear flows.

In the conditions for which simple shear flows are quantitatively well predicted, i.e., when using hard, frictionless particles, the theory is applied to the Couette flow configuration. In the Couette configuration, the granular material is sheared between two parallel planes, having infinite length, one at rest and the other moving at constant velocity. The granular material is an assembly of identical, frictionless spheres, and the inter-particle collisions are characterized by the coefficient of restitution (ratio of the relative velocity between two impending particles after and before a collision). The walls are made bumpy by gluing particles in a regular array, and the bumpiness of the walls is defined in relation with the distance between the edges of two adjacent glued spheres. The resulting flow fields are non homogeneous and vary along the flow depth. In this case, the energy diffusion cannot be neglected, and the set of differential equations deriving from the proposed theory is numerically solved with appropriate boundary conditions.
In order to make comparisons between the theory and the numerical results, 3D numerical simulations have been performed using the discrete element method (DEM). The simulations are carried out under the constant volume condition, and periodic boundary conditions are applied along the flow and the transversal direction. The influence of the inelasticity of the particles (i.e., the coefficient of restitution) and the boundary conditions (i.e., the bumpiness of the walls) has been investigated.
The theory is in very good agreement with the numerical results when using appropriate boundary conditions. A peculiar behavior has been highlighted by the simulations when using high bumpiness: some flowing particles get stuck in the gaps between wall spheres, making the bumpy walls disordered and more dissipative than expected.

In short, this thesis focuses on the mechanical behavior of granular materials under steady conditions. Homogeneous and inhomogeneous granular shear flows are analyzed in order to investigate the the link between the collective behavior and properties of individual particles, and to develop a consistent constitutive model.

Acknowledgements

Many people accompanied me through this work, during good and bad times, making my Ph.D. an unforgettable experience.

First of all, I wish to thank my supervisors Dr. Diego Berzi and Prof. Claudio di Prisco for giving me the chance to undertake this experience and for introducing me in the amazing world of scientific research. They have always been patient, available and supportive, and gave me all the freedom and the confidence I needed.

I wish to sincerely thank Diego for his guidance, understanding, patience, and most importantly, his friendship during these three years. He has been a smart and funny supervisor, always smiling and enthusiastic. I learned a lot from him, not only about science but also how to be a good teacher. He helped me in all the time of research and writing of this thesis, and allowed me to grow as a research scientist. It has been an honor to be his first Ph.D. student.

I would like to express my immense gratitude to Prof. Claudio di Prisco, who conceived this work and the idea of building a research group on granular flows at Politecnico di Milano. He has oriented and supported me with promptness and care, and have always been patient and encouraging in times of new ideas and difficulties. His precious insights and immense knowledge are a model to me.

I would like to give special thanks to Prof. Patrick Richard for his collaboration and hospitality during my stay in Rennes. The second part of this thesis would not have been possible without his guidance and persistent help on granular physics and numerical simulations.

Many thanks goes to Dr. Nicolas Brodu, he helped me setting up many simulations and solving several problems using the DEM code.

I do not know how to express my gratitude to my parents and my brother, for their infinite support and unconditional love throughout everything.

Finally, I wish to thank Francesco, to make me happy everyday.

Contents

List of Figures

List of Tables

1. Introduction

1.1. Granular flows

According to the definition, granular materials are large collections of discrete solid particles with sizes large enough that Brownian motion is irrelevant [2]. Classical examples of granular materials are sand, soil and snow, but their are widely diffused also in daily life: food products like seeds, rice, corns, sugar and coffee, chemical and pharmaceutical products like pills and powders, building materials such as gravel, are few amongst many examples of granular materials. Also, the motion of red blood cells or cars in the traffic can be seen as a granular flows. Granular materials are diverse in shapes and sizes, ranging from micron sized of powders to few meters sized of blocks in rock avalanches. Due to the large number of industrial processes and applications involving solid particles flowing, the flow of granular materials has been the subject of many scientific works (Ref. [38] and references therein). Storing, transporting and manipulating pills, seeds, soils and powders, are a common matters in pharmaceutical, chemical, agricultural, mineral and construction-based industries. Above all, research on granular flows has been strongly motivated by the description and prediction of natural hazards such as landslides, rock avalanches and debris flows. Furthermore, the study of formation and motion of desert dunes are the subject of important studies all around the world, often involving granular theories, as well as the study of ripples formations in the sand under shallow sea waters can solve important emergencies on many coasts.
The discontinuous and inhomogeneous nature of granular materials leads to complex mechanical behaviors, even in the case of simple flow conditions (i.e., elementary geometries, stationary motions) or when the granular matter is particularly treatable (i.e., dry, no complex shapes of the grains and no polydispersity, etc). As a consequence, the study of such medium normally involves interdisciplinary concepts like rheology, plasticity and viscosity and requires both soil mechanics and fluid dynamics tools.
Given that a discontinuous description of the motion of each single grain is often prohibitive, due to the large number of particles involved, the macroscopic behavior of the whole system is usually treated in the framework of continuum mechanics. A continuum description of granular dynamics has to incorporate the micro-mechanical properties of the single grains and an averaging process over the number of particles which composes the material. Then, a continuum mechanics model consists of solving a set of partial differential equations given by the conservation of mass, momentum and energy, supplemented with boundary conditions and constitutive equations which characterize the behavior of the material under consideration. In particular, the constitutive relations relate stresses and deformations, taking into account the physics of the grain-grain interaction. At the microscale level, two mechanisms of interaction between particles can be recognized: enduring contacts among grains, which are involved in force chains, and inelastic collisions. Both the mechanisms are characterized by two salient features: friction and inelasticity, which make the particle-particle interactions dissipative. Whenever grains interact, through collisions or enduring contacts, they lose part of their energy, and the global energy lost in the system is transferred to heat and then dispersed to the environment.

1. Introduction

As a consequence of energy dissipation, granular systems are always in non-equilibrium states, and a steady state can be reached and maintained only by pumping energy into the system [46]. Also, homogeneous solutions of the equations of continuum mechanics are often unstable. Clustering in dilute granular systems and shear bands formation in shear flows are examples of instabilities which affect granular flows. Another key characteristic of granular materials is that, due to the macroscopic nature of grains, and, in particular, to their masses (usually of the order of 10^{20} molecular masses), the thermal temperature plays a negligible role in their dynamics. Consequently, the thermal energy of the system is always many orders of magnitude smaller than the kinetic and potential energy. Irrelevance of thermal temperature and dissipative interactions make grains behavior very different from that of the molecules of fluids and gases, and this is why classical theories like thermodynamics and statistical mechanics are not sufficient to describe granular flows. Depending on both the micromechanical properties of the grains (among them, friction and inelasticity) and the macroscopic characteristics of the flow (i.e., velocity and concentration), granular flows exhibit different behaviors, commonly interpreted as flow regimes. Considering, for example, a landslide: immediately after the triggering, the soil behaves like a solid and a sliding motion takes place; but, if the velocity of the motion is large enough, the landslides evolves to a fluid-like process and the material starts to flow. Whereas the study of the initiation is the domain of soil mechanics, the propagation phase has been widely investigated in fluid dynamics.
When the system is very dense, its response is governed by the enduring contacts among grains which are involved in force chains spanning the whole domain; the deformations are extremely slow because the entire network of contacts has to be continuously re-arranged. In these conditions, the granular material behaves like a solid and the corresponding flow regime is said quasi-static. On the other hand, when the particles are widely spaced, force chains are inhibited and the energy of the system is totally dissipated through collisions. As a consequence, the medium is strongly agitated, the particles are free to move in all directions and the deformations are rapid. There, the material response can be assimilated to that of a gas, and the flow regime is called collisional. When the grains interact both through force chains and through collisions, the material is in the transition phase between the two extreme behaviors.
Slowly deforming quasi-static dense granular materials has been mainly investigated in the framework of geomechanics. There, the majority of the constitutive models are based on the theories of elastoplasticity and viscoplasticity [33, 69, 98, 107, 121]. In those models, the granular material reaches a limit condition in which it continues to (plastically) deform indefinitely without further change in stresses and volume. This attractor state is known as critical state. The critical state is defined as a non-evolving state reached after a progressive increase in strain, at a vanishingly small strain rate [93, 106, 110].
The collisional regime has been largely studied in the context of kinetic theories of granular gases [23, 45, 57]. In those theories, the particles are assumed to interact mainly through instantaneous, binary and uncorrelated collisions. In analogy with the molecular kinetic energy determining the thermodynamic temperature of a gas, a state variable of the system is introduced, the granular temperature. The granular temperature is related with the particle velocity fluctuations and represents a measure of the degree of agitation of the system. Standard Kinetic Theories are unable to take into account the correlated motion among the particles forming clusters occurring at high concentrations. Recently, Jenkins [52, 53] proposed the so called Extended Kinetic Theory with the intent of incorporating such an effect. Nevertheless, kinetic theories fail in reproducing granular flows at high concentration, when force chains develop.

There are several practical problems where the granular material encompasses a transition from a solid to a more gaseous state, thus suggesting that a collaboration between the two above mentioned communities would be fruitful. The landslide risk evaluation, requiring the modeling of both the inception and the evolution of the gravitational collapse, is the tipical example. Moreover, the increasing success of computational tools in handling large deformations suggests that such an ambitious goal is now possible and stimulates the need for constitutive models capable of simulating the mechanical response of granular materials under both quasi-static and collisional conditions. A first step in this direction is the extension of the critical state concept, interpreted hereafter as a sort of limit condition for the steady state at vanishingly small strain rate, by employing the granular temperature as an additional state variable for the system.

1.2. Research aims and approaches

This thesis focuses on the plane shear flow of an ideal granular material, composed of identical, inelastic spheres, under steady conditions. The plane shear configuration is the simplest geometry which allows to analyze the rheology of granular materials, i.e., to study the constitutive relations which relate stresses and deformations [44]. In this simple configuration, the flow is assumed to be one-dimensional and the granular material is sheared between two walls, one at rest and the other moving at constant velocity. Here, the flow behavior is influenced by a number of factors, including the particle properties (density, friction, inelasticity and stiffness), the relative width of the flow gap, the roughness of the walls and the imposed velocity of the moving plane. In particular, the constitutive behavior of granular systems is studied in both the cases of homogeneous and inhomogeneous shearing, called simple shear flow and Couette flow, respectevely.
The purposes of the present research are:

- to develop general, physically based constitutive equations for granular flows, in the framework of continuum mechanics. The theory must be able to deal with the phase transition, where both enduring contacts among particles involved in force chains and collisions are considered, including, as special cases, the aforementioned collisional and quasi-static approaches.

- To perform Soft-Sphere Discrete Element Method simulations, missing in the literature, on inhomogeneous steady, plane shear flows of frictionless spheres, where the walls are made bumpy by gluing particles in a regular array.

The proposed constitutive model is derived under the main assumption that the energy and the total stress are given by the linear sum of a quasi-static and a collisional component, accounting, respectively, for the force chains and the collisions. The quasi-static and the collisional contributions are modeled in the context of the critical state theory of soil mechanics and the kinetic theory of granular gases, respectively.
The simulations have been carried out using the Soft-Sphere Discrete Element Method. The SS-DEM technique simulates the motion of each particle and computes the interaction forces between particles at the contacts. SS-DEM simulations provide physical insights into both the microscopic and the macroscopic dynamics of the system. The data obtained from numerical simulations can be used to test constitutive models and boundary conditions. In this thesis, we used the results of the SS-DEM numerical simulations to validate the collisional component of the constitutive model and to propose boundary conditions appropriated for this kind of bumpy walls.

1.3. Outline of the dissertation

Chapter 2 presents some background information on the behavior of granular flows with brief reviews of Molecular Dynamics simulations and continuum mechanics models.
Chapter 3 provides a summary description of the kinetic theory of granular gases, which is the theoretical model mostly adopted throughout the thesis.
Chapter 4 describes the constitutive approach developed in this work. The model is based on the fundamental assumption that the energy of the system is dissipated thorugh two mechanisms, collisions and enduring contacts among grains involved in force chains. The two mechanisms are modeled independently by using the kinetic theory, properly modified, and the critical state theory of soil mechanics. The complete set of constitutive relations is derived for the case of a collection of identical spheres sheared under steady conditions.
In Chapter 5, the constitutive model is applied to the steady, homogeneous shear flows of a mixture of identical spheres, usually called simple shear flows. A critical discussion on the salient properties of the theory is proposed and the comparison with experimental and numerical results found in literature is illustrated.
Chapter 6 is devoted to the study of non homogeneous shear flows of frictionless and hard spheres, under steady conditions, at fixed average concentration. The set of differential equations deriving from the proposed theory is numerically solved with appropriate boundary conditions. Also, numerical simulations have been carried out using a Soft-Sphere Discrete Element Method code. The SS-DEM method is briefly introduced together with the contact model adopted. Finally, the results of the numerical simulations are compared to those obtained from the numerical integration of the equations.
Chapter 7 summarizes the main conclusions and possible extensions to this work.

2. State of the art

This chapter surveys the literature and background on granular flows, in general, and the principal results regarding steady, plane shear flows, in particular.

2.1. Background

Granular materials are collections of discrete particles characterized by loss of energy whenever the particles interact. Due to their microscopic, discrete nature and their macroscopic behavior, granular materials are treated in both the frameworks of discontinuum and continuum mechanics.
In the realm of discontinuum mechanics, several numerical techniques have been developed, able to reproduce the single particle motions and to control the micro-mechanical properties of the grains. The Molecular Dynamics or Discrete Element Methods (DEM) is the term given to the numerical analysis procedure that simulates the behavior within discontinuum mechanics. There, the material is considered as an assembly of discrete particles, and by applying the micro-mechanical properties and the interaction-contact laws, the dynamic behavior can be studied by integrating the equations of motion of each single grain.
On the other hand, continuum models give a macroscopic view to investigate granular material behaviors. Continuum mechanics theories solve the conservation equations of the whole medium, i.e., the balance of mass, momentum and, when necessary, energy. Although the balance laws are, somehow, easily deducible, the big challenge is the definition of the constitutive relations. The latter relate stresses and deformations, taking into account the physics of the grain-grain interaction. The constitutive relations have to be able to capture the macroscopic behavior of the system, incorporating the microscale particle interaction dynamics.
A granular flow can undergo different constitutive behaviors depending on both the micro-mechanical properties of the particles and the macroscopic characteristic of the flow (i.e., velocity and concentration). The micro-mechanical properties which play a fondamental role in the motion of a granular material and in the regime transition are the inter-particle friction and the inelasticity of the particles, which make the grain-grain interactions dissipative.
In the literature, three different granular flow regimes have been identified [38]:

- Collisional regime: characterized by low concentration and rapid deformations; here, the medium is strongly agitated, the particles are widely spaced and interact only through collisions (gas-like behavior).
- Quasi-static regime: characterized by high concentrations and enduring, frictional contacts among the grains, which are involved in force chains spanning the entire domain; the motion of the medium is slow given that at every step the entire network of contacts has to be re-arranged (solid-like behavior).
- Intermediate regime: the grains interact both through enduring contacts and through collisions; (liquid-like behavior).

Of course, the most ambitious purpose of a theoretical model is to deal with the phase transition between the different regimes, and it requires both soil mechanics and fluid dynamics tools.
Several flow configurations have been studied with both discontinuous and continuous approaches. The six geometries mostly studied are those in which a "simple" shear is achieved and rheological properties can be measured [44] (Fig. 2.1). These configurations are divided in confined and free surface flows. In Fig. 2.1, the three pictures on the top (a, b and c) represent the most commonly studied confined flows, which are the plane shear geometry, the annular shear and the vertical-chute flow configuration. The three flow configurations in the bottom (d, e and f) are the free surface flows: inclined plane, flow at the surface of a pile and flow in a rotating drum.

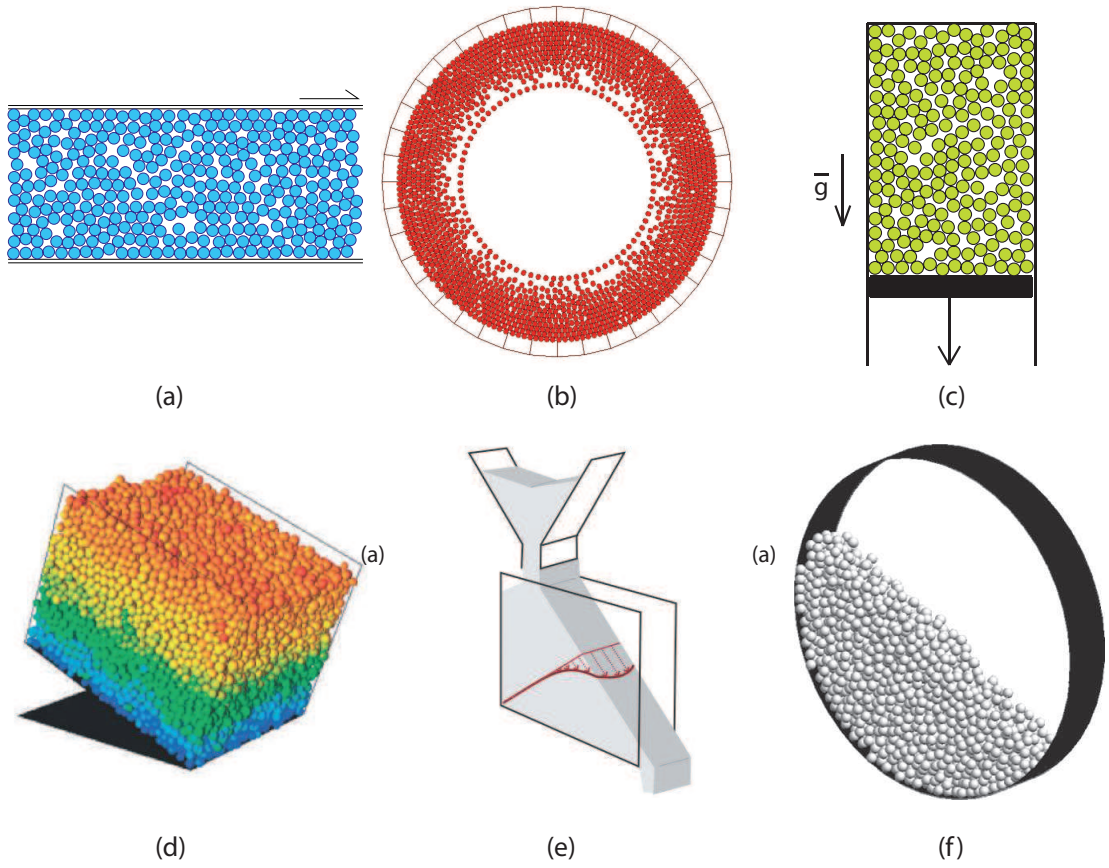

Figure 2.1.: Example of granular flow configurations: plane shear (a), annular shear (b), vertical-chute flow (c), inclined plane (d), flow at the surface of a pile (e), rotating drum (f).

The present work focuses on the steady flow of granular materials in the plane shear configuration (Fig. 2.1a), in which the granular material is sheared between two parallel planes, one at rest and the other moving at constant, fixed velocity, in absence of pressure gradient. Both the cases of homogeneous and non homogeneous shearing are analyzed. Simple shear flows is the name given to homogeneous, plane shear flows in steady conditions, whereas the non homogeneous flows are known as Couette flows. In the second case, the influence of the boundaries cannot be neglected and continuum mechanics models require appropriate boundary conditions in order to close the system of (differential) equations.

2.2. Review of Molecular Dynamics simulations

Molecular Dynamics (MD) method is essentially the simultaneous numerical solution of Newton's equation of motion for many particles, and was originally introduced in physics to simulate the motion of molecules [29]. This numerical technique computes, at each time step, the position, velocity and acceleration of each simulated particle. Through ensemble averaging of the respective positions and velocities of the particles, the macroscopic fields of the whole system, such as the density and the mean velocity, can be obtained. This helps in revealing the insight of the granular behaviour which is difficult to capture in experimental methods. MD simulations are flexible, allowing the definition of the micromechanical properties of the grains and the use of flow conditions usually forbidden in laboratory, for example unlimited boundaries or steady conditions. With MD methods, one can perform simulations using ideal grains, characterized by micromechanical particles not possible in the Nature but which are useful to understand the physics of the global behavior. In such a way, the influence of several micromechanical properties can be analyzed separately from the others, providing a complete description of the role of each particle property. Examples of ideal grains which cannot be found in the Nature, but which have been largely investigated, are frictionless, rigid and perfectly elastic spheres. Apart from their versatile applications and benefits, these models are still computer simulations, hence having limitations such as excessive computational requirements, round off errors and truncation errors.
Molecular Dynamics simulation methods include three different techniques: the Event-Driven molecular dynamics (ED), the Contact Dynamics method (CD), and the Soft-Sphere Discrete Element Method (SS-DEM). In the first two methods, the particles are assumed to be infinitely rigid, whereas in the third method deformations of particles during contacts are modeled allowing a small overlap between grains. All the MD methods simulate the inelastic and frictional nature of the contacts among grains through macroscopic coefficients (i.e., the coefficients of restitutions and the interparticle friction coefficient).
In the SS-DEM methods, all the forces acting on each particle are computed on the basis of the positions of the particles. The deformability of the grains is taken into account allowing the overlap at the contacts. Then, the Newton's equations of motion are explicitly integrated for each particle, and the new particle positions are obtained. The fixed time step is imposed small enough to resolve the deformation of the contact elements during the course of the particle interactions. The SS-DEM method has been used in this work to perform numerical simulations of granular flows in the Couette configuration, and will be discussed in detail in Section 6.2.
The fundamental assumption in the Event-Driven method is that grains interact by instantaneous collisions. As a consequence, the grains are assumed to be rigid and non deformable, and the collisions are binary (involve only two particles). Then, the trajectories of the particles follow an undisturbed motion until an event, i.e., a collision, occurs [79, 101]. The ED method consists of two steps: first, all potential collisions between each pair of particles are identified, and, secondly, the potential collision whose time is the smallest is detected [84]. Then, the algorithm computes the velocities and the positions of all particles at that time, according to Newton's law. The velocities (and angular velocities) of the particles change according to a collision rule, which relates the post-collisional velocities to the pre-collisional ones, defining completely the interactions among grains. The (variable) time advancement in the ED simulation is dictated by the interval between collisions. Then, in contrast to the SS-DEM method where the time step is fixed, ED techniques employ a variable time step adapted to the problem. Event-Driven methods

are typically faster than SS-DEM, when applied to dilute systems, because (i) they do not require the computation of interaction forces; (ii) the positions and the velocities of the particles are computed only at the collisions, and no computation time is wasted for computing them in the particles free motion. On the other hand, ED methods are impractical for dense flows, in which collisions are very frequent, particles develop persistent contacts, and the rigidity assumption becomes invalid [2].
The Contact Dynamic method treats the particles as rigid, non-overlapping and frictional [32]. In this method, the small elastic response times and displacements characterizing the contact interactions are neglected and the granular dynamics is formulated at the scale of particles rearrangements [51, 103]. The CD method is based on a "nonsmooth" formulation of the equations of motion in which the accelerations are replaced by possible velocity jumps resulting from collisions. The interactions among particles are described by contact laws (and not force laws). The contact laws are formulated in terms of kinematic constraints, which impose the condition of impenetrability of the grains in the normal direction (collisional interaction), and the Coulomb law in the tangential direction (frictional interaction). The frictional and collisional interactions are described as "complementarity relations" between the relative velocities and the corresponding forces at the contact points [35]. As a consequence of the complementary relations, the contacts are treated as strictly nonsmooth and velocity jumps are expected. Given a contact network, all the kinematic constraints are imposed in an exact form, i.e., without introducing further regularizing or damping parameters. The kinematic constraints are simultaneously taken into account together with the equations of motion, in order to compute the velocities and the contact forces in the system at each time step, through an iterative procedure. The formulation of the contact laws at the velocity level implies an implicit time-stepping scheme, together with an explicit treatment of the evolution of the contact network. The implicit time integration makes the CD method unconditionally stable, but the uniqueness of the solution at each time step is not guaranteed. However, the variability of the solutions is generally below numerical precision [103].

MD simulations have been successfully used to analyze the rheology of granular flows and the transition among the different flow regimes. A very large number of numerical simulations have been carried out on various configurations and geometries, so that is quite impossible to make a list of these works. Collections of results can be found in GDR-MiDi [44] and in Delannay et al. [32]. This work focuses on steady, plane shear flows of granular materials, then just a (non exhaustive) list of numerical results obtained on this flow configuration is reported below.
As previously stated, homogeneous shearing characterizes simple shear flows. In numerical simulations, simple shear flows can be obtained by imposing the Lees-Edwards [73] periodic boundary conditions in the shearing direction. ED, CD and SS-DEM simulations of simple shear flows have been performed using disks and spheres. Babic et al. [6] performed 2D SS-DEM simulations of disks to study the relationships between the stresses and shear rate and speculated the existence of a "regime chart" to classify the flow regimes. A more intensive study of the stress-strain rate relation was conducted by Campbell [24], Ji and Shen [61, 62] and Chialvo et al. [28], independently, carring out 3D simulations of soft frictional spheres at imposed concentration. In those works, the authors derived a flowmap of the various flow regimes and analyzed the transition among them. da Cruz et al. [30] studied the simple shear flows of a collection of disks prescribing the pressure and the shear rate, and proposed constitutive relations in terms of dimensionless quantities. The effect of velocity correlation on the energy dissipation rate and the stresses were investi-

gated by Mitarai and Nakanishi [88] by performing ED simulations of frictionless spheres. Estrada et al. [35] carried out a set of CD simulations in order to study the steady-state strength properties and microstructure of sheared granular media. More recently, Chialvo and Sundaresan [27] investigated the simple shear flows of frictionless and frictional particles in the collisional regime through 3D SS-DEM simulations, measuring the stresses and the granular temperature (mean square of the velocity fluctuations) in a wide range of imposed concentrations.
Concerning the Couette flows (i.e., inhomogeneous shearing), 2D simulations using frictional spheres and flat, frictional walls have been performed using both CD [114] and SS-DEM [68] method; 3D SS-DEM simulations using frictional particles were carried out by Liu and Rosato [74], adopting bumpy walls composed of regularly glued semi-spheres and imposing periodic boundary conditions in the flow and transversal direction; Xu et al. [130] solved the kinetic theory equations in rectilinear or axisymmetric rectangular channels and compared the results with Molecular Dynamics simulations obtained using walls made bumpy by gluing semi-cylinders at them. Also, sets of physical experiments have been performed: Orlando and Shen [95] carried out experiments on the flows of glass spheres in an annular shear cell, where the influence of the boundaries, the average concentration and the particle to apparatus size ratio is investigated; Miller et al. [85] performed experiments using a special device named Stadium Shear, that can produce plane shear of a 2D granular material.

2.3. Review of continuum mechanics models

The goal of a theoretical model is to describe and to predict the mechanical behavior of the whole granular system, starting for the physics of the grain-grain interaction. The most of the theoretical models are in the framework of continuum mechanics. Then, they require to write and to solve the motion equations of the material, dealing with the rheology.
A large number of constitutive relations have been proposed to account for the irreversible, time-dependent mechanical behavior of granular media in the quasi-static regime. Those phenomenological constitutive models mainly arise from soil mechanics and are based on plasticity and viscoplasticity theory [33, 69, 98, 107, 121]. Many of them have been conceived by starting from the well known critical state theory [93, 110]. According to this theory, the granular material approaches a certain attractor, called the critical state. This non-evolving state, reached after a progressive increase in strain, at a vanishingly small strain rate, is independent of the initial arrangement. At the critical state, an ideal mechanism of yielding is assumed to develop within the specimen: the external work is totally dissipated by frictional processes at the contact level (disregarding both crushing and damage), unlimited shear strains develop, the microstructure does not evolve, and consequently, the concentration remains constant.
On the contrary, most of the works published within the granular flow community (e.g., see [45]) deal with the rheology of granular materials at large strain rates and low to moderate concentration, i.e., in the collisional regime. One of the first rheological models for granular flows in the collisional regime was proposed in 1954 by Bagnold [7]. This empirical model, derived from experiments in two-dimensional plane shear flows, basically states that the stresses are proportional to the square of the strain rate. This simple law, now known as “Bagnold scaling”, has been the first to understand the physics of granular dynamics at large deformations and has been verified for dry grains in a number of experiments and simulations [30, 75, 102, 116].

The collisional regime has beens largely studied in the context of kinetic theories of granular gases [23, 40, 45, 59, 80, 108]. In those works, the inelastic collisions associated with the random motion of the grains represent the main mechanism to dissipate the energy of the system. The kinetic theories take into consideration granular gaseous or collisional states, in which force chains within the medium, forming the granular skeleton, disappear. In this context, the granular temperature, which represents a measure of the degree of agitation of the system, is introduced. Classic kinetic theories assume that the particles interact mainly through instantaneous, binary and uncorrelated collisions. When the granular material becomes denser, the assumption of chaotic, binary, instantaneous collisions fails [24, 71, 88]. Jenkins [52, 53] has recently extended the kinetic theories to account for the decrease in the energy dissipation due to the existence of correlated motion among the particles occurring at high concentration. Moreover, an heuristic extension of kinetic theories to deal with non-instantaneous inter-particle collisions, due to the finite stiffness of the particles, has been suggested by Hwang and Hutter [49]. The possibility of sticking-sliding collisions has also been included in the theory in an approximate way [54]. The constitutive model proposed in this work is largely based on kinetic theories of granular gases; then, a summary description of them is presented in Chapter 3. Nevertheless, kinetic theories are not capable of capturing the roughly rate-independent behavior observed at large concentration, when force chains develop within the medium [30, 82]. On the other side, the constitutive models proposed within the soil mechanics community do not incorporate the granular temperature as a state variable of the problem. Therefore, they are unable to deal with the phase-transition of granular materials - from a solid-like to a fluid-like state, and vice-versa.

More recently, several theories have been developed to model the phase transition and, in particular, the behavior of granular materials in the intermediate regime. The French research group GDR-MiDi [44] has suggested that dense granular materials obey to a local, phenomenological rheology that can be expressed in terms of two relations between three non-dimensional quantities: concentration, shear to normal stress ratio and inertial parameter (ratio of the time scales associated with the motion perpendicular and parallel to the flow, respectively). Various constitutive relations, based on the 'GDR MiDi rheology, have been developed [30, 31, 65, 67]. Despite the notable results obtained in modeling many different configurations of dense granular flows [12, 13, 14, 66, 97], the GDR MiDi rheology does not apply when there is an additional time scale associated with the particle velocity fluctuations [53], whose intensity is provided by the granular temperature; in fact, the role of the latter cannot be disregarded in regions of thickness some diameters close to the boundaries (free surface, rigid and/or erodible bottom) [70, 116].

Most of the constitutive models used to predict the behavior of granular flows in the whole range of flow regimes are based on additive decomposition of the stress tensor into the sum of "rate-dependent" and "rate-independent" contributions [16, 63, 64, 72, 78, 108]. Savage [108] assumed a plastic, frictional behavior and the presence of Gaussian fluctuations of the strain rate and stresses in the planar flow of a dense granular material. By averaging strain rate fluctuations, Savage obtained a constitutive relation in which the shear stress has two contributions: a viscous, rate-dependent part, and a strain rate-independent part. Also, the theory assumes the viscous shear stress to diverge as the density approaches the close packing limit. In the theories proposed by Johnson and Jackson [63, 64], Louge [78] and Lee and Huang [72], the stress tensor is given by the sum of a rate-independent part and a rate-dependent part. In all those works, the rate-independent part (called "frictional" in [63], associated to "enduring contacts" in [78] and said "static" in [72]) is defined by a Coulomb law relation between the the shear and the normal stresses. The

rate-dependent contribution ("collisional", "impulsive interactions" or "kinetic"), is modeled by using a kinetic theory developed for dilute flows, that does not take into account the breaking of the molecular chaos assumption [26], at high concentrations. In these models, the role of particle stiffness is not taken into account, so that the constitutive relation for the frictional rate-independent part is not well physically based.

3. Kinetic theory of granular gases

The approach followed in this thesis for modeling granular flows, which is presented in the upcoming Section 4.2, is largely based on the kinetic theory of granular gases. This Section is devoted to a summary description of the kinetic theory of granular gases, and is largely based on: Brilliantov and Pöschel [20], Garzó et al. [42, 43], Goldhirsch [45, 46], Pöschel and Luding [100].

The term "granular gas" is used in analogy with a (classic) molecular gas, where the molecules are largely spaced and free to move in each direction, interacting only through collisions. The main difference between molecular and granular gases is that in the latter grains are inelastic (i.e., the collisions are dissipative), so that part of the energy of the system is irreversibly lost whenever particles interact. Consequently, granular gases are always in *non-equilibrium* states and it is always necessary to pump energy into a granular gas in order to maintain it fluidized [46]. Furthermore, grains undergo attrition, breakup, coagulation and other processes, which are rare for molecular gases at not-too-high temperatures. Also, granular systems do not usually possess the strong scale separation that characterizes molecular systems, except in the case of nearly-elastic interactions. This fact has numerous consequences, one of which is the sizeable normal stress differences in granular gases.
As in the case of molecular gases (or liquids), one can define macroscopic fields for granular gases, such as the granular temperature, T, the velocity, $\mathbf{u}$, and the mass density, ρ [45]. The definition of these fields for granular materials requires the introduction of the notion of average over the microscopic scales. For an ordinary gas, the macroscopic velocity field is given by the average over the single molecule velocity, and the difference between the velocity of a molecule and the macroscopic velocity is known as the fluctuating (or peculiar) velocity of that molecule. The average of the square of the fluctuating velocities of the molecules is proportional to the local thermodynamic temperature of the gas, by definition. This definition of thermodinamic temperature comes from statistical mechanics and has been proved to be the same as that defined using the standard concepts of energy and entropy. But the statistical mechanics definition does not require to refer to a state of equilibrium of the system [45], then allows to define temperature even for systems which are far from an equilibrium state. Similarly to ordinary gases, the macroscopic velocity field of a granular system is defined as the average over single grain velocity and the granular temperature is introduced as the mean square of the velocity fluctuations of the grains. Hence, there is an evident analogy between the grain fluctuation kinetik energy of granular systems and the molecular kinetic energy that determines the thermodynamic temperature of a gas.
Kinetic theories assume that particles can interact only through dissipative collisions, and they have been proved to succeed, describing accurately the beviavior of a granular system, whenever the force chains do not span the entire domain of the granular medium. Although the application of kinetic theory to granular gases involves several problems, for example, the lack of scale separation, the long range correlations, etc [45], the granular hydrodynamic equations derived by the kinetic theory of granular gases well describe the dynamics of granular flows.

Kinetic equation and distribution function

Following the statistical mechanics approach, kinetic theory deals with the probability distribution functions describing the state of a granular gas [2]. The corresponding equations, similar to Boltzmann equations for rarefied gases, can be rigorously derived for the dilute gas of inelastically colliding particles.
In the context of kinetic theory, the macroscopic properties of granular gases are governed by the single-particle distribution function. The single-particle distribution function, $f(\mathbf{v}, \mathbf{x}, t)$, is defined as the probability to find particles with velocity $\mathbf{v}$ at point $\mathbf{x}$ at time t and is determined by a certain time evolution integral equation (the kinetic equation). Two forms of the time evolution equation for f have been used, the Boltzmann equation and the Enskog equation, leading to two different classes of kinetic theory. Whereas the validity of kinetic theories derived by the Boltzmann equation is restricted to dilute systems of particles, those obtained by using the Enskog equation extend to higher density gases.
For those theories that employ the Enskog equation, two different approaches are possible: the Standard Enskog Theory (SET) and the Revised Enskog Theory (RET). The difference between SET and RET traces to the choice of the two-particle distribution function [43], $f_2(\mathbf{v}_1, \mathbf{x}_1, \mathbf{v}_2, \mathbf{x}_2, t)$, appearing in the Enskog equation, and which is defined as the probability that at time t, spheres with velocities near $\mathbf{v}_1$ and $\mathbf{v}_2$ will be located near $\mathbf{x}_1$ and $\mathbf{x}_2$.

Hydrodynamic equations of motion

Independently of the adopted starting equation, the macroscopic variables of interest of the continuum medium (density, velocity and granular temperature) are defined exactly in terms of moments of f, and the macroscopic, "hydrodynamic" balance equations of motion are obtained by appropriate manipulation of the time evolution equation for f. Those resemble the Navier Stokes equations with one (very important) difference: the equation for the energy density (or granular temperature) contains a "sink term" that represents the loss of energy due to the inelasticity of the collisions [46]. This term is responsible for the existence of steady granular shear flows (else the work by shear would have heated the granular system indefinitely) and for many other phenomena that characterize granular gases.
The balance equations become a closed set of equations for the hydrodynamic fields once the constitutive relations are given and are expressed as functionals of these fileds. The constitutive relations are explicit functionals of f; so the desired forms are obtained from a solution to the kinetic equation (Boltzmann or Enskog equation) that expresses the space and time dependence of f entirely in terms of the hydrodynamic fields. Such a solution is called a "normal" solution [18].

Solution method

In principle, the solution to the kinetic equation is equivalent to specifying all moments of the distribution function. Equations for the moments are obtained by taking moments of the time evolution equation of f, leading to a hierarchy of equations coupling lower order moments to those of higher order. Then, the set of kinetic equations is not closed. Two closures of the kinetic equations have been proposed, all of which involve the finding of

approximations for the distribution function, f. The first approximation is called Grad's moment method and consists in truncating the hierarchy of momentum equations. In the framework of this method, f is modeled by a Gaussian (or Maxwellian) function multiplied by a polynomial in the components of the fluctuating velocity. This modification is substituted in the Boltzmann or Enskog equation, leading to equations of motion for the coefficients of these polynomials [45]. The latter are then solved, for example, by assuming scale separation or a steady state. The main problem of the Grad's method is that it involves a fit to the distribution function and is not systematic.
The second approach is the Chapman-Enskog procedure, and involves a perturbative expansion about low Knudsen numbers ϵ (a non-dimensional measure of gradients, defined as the ratio of the mean free path to the scale over which the hydrodynamic fields vary) or "small gradients", and thus is not applicable to systems in which free-molecular (non-continuum) effects play a non-negligible role [43]. The Grad's moment method, does not contain similar restrictions, though the derivation is necessarily more complex and thus has not been performed without resorting to other simplifying assumptions (e.g., equipartition of energy). However, in this thesis the Grad's moment method is not employed and only the Chapman-Enskog expansion will be described in detail.
The Chapman-Enskog expansion is a systematic method for constructing a normal solution as an expansion in powers of the Knudsen number ϵ, or spatial gradients of the fields. When the gradient vanishes (zeroth order of the expansion), the kinetic theory determines the form of the distribution function to be the 'local equilibrium' Maxwellian for molecular fluids. However, in the presence of dissipation (inelastic particles) the kinetic theory requires a different solution at zeroth order, the "local homogeneous cooling" (HCS) distribution. The HCS distribution agrees with the local Maxwellian only when the particles are elastic. Following these considerations, two different approaches of the Chapman-Enskog procedure have been developed. The first is based on the observation that in the limit of elastic collisions and when the gradients vanish, the distribution function of the grain velocities is Maxwellian, corresponding to a state of (local) equilibrium. This limit is not singular and therefore one can expand the solution in two small parameters around this state of equilibrium: the Knudsen number ϵ and the degree of inelasticity, defined as $(1-e_n^2)$, where e_n is the coefficient of normal restitution. In this case, the lowest order term is indeed the Maxwellian. Such a double expansion is necessarily limited to asymptotically weak dissipation, i.e. is restricted to the case of nearly-elastic collisions.
The second approach is based on an expansion in the Knudsen number (or gradients) without any other small parameters, with HCS as the leading order solution and hence no a priori limitation on the degree of dissipation. Both the last two approaches produce constitutive relations, which agree with each other in the common domain of validity (nearly-elastic collisions). In this thesis, the kinetic theory in the form derived by Garzó and Dufty [40] is adopted, which employs the second approach, then only this one will be accurately described in the following.
In the most of kinetic theories that employ the Chapman-Enskog procedure, all expansions are carried out to first order in spatial gradients (Navier Stokes order). This assumptions requires that the gradients of the macroscopic fields are not large, which means that the conditions for the solution are restricted to small variations of the hydrodynamic fields over distances of the order of the mean free path [45]. Nonetheless, evidence of higher-order effects has been noted in a range of granular flows, and Burnett order effects (second order in spatial gradients) in particular have been shown to be linked to the anisotropy in the stress tensor.

Summary of different kinetic theories

As can be easily deduced, several kinetic theories have been proposed in the literature. Garzó et al. [43] summerized and classified a collection of previous works based on kinetic theory on the basis of: the dimensionality of the particles (2D disks or 3D spheres); the starting kinetic equation: Boltzmann (limited to dilute systems) or Enskog, and the specific mechanics and assumptions used in the derivation process (SET or RET); the solution method: Chapman-Enskog (CE) or Grad's moment method (Grad); the order of expansion in the Knudsen number (first Navier Stokes order or second Burnett order); the eventual order of expansion in the degree of inelasticity (which limits the validity of the solution to nearly-elastic particles). The resulted list is reported in Tab. 3.1, with some integration.

Table 3.1.: Classification of kinetic theories.

Reference	Dimension	Kinetic theory	Solution method	Exp. or. in ϵ	Exp. or. in $(1-e_n^2)$
Garzó and Dufty [41]	3D	Boltzmann	CE	first	-
Serero et al. [112]	3D	Boltzmann	CE	first	first
Sela and Goldhirsch [111]	3D	Boltzmann	CE	second	first
Brey et al. [18]	3D	Boltzmann	CE	second	-
Zamankhan [131]	3D	Enskog RET	Grad	-	-
Alam et al. [1]	2D	Enskog RET	CE	first	first
Willits and Arnarson [127]	2D	Enskog RET	CE	first	first
Jenkins and Mancini [55]	2D and 3D	Enskog SET	CE	first	first
Rahaman et al. [104]	3D	Enskog SET	CE	first	first
Jenkins and Mancini [56]	3D	Enskog RET	CE	first	first
Arnarson and Willits [3]	3D	Enskog RET	CE	first	first
Garzó and Dufty [40]	2D and 3D	Enskog RET	CE	first	-

Standard vs Extended Kinetic Theory

All the kinetic theories appearing in Tab. 3.1 fall within the context of Standard Kinetic Theory, i.e., are developed under very restrictive assumptions:

- spherical particles;
- monodisperse systems;
- frictionless particles;
- constant coefficient of restitution;
- rigid particles (i.e., instantaneous collisions);
- binary collisions;
- molecular chaos (i.e., uncorrelated motion).

The kinetic theories based on the Boltzmann equation requires the additional assumption of dilute systems (low concentration of the particles). Also, if the Chapman-Enskog procedure is employed as the solution method and the expansion in the Knudsen number is

limited to the first Navier Stokes order, the gradients of the macroscopic fields are supposed to be not large. Finally, if also the expansion in the degree of inelasticity is adopted, an extra hypothesis requires that the collisions are nearly-elastic.

Several modifications to the Standard Kinetic Theories have been introduced in the literature in order to take into account different effects: inter-particle friction [47, 57, 60, 80, 81]; dependence of the coefficient of restitution on the relative velocity [19]; nonspherical grains [99]; polydispersivity [41].
Finally, the class of kinetic theories which incorporates the influence of correlated motion is called Extended Kinetic Theory. Numerical simulations and experiments have shown that when simultaneous interactions between more than two particles become likely, i.e. when the particle velocities are correlated, small groups of particles overlap [75, 76, 86] and/or interact through repeated, weak, "chattering" collisions [88]. The presence of clusters of particles and force chains influences the energy dissipation. Within the context of kinetic theory, Jenkins [52, 53] has introduced a length associated with the size of particle clusters into the expression of the energy dissipation, which accounts for the effect of correlated motion.

Outline of the Chapter

The present Chapter is outlined in the following way. Section 3.1 is devoted to a summary description of the Standard Kinetic Theories. In this framework, the Boltzmann equation is first introduced, then the hydrodynamic equations of the motion are derived and the Chapman-Enskog procedure is presented. The Standard Kinetic Theory derived from the Enskog equation, in the form proposed by Garzó and Dufty [40], is then discussed. The modification introduced by Jenkins and Zhang [60] in order to account for the role played by the inter-particle friction is finally described. Section 3.2 concerns with the Extended Kinetic Theory proposed by Jenkins [52, 53], which incorporates the effect of correlated motion of particles and extends the validity of kinetic theory to dense granular flows.

3.1. Standard Kinetic Theory

3.1.1. The Boltzmann equation

Let's consider an assembly of smooth, frictionless spheres with a diameter d and a mass m. The collision between two grains is inelastic and part of the kinetic energy is lost during the collision. The grains are assumed to be rigid, then the collisions are instantaneous. The inelastic, instantaneous collision between two particles can be described introducing the coefficient of normal restitution, e_n, which relates the relative particle velocities before and after the collision. Here, the particles are assumed to be frictionless, then the relative velocities of the colliding particles have only normal component. In this case, the normal coefficient of restitution is the unique material parameter characterizing the collision, and is named simply coefficient of restitution. Considering two particles, labeled 1 and 2, and their velocities, $\mathbf{v}_i$ and $\mathbf{v}_i'$, $i = 1, 2$, respectively before and after a collision, the dynamics of the collision is described by:

$$\mathbf{g}' \cdot \mathbf{n} = -e_n \left(\mathbf{g} \cdot \mathbf{n} \right). \tag{3.1}$$

There, $\mathbf{n}$ is the unit vector from the center of particle 1 to that of particle 2, and $\mathbf{g} = (\mathbf{v}_1 - \mathbf{v}_2)$ and $\mathbf{g}' = (\mathbf{v}_1' - \mathbf{v}_2')$ are the relative velocities before and after the collision.

Then, the coefficient of restitution is a single parameter which capture the inelasticity of collisions. In general, the coefficient of restitution depends on the relative velocity and the duration time of the collision, but here the simplest case for which e_n is a constant and $0 < e_n < 1$ is considered. When $e_n = 1$, the relative velocity before the collision is totally recovered, then particles are perfectly elastic. Whereas, $e_n < 1$ means that the spheres lose part of their velocity, and then of their kinetic energy, during the collision.
Considering the granular matter as an assembly of a large number of grains, in the kinetic theory the approach of the statistical mechanics for the description of the macroscopic properties of granular gases is adopted. The macroscopic (or hydrodynamic) properties of interest are governed by the single-particle distribution function. The single-particle distribution function at point $\mathbf{x}$ and time t, $f(\mathbf{v}, \mathbf{x}, t)$, is defined as the number density n of particles having velocity $\mathbf{v}$ at point $\mathbf{x}$ at time t. In other words, f/n is the probability density for a particle at point $\mathbf{x}$ at time t to have a velocity $\mathbf{v}$. The number n of particles per unit volume at $\mathbf{x}$ and t is then given by

$$n(\mathbf{x}, t) = \int f(\mathbf{v}, \mathbf{x}, t) d\mathbf{v}.$$

where the integration is over the entire volume of velocity space. The global number of particles in the system, at time t, is $N(t) = \int n(\mathbf{x}, t) d\mathbf{x}$. The average $\langle\ \rangle$ of a particle property X is defined in terms of n and the velocity distribution function f by

$$\langle X \rangle = \frac{1}{n(\mathbf{x}, t)} \int X f(\mathbf{v}, \mathbf{x}, t) d\mathbf{v}.$$

Following the standard procedures of kinetic theory, the time evolution of the single-particle distribution, in absence of external forces, can be described by

$$\left(\frac{\partial f}{\partial t} + \mathbf{v} \cdot \frac{\partial}{\partial \mathbf{x}} \right) f(\mathbf{v}, \mathbf{x}, t) = \left(\frac{\partial f}{\partial t} \right)_{\text{col}}, \tag{3.2}$$

where $(\partial f/\partial t)_{\text{col}}$ represents the rate of change due to the collisions among the particles. Eq. (3.2) is a non-linear integro-differential equation for $f(\mathbf{v}, \mathbf{x}, t)$. Note that the left-hand-side of Eq. (3.2) is independent of the nature of the collisions. By assuming the particle collisions to be binary, the change rate $(\partial f/\partial t)_{\text{col}}$ depends on the two-particle distribution function, $f_2(\mathbf{v}_1, \mathbf{x}_1, \mathbf{v}_2, \mathbf{x}_2, t)$, which is defined as the probability that at time t, spheres with velocities near $\mathbf{v}_1$ and $\mathbf{v}_2$ will be located near $\mathbf{x}_1$ and $\mathbf{x}_2$, respectively.
Then, the change rate is, in general, defined as

$$\begin{aligned} \left(\frac{\partial f}{\partial t} \right)_{\text{col}} = \mathrm{d}^2 \int d\mathbf{v}_2 \int \Theta\left(\mathbf{g} \cdot \mathbf{n}\right) \left(\mathbf{g} \cdot \mathbf{n}\right) \Big[\frac{1}{e_n^2} f_2\left(\mathbf{v}_1', \mathbf{x}_1, \mathbf{v}_2', \mathbf{x}_1 - \mathrm{d}\mathbf{n}, t\right) + \\ - f_2\left(\mathbf{v}_1, \mathbf{x}_1, \mathbf{v}_2, \mathbf{x}_1 + \mathrm{d}\mathbf{n}, t\right) \Big] d\mathbf{n}. \end{aligned} \tag{3.3}$$

The position $\mathbf{x}_2$ appears only for $\mathbf{x}_2 = \mathbf{x}_1 \pm \mathrm{d}\mathbf{n}$ and this means that the two particles are at contact. The Heaviside step function Θ assures that the relative velocities $\mathbf{g}$ are such that a collision takes place.
Eq. (3.2) becomes a kinetic theory (i.e., closed equations for f) only after specifying f_2 as a function (or a functional) of f. In the classic kinetic theory, two assumptions allow to simplify the expression of the change rate. First, the system is assumed to be dilute, (the granular gas is rarefied). In this case, the velocity distribution function does not change with slightly changing the position:

$$f_2(\mathbf{v}_1, \mathbf{x}_1, \mathbf{v}_2, \mathbf{x}_1 + \mathrm{d}\mathbf{n}, t) \cong f_2(\mathbf{v}_1, \mathbf{x}_1, \mathbf{v}_2, \mathbf{x}_1, t).$$

Second, the correlations between colliding particles are neglected, so that the two-particle distribution function can be decomposed into the single-particle distribution functions as

$$f_2(\mathbf{v}_1, \mathbf{x}_1, \mathbf{v}_2, \mathbf{x}_1, t) = f(\mathbf{v}_1, \mathbf{x}_1, t) f(\mathbf{v}_2, \mathbf{x}_1, t).$$

The second assumption is known as "molecular chaos" hypothesis.
Using the two assumptions above, Eq. (3.2) can be rewritten as

$$\left(\frac{\partial}{\partial t} + \mathbf{v}_1 \cdot \frac{\partial}{\partial \mathbf{x}_1}\right) f(\mathbf{v}_1, \mathbf{x}_1, t) = I\left(f, f\right), \tag{3.4}$$

where $I\left(f, f\right)$ is called binary collision integral and is given by

$$\begin{aligned} I\left(f, f\right) = \mathrm{d}^2 \int d\mathbf{v}_2 \int \Theta\left(\mathbf{g} \cdot \mathbf{n}\right)\left(\mathbf{g} \cdot \mathbf{n}\right) \Big[\frac{1}{e_n^2} f\left(\mathbf{v}_1', \mathbf{x}_1, t\right) f\left(\mathbf{v}_2', \mathbf{x}_1, t\right) + \\ - f\left(\mathbf{v}_1, \mathbf{x}_1, t\right) f\left(\mathbf{v}_2, \mathbf{x}_1, t\right) \Big] d\mathbf{n}, \end{aligned} \tag{3.5}$$

Eq. (3.4) is the Boltzmann equation, first derived by Boltzmann in 1872, and holds only under the following assumptions:

(I) spherical particles;

(II) monodisperse systems;

(III) frictionless particles;

(IV) constant coefficient of restitution;

(V) rigid particles (i.e., instantaneous collisions);

(VI) binary collisions;

(VII) dilute systems;

(VIII) molecular chaos (i.e., uncorrelated motion).

Due to the dissipative nature of the collisions in granular material, the velocity distribution function has been modified in order to take into account the inelasticity of the particles, and the Boltzmann equation has been derived in a little different way from the case of molecular gases.
By multiplying a generic function of the velocity, $\psi(\mathbf{v}_1)$, to the Boltzmann equation (3.4) and integrate over $\mathbf{v}_1$, the transport equation for $\psi(\mathbf{v}_1)$ is obtained:

$$\frac{\partial}{\partial t}\left\langle n\psi \right\rangle + \frac{\partial}{\partial \mathbf{x}_1} \cdot \left\langle n\psi \mathbf{v}_1 \right\rangle = \int \psi(\mathbf{v}_1) I(f, f) d\mathbf{v}_1, \tag{3.6}$$

We notice that the time derivative and the integral over $\mathbf{v}_1$ can be exchanged and the gradient does not act on $\mathbf{v}$.
For a generic function of the the velocity $\psi(\mathbf{v}_1)$, the binary collision integral satisfies the following property:

$$\begin{aligned} \int \psi(\mathbf{v}_1) I(f, f) d\mathbf{v}_1 = \frac{\mathrm{d}^2}{2} \int d\mathbf{v}_1 \int d\mathbf{v}_2 \int \Theta\left(\mathbf{g} \cdot \mathbf{n}\right)\left(\mathbf{g} \cdot \mathbf{n}\right) \left\{ \left[\psi(\mathbf{v}_1') + \psi(\mathbf{v}_2')\right] + \right. \\ \left. - \left[\psi(\mathbf{v}_1) + \psi(\mathbf{v}_2)\right] \right\} f\left(\mathbf{v}_1, \mathbf{x}_1, t\right) f\left(\mathbf{v}_2, \mathbf{x}_1, t\right) d\mathbf{n}. \end{aligned}$$

We call collisional invariant each quantity $\tilde{\psi}(\mathbf{v})$ which does not change in a collision, i.e., $\tilde{\psi}(\mathbf{v}_1') + \tilde{\psi}(\mathbf{v}_2') = \tilde{\psi}(\mathbf{v}_1) + \tilde{\psi}(\mathbf{v}_2)$, implying that $\int \tilde{\psi}(\mathbf{v}) I(f,f) d\mathbf{v} = 0$. An elastic binary collision is characterized by the conservation of mass m, momentum $m\mathbf{v}$ and kinetic energy $m|\mathbf{v}|^2/2$, which are then the collisional invariants in the elastic case ($e = 1$). For inelastic collisions, the mass and the momentum are conservative quantities, but not the kinetic energy.
The three independent, hydrodynamic mean fields are introduced, as the averages of m, $m\mathbf{v}$ and $m|\mathbf{v}|^2/2$:

- the mean mass density of the system:

$$\rho = mn = m \int f(\mathbf{v}, \mathbf{x}, t) d\mathbf{v};$$

- the mean velocity of the flow:

$$\mathbf{u} = \langle \mathbf{v} \rangle = \frac{1}{n} \int f(\mathbf{v}, \mathbf{x}, t) \mathbf{v} d\mathbf{v};$$

- the macroscopic granular temperature, T:

$$\frac{3}{2} T = \frac{1}{2} \langle V^2 \rangle = \frac{1}{n} \int \frac{1}{2} V^2 f(\mathbf{v}, \mathbf{x}, t) d\mathbf{v} \tag{3.7}$$

where $\mathbf{V} = \mathbf{v} - \mathbf{u}$ is the particle fluctuating velocity, and $V = |\mathbf{V}|$ its magnitude. T is the average fluctuating kinetic energy per unit of mass of a resting system of grains, as the temperature in the theory of molecular gases. It is important to stress that the internal thermodynamic temperature of the grains is a very different entity whose value is usually not of much interest in the field of granular flows [45].

3.1.2. Hydrodynamic equations of motion

The balance laws for ρ, $\mathbf{u}$ and T result from the transport equation (3.6) when ψ is taken to be m, $m\mathbf{v}_1$ and $m|\mathbf{v}_1|^2/2$, respectively. Note that for the mass and the momentum, the right-hand-side of the transport equation (3.6) vanishes; this does not happen for the kinetic energy if the collisions are inelastic.
The mass balance reads

$$\frac{D\rho}{Dt} + \rho \nabla \cdot \mathbf{u} = 0, \tag{3.8}$$

where the material derivative is defined with respect to the mean velocity: $D/Dt = \partial/\partial t + \mathbf{u} \cdot \nabla$.
The momentum balance equation, in absence of external forces, is given by:

$$\rho \frac{D\mathbf{u}}{Dt} = -\nabla \cdot \boldsymbol{\sigma}, \tag{3.9}$$

where $\boldsymbol{\sigma}$ is the stress tensor.
Finally, the balance of fluctuating energy, which describes the time development of the granular temperature, is:

$$\frac{3}{2} \rho \frac{DT}{Dt} = -\boldsymbol{\sigma} : \dot{\boldsymbol{\varepsilon}} - \nabla \cdot \mathbf{q} - \Gamma. \tag{3.10}$$

Here, $\mathbf{q}$ and Γ are, respectively, the flux of fluctuating energy and the collisional rate of dissipation of fluctuating energy per unit volume, whereas the strain rate tensor, $\dot{\boldsymbol{\varepsilon}}$, is given by the symmetric part of the velocity gradient:

$$\dot{\boldsymbol{\varepsilon}} = \frac{1}{2}\left(\nabla\mathbf{u} + \nabla^t\mathbf{u}\right). \tag{3.11}$$

The : denotes the tensorial product: $\mathbf{A} : \mathbf{B} = A_{ij}B_{ij}$ and the superscript t represents transposition. Here and in the following, the summation rule is used for twice appearence of the indices.
Equations (3.8)-(3.10) have to be supplemented by the constitutive relations for the stress tensor $\boldsymbol{\sigma}$, energy flux $\mathbf{q}$, and energy dissipation rate Γ. Their forms, following the integral procedure, read:

$$\sigma_{ij} = m\int V_iV_jf(\mathbf{v},\mathbf{x},t)d\mathbf{v}, \tag{3.12}$$

$$\mathbf{q} = \frac{m}{2}\int \mathbf{V}V^2f(\mathbf{v},\mathbf{x},t)d\mathbf{v}, \tag{3.13}$$

$$\Gamma = -\frac{m}{2}\int |\mathbf{v}|^2\, I(f,f)d\mathbf{v}. \tag{3.14}$$

From Eq. (3.12), using the definition of granular temperature Eq. (3.7), the stress tensor can be written as

$$\boldsymbol{\sigma} = p\mathbf{I} + \rho\left\langle\mathbf{D}\right\rangle,$$

where $\mathbf{I}$ is the identity matrix, $p = \rho T$ is the hydrostatic pressure, and $\mathbf{D}$ is the deviatoric part of the stress tensor:

$$D_{ij} = V_iV_j - \frac{1}{3}V^2\delta_{ij},$$

being δ_{ij} the Kronecker's symbol. Using the expression of the binary collision integral (3.5), the rate of dissipation of fluctuating energy can be expressed as

$$\Gamma = \left(1-e_n^2\right)\frac{\pi m\mathrm{d}^2}{16}\int d\mathbf{v}_1\int |\mathbf{g}|^3\, f(\mathbf{v}_1,\mathbf{x},t)f(\mathbf{v}_2,\mathbf{x},t)d\mathbf{v}_2. \tag{3.15}$$

The dissipation rate is the consequence of the inelasticity of the particles, and vanishes when $e_n = 1$. The set of hydrodynamic equations (3.8)-(3.10) is not close, since requires the additional constitutive equations for $\boldsymbol{\sigma}$, $\mathbf{q}$ and Γ which depend on higher moments of the single-particle distribution function f. The constitutive relations $\boldsymbol{\sigma}$, $\mathbf{q}$ and Γ have been provided by the Chapman-Enskog procedure, under the hypothesis of small gradients.

3.1.3. Chapman-Enskog procedure

The Chapman-Enskog theory is a closure of the hydrodynamic equations of motion (3.8)-(3.10), under two main assumptions. The first assumption is that the mean free path, λ, that is the average distance traveled by a particle between two successive collisions, is small with respect to the macroscopic scale length, L, at which the hydrodynamic fields vary. The mean free path is computed as $\lambda = \left(\sqrt{2}\pi n\mathrm{d}^2\right)^{-1}$. In the Chapman-Enskog procedure, the Knudsen number is introduced, $\epsilon = \lambda/L$, as a non-dimensional measure of gradients. The spatial scale of the problem changes from $\mathbf{x}$ to $\epsilon\mathbf{x}$, so that all gradients

are trasformed as $\nabla \longrightarrow \epsilon\nabla$. The first assumption ensure that ϵ is small, then the stress tensor and the heat flux can be approximated as linear in the gradient:

$$\sigma_{ij} = p\delta_{ij} - \tilde{\eta}\epsilon\left(\frac{\partial u_i}{\partial x_j} + \frac{\partial u_j}{\partial x_i} - \frac{2}{3}\delta_{ij}\nabla\cdot\mathbf{u}\right), \tag{3.16a}$$

$$\mathbf{q} = -\epsilon\left(\tilde{\kappa}\nabla T + \tilde{\mu}\nabla\rho\right), \tag{3.16b}$$

where p is the hydrostatic pressure, as already stated, and $\tilde{\eta}$, $\tilde{\kappa}$ and $\tilde{\mu}$ are the shear viscosity, the thermal conductivity and the coefficient of the density gradient, respectively. We notice that the tilde denotes coefficients deriving from the Boltzmann equation, and then valid in the low density limit. Then, the microscopic expressions of these coefficient have to be derived.
Also, given that the gradient is scaled as $\epsilon\nabla$, the hydrodynamic equations, with the stress tensor and the energy flux computed using Eqs. (3.16), are also scaled as

$$\frac{\partial\rho}{\partial t} = -\epsilon\nabla\cdot(\rho\mathbf{u}), \tag{3.17a}$$

$$\frac{\partial\mathbf{u}}{\partial t} = -\epsilon\left(\mathbf{u}\cdot\nabla\mathbf{u} + \frac{1}{\rho}\nabla p\right) + \epsilon^2\frac{\tilde{\eta}}{\rho}\left[\nabla^2\mathbf{u} + \frac{1}{3}\nabla\left(\nabla\cdot\mathbf{u}\right)\right], \tag{3.17b}$$

$$\frac{\partial T}{\partial t} = -\frac{2\Gamma}{3\rho} - \epsilon\left[\mathbf{u}\cdot\nabla T + \frac{2}{3\rho}p\left(\nabla\cdot\mathbf{u}\right)\right] + \epsilon^2\mathcal{G}, \tag{3.17c}$$

with

$$\mathcal{G} = \frac{2}{3\rho}\left(\tilde{\kappa}\nabla^2 T + \tilde{\mu}\nabla^2\rho\right) + \frac{2\tilde{\eta}}{3\rho}\left[\left(\frac{\partial u_j}{\partial x_i}\right)\left(\frac{\partial u_i}{\partial x_j}\right) + \left(\frac{\partial u_i}{\partial x_j}\right)\left(\frac{\partial u_i}{\partial x_j}\right) - \frac{2}{3}\left(\nabla\cdot\mathbf{u}\right)^2\right],$$

being ∇^2 the Laplacian operator.
The second assumption of the Chapman-Enskog procedure requires that the single-particle distribution function depends on $\mathbf{x}$ and t only through the hydrodynamic mean variables, $\rho(\mathbf{x},t)$, $\mathbf{u}(\mathbf{x},t)$ and $T(\mathbf{x},t)$. Therefore, the time and spatial derivative of $f(\mathbf{v},\mathbf{x},t)$ are given, respectively, by

$$\frac{\partial f}{\partial t} = \frac{\partial f}{\partial\rho}\frac{\partial\rho}{\partial t} + \frac{\partial f}{\partial\mathbf{u}}\cdot\frac{\partial\mathbf{u}}{\partial t} + \frac{\partial f}{\partial T}\frac{\partial T}{\partial t},$$
$$\nabla f = \frac{\partial f}{\partial\rho}\nabla\rho + \frac{\partial f}{\partial\mathbf{u}}\cdot\nabla\mathbf{u} + \frac{\partial f}{\partial T}\nabla T.$$

This assumption is based on scale separation: it is assumed that the system locally equilibrates on a timescale that is shorter than the macroscopic timescales [45].
For consistency with the above assumptions, time scales which measure the time variations associated to growing powers of ϵ can be introduced:

$$\frac{\partial}{\partial t} = \frac{\partial^{(0)}}{\partial t} + \epsilon\frac{\partial^{(1)}}{\partial t} + \epsilon^2\frac{\partial^{(2)}}{\partial t} + \ldots$$

and the velocity distribution function is expanded into the series of the gradient

$$f = f^{(0)} + \epsilon f^{(1)} + \epsilon^2 f^{(2)} + \ldots$$

The expansions are put into the Boltzmann equation (3.4), leading to

$$\left(\frac{\partial^{(0)}}{\partial t} + \epsilon\frac{\partial^{(1)}}{\partial t} + \ldots + \epsilon\mathbf{v}\cdot\nabla\right)\left(f^{(0)} + \epsilon f^{(1)} + \ldots\right) = I\left(f^{(0)} + \epsilon f^{(1)} + \ldots, f^{(0)} + \epsilon f^{(1)} + \ldots\right). \tag{3.18}$$

The rate of dissipation of fluctuating energy is also expanded into the serie of ϵ:

$$\Gamma = \Gamma^{(0)} + \epsilon\Gamma^{(1)} + \epsilon^2\Gamma^{(2)} + \dots$$

where $\Gamma^{(r)}$ are computed using (3.15) with the corresponding $r-$th order distribution function $f^{(r)}$. In Eq. (3.18), terms at the same order in ϵ can be solved separately (supplemented by Eqs. (3.17) for the hydrodynamic variables); this must be executed in order of growing powers of ϵ, since at each order the solution at smaller order is needed.
The zeroth order in the Chapman-Enskog expansion begets the Euler equations, the first order yields the Navier-Stokes equation, and next are the Burnett and super-Burnett orders [45].

Zeroth order

At the zeroth (Euler) order, the Boltzmann equation (3.18) and the hydrodynamic equations (3.17) read

$$\frac{\partial^{(0)}}{\partial t} f^{(0)} = I(f^{(0)}, f^{(0)}), \tag{3.19a}$$

$$\frac{\partial^{(0)}}{\partial t} \rho = 0, \tag{3.19b}$$

$$\frac{\partial^{(0)}}{\partial t} \mathbf{u} = 0, \tag{3.19c}$$

$$\frac{\partial^{(0)}}{\partial t} T = -\frac{2\Gamma^{(0)}}{3\rho}. \tag{3.19d}$$

This set of equations describes a spatially homogeneous situation, where the density is uniform, ρ =const, and the velocity field is zero, $\mathbf{u} = \mathbf{0}$; then, the distribution functions are independent of the space and the system behaves like an equilibrium state at each time instant, except for the decay of the granular temperature. The formal expressions of the zeroth order of the distribution function, $f^{(0)}$, and the rate of dissipation of fluctuating energy, $\Gamma^{(0)}$, can be evaluated using Eqs. (3.19). The constitutive relations for $\boldsymbol{\sigma}$ and $\mathbf{q}$ (3.16) become

$$\sigma_{ij} = p\delta_{ij}$$

$$\mathbf{q} = \mathbf{0}$$

Then the stress tensor is isotropic and is completely described by the hydrostatic pressure $p = \rho T$.

First order

For the first order in ϵ (Navier Stokes order), the analysis is similar although more complicated. The stress tensor and the energy flux read, respectively

$$\sigma_{ij} = p\delta_{ij} - \tilde{\eta}\left(\frac{\partial u_i}{\partial x_j} + \frac{\partial u_j}{\partial x_i} - \frac{2}{3}\delta_{ij}\nabla\cdot\mathbf{u}\right), \tag{3.20}$$

$$\mathbf{q} = -\tilde{\kappa}\nabla T - \tilde{\mu}\nabla\rho. \tag{3.21}$$

Knowledge of $f^{(0)}$ allows to write an expression for $f^{(1)}$, then comparing the expressions (3.20)-(3.21) with the original definitions of $\boldsymbol{\sigma}$ and $\mathbf{q}$, (3.12)-(3.13), respectively, and using

$f = f^{(0)} + f^{(1)}$, the formal expressions for the shear viscosity, the thermal conductivity and the coefficient of the density gradient are given by:

$$\tilde{\eta} = -\frac{1}{10}\int \mathbf{D} : \boldsymbol{\gamma} d\mathbf{v}, \tag{3.22a}$$

$$\tilde{\kappa} = -\frac{1}{3T}\int \mathbf{S} \cdot \boldsymbol{\alpha} d\mathbf{v}, \tag{3.22b}$$

$$\tilde{\mu} = -\frac{1}{3\rho}\int \mathbf{S} \cdot \boldsymbol{\beta} d\mathbf{v}, \tag{3.22c}$$

where $\mathbf{S} = \left(V^2 - 5T\right)\mathbf{V}/2$ and $\mathbf{D}$ was previously introduced. The expressions of $\boldsymbol{\alpha}$, $\boldsymbol{\beta}$ and $\boldsymbol{\gamma}$ are obtained putting the expression of $f^{(1)}$ into the first order Boltzmann equation and comparing terms with the same gradients. In order to do that, the expression of $f^{(0)}$ has to be provided.

In the case of elastic collisions ($e_n = 1$), the first order set of equations describes transport without dissipation (i.e., there are no viscosity and thermal conductivity) and $f^{(0)}$ is the Maxwellian distribution function, which represents the local equilibrium distribution function:

$$f^{(0)}_{(e_n=1)}(\mathbf{v}) = \frac{n}{(2\pi T)^{3/2}} \exp\left(-\frac{|\mathbf{v}|^2}{2T}\right). \tag{3.23}$$

The above coefficients can be analytically deduced:

$$\tilde{\eta}_{(e_n=1)} = \frac{5}{96}\rho_p d\sqrt{\pi T}, \tag{3.24a}$$

$$\tilde{\kappa}_{(e_n=1)} = \frac{15}{4}\tilde{\eta}_{(e_n=1)}, \tag{3.24b}$$

$$\tilde{\mu}_{(e_n=1)} = 0, \tag{3.24c}$$

being $\rho_p = 6m/\left(\pi \mathrm{d}^3\right)$ the particle density.

In the inelastic case, i.e., $e_n < 1$, $f^{(0)}$ is not known analytically, but, if not too much energy is dissipated in collisions (nearly elastic collisions), it is plausible to assume that the velocity distribution function does not differ much from the Maxwellian. This is a furter assumption which means that when the gradients are not 'too large' the correction to the local equilibrium distribution function is a 'small' perturbation. Then, $f^{(0)}$ can be expressed as an expansion in Sonine polynomials of the Maxwellian distribution function. For instance, truncating $f^{(0)}$ at the second Sonine polynomials, we obtain:

$$\begin{aligned}
\tilde{\eta} &= \tilde{\eta}_{(e_n=1)}\tilde{\eta}^*, \\
\tilde{\kappa} &= \tilde{\kappa}_{(e_n=1)}\tilde{\kappa}^*, \\
\tilde{\mu} &= \frac{T}{\rho}\tilde{\kappa}_{(e_n=1)}\tilde{\mu}^*,
\end{aligned}$$

where we defined

$$\tilde{\eta}^* = \frac{24}{(1+e_n)(13-e_n)}\left[1+\frac{3\,(4-3e_n)}{8\,(13-e_n)}a_2\right]$$
$$\tilde{\kappa}^* = \frac{32}{2(1+e_n)(9+7e_n)}\left[1+\frac{797+211e_n}{32\,(9+7e_n)}a_2\right]$$
$$\tilde{\mu}^* = \frac{640(1-e_n)\,[1+h(e_n)a_2]}{(1+e_n)(9+7e_n)(19-3e_n)}$$
$$h(e_n) = \frac{50201-30971e_n-7253e_n^2+4407e_n^3}{80(1-e_n)(19-3e_n)(9+7e_n)},$$

and a_2 is the second Soline coefficient:

$$a_2 = \frac{16(1-e_n)\left(1-2e_n^2\right)}{81-17e_n+30e_n^2(1-e_n)}.$$

3.1.4. The Enskog equation

The validity of the Standard Kinetic Theory derived using the Boltzmann equation is restricted to dilute systems of particles. This conditions is necessary to consider valid the "molecular chaos" assumption, which states the independence of colliding particles, and leads to the Boltzmann equation. In principle, in fact, two colliding particles can be correlated due to an intersection of their collisional histories: one simple possibility is that they may have collided some time before or, alternatively, they may have collided with particles that have collided before. Moreover, the spatial extension of particles (i.e. the fact that they are not really pointlike) restricts the possibilities of motion, and, as a consequence, the degree of independence (this is the so called excluded volume effect). All these kinds of correlations become relevant when the granular gas is not rarefied but (either moderately or highly) dense.
In 1922 Enskog [26] proposed a generalization of the Boltzmann equation, the Enskog equation, in order to extend the classic kinetic theory to higher density gases. This section is devoted to the kinetic theory based on the Enskog equation, called the Standard Enskog Theory (SET), and a subsequent extension of this, the Revised Enskog Theory (RET), proposed in 1972 by van Beijeren and Ernst [119, 120]. The section is mainly based on [43].
As previously stated, two kinetic theories have been used in the development of hydrodynamic equations for gases, namely the Boltzmann equation, which has led to the classical kinetic theory, and the Enskog equation for hard spheres. The difference between these two equations stems from the treatment of the two-particle distribution function f_2 in the equation of the change rate (3.3) [43]. For the Boltzmann equation, f_2 is assumed equal to the product of the two single-particle distribution functions. This lack of spatial and pre-collisional velocity correlations between the two particles restricts the Boltzmann equation to dilute systems. Enskog [26] introduced two crucial changes in the collision integral [91]: (i) the difference in position between the centers of a colliding pair of molecules is taken into account; (ii) the collision frequency is increased by a factor that accounts for the spatial correlations between the two colliding molecules. The two-particle distribution function, in the Enskog formulation, reads:

$$f_2(\mathbf{v}_1,\mathbf{x}_1,\mathbf{v}_2,\mathbf{x}_2,t) = \chi\left[\mathrm{d}|n(\mathbf{x}+\mathrm{d}\mathbf{n}/2)\right] f(\mathbf{v}_1,\mathbf{x}_1,t) f(\mathbf{v}_2,\mathbf{x}_2,t). \tag{3.25}$$

Here, $\chi\left[\mathrm{d}|n(\mathbf{x}+\mathrm{d}\mathbf{n}/2)\right]$ is the equilibrium pair correlation function for $|\mathbf{x}_1-\mathbf{x}_2| = \mathrm{d}$, and is a function of the number density n evaluated at the contact point $(\mathbf{x}+\mathrm{d}\mathbf{n}/2)$.

The function $\chi\left[\mathrm{d}|n\right]$ is the equilibrium value of the pair correlation function at contact corresponding to a uniform density n (the Enskog approximation). More specifically, χ accounts for excluded volume effects encountered in denser flows, and thus the corresponding Enskog kinetic theory is applicable to moderately dense flows. Using the new form of the two-particle distribution function into the definition of the rate of change due to the collisions $\left(\partial f/\partial t\right)_{\mathrm{col}}$ in Eq. (3.2), the Enskog equation is obtained instead of the Boltzmann equation, which is at the basis of the SET. Although the Enskog theory ignores the possibility of correlations in the velocities before collision, accounting just for positional correlations, it leads to transport coefficients that are in good agreement with experimental and simulation values over a wide range of densities [91]. The Enskog approximation is expected to deteriorate at higher densities as ring collisions and their associated velocity correlations become important.

In 1972, van Beijeren and Ernst [119, 120] proposed a modification to the SET, known as the Revised Enskog Theory (RET). The difference between SET and RET traces to the choice of the pair correlation function in the two-particle distribution function. In SET, the pair correlation function χ is a function of concentration (i.e., depends on the local value only) at a single position of interest, whereas for RET the new pair correlation function, g_0, is treated as a functional of concentration (i.e., depends on the local value and its gradient) at the two particle centers. Then, in RET the two-particle distribution function is defined as

$$f_2(\mathbf{v}_1, \mathbf{x}_1, \mathbf{v}_2, \mathbf{x}_2, t) = g_0\left[\mathbf{x}_1, \mathbf{x}_2 | n(t)\right] f(\mathbf{v}_1, \mathbf{x}_1, t) f(\mathbf{v}_2, \mathbf{x}_2, t),$$

Here, $g_0\left[\mathbf{x}_1, \mathbf{x}_2 | n(t)\right]$ is the equilibrium pair correlation function, also called radial distribution function, as a functional of the non-equilibrium density $n(\mathbf{x}_1, t)$, and takes into account the spatial non-uniformities in a non-uniform state.
The RET and the SET lead to different predictions in non-homogeneous states. Therefore the difference between both theories is relevant in states far from equilibrium, as well as in equilibrium crystal and (metastable) glassy states [91].
The rate of change due to the collisions $\left(\partial f/\partial t\right)_{\mathrm{col}}$ in Eq. (3.2) depends on the new two-particle distribution function, and the corresponding of the Boltzmann equation is the Enskog equation for the time evolution of the single-particle distribution function:

$$\left(\frac{\partial}{\partial t} + \mathbf{v}_1 \cdot \frac{\partial}{\partial \mathbf{x}_1}\right) f(\mathbf{x}_1, \mathbf{v}_1, t) = J_E\left[\mathbf{x}_1, \mathbf{v}_1 | f(t)\right], \tag{3.26}$$

where $J_E\left[\mathbf{x}_1, \mathbf{v}_1 | f(t)\right]$ is called the Enskog collisional operator and is given by

$$\begin{aligned} J_E\left[\mathbf{x}_1, \mathbf{v}_1 | f(t)\right] = & \mathrm{d}^2 \int d\mathbf{v}_2 \int \Theta\left(\mathbf{g}\cdot\mathbf{n}\right)\left(\mathbf{g}\cdot\mathbf{n}\right)\left[\frac{1}{e_n^2} f_2\left(\mathbf{v}_1', \mathbf{x}_1, \mathbf{v}_2', \mathbf{x}_1 - \mathrm{d}\mathbf{n}, t\right) + \right. \\ & \left. - f_2\left(\mathbf{v}_1, \mathbf{x}_1, \mathbf{v}_2, \mathbf{x}_1 + \mathrm{d}\mathbf{n}, t\right)\right] d\mathbf{n}. \end{aligned} \tag{3.27}$$

As for the Boltzmann equation, the macroscopic balance equations for ρ, $\mathbf{u}$ and T follow directly from Eq. (3.26) by multipling by m, $m\mathbf{v}_1$ and $m\left|\mathbf{v}_1\right|^2$ and integrating over $\mathbf{v}_1$, and coincide with Eqs. (3.8)-(3.10). The constitutive relations for the stress tensor and the energy flux are now given by the following expressions:

$$\boldsymbol{\sigma} = \boldsymbol{\sigma}^k + \boldsymbol{\sigma}^c, \tag{3.28}$$

$$\mathbf{q} = \mathbf{q}^k + \mathbf{q}^c, \tag{3.29}$$

where the superscripts k and c denote the "kinetic" (or streaming) and the "collisional transfer" contributions, respectively. A primary consequence of the Enskog theory is that it leads to a collisional transfer of momentum and energy that can be expressed in terms of f_2. The kinetic contributions are defined as the quantities for the dilute case, then by Eqs. (3.12) and (3.13). The collisional transfer contributions are expressed as function of f_2 [17]:

$$\begin{aligned}\sigma_{ij}^{c} =& \frac{1+e_n}{4} m\mathrm{d}^3 \int d\mathbf{v}_1 \int d\mathbf{v}_2 \int \Theta\left(\mathbf{g}\cdot\mathbf{n}\right) \times \\ & \left(\mathbf{g}\cdot\mathbf{n}\right)^2 \mathbf{n}\ \mathbf{n}\ d\mathbf{n} \int_0^1 f_2\left[\mathbf{v}_1, \mathbf{x}-(1-\lambda)\mathrm{d}\mathbf{n}, \mathbf{v}_2, \mathbf{x}+\lambda\mathrm{d}\mathbf{n}, t\right] d\lambda\end{aligned} \tag{3.30}$$

$$\begin{aligned}\mathbf{q}^{c} =& \frac{1+e_n}{4} m\mathrm{d}^3 \int d\mathbf{v}_1 \int d\mathbf{v}_2 \int \Theta\left(\mathbf{g}\cdot\mathbf{n}\right) \times \\ & \left(\mathbf{g}\cdot\mathbf{n}\right)^2 \left(\mathbf{G}\cdot\mathbf{n}\right) \mathbf{n}\ d\mathbf{n} \int_0^1 f_2\left[\mathbf{v}_1, \mathbf{x}-(1-\lambda)\mathrm{d}\mathbf{n}, \mathbf{v}_2, \mathbf{x}+\lambda\mathrm{d}\mathbf{n}, t\right] d\lambda.\end{aligned} \tag{3.31}$$

Finally, the constitutive relation for the rate of dissipation of fluctuating energy Γ is changed into

$$\Gamma = \left(1-e_n\right)^2 \frac{\pi m \mathrm{d}^2}{16} \int d\mathbf{v}_1 \int d\mathbf{v}_2 \int \Theta\left(\mathbf{g}\cdot\mathbf{n}\right)\left(\mathbf{g}\cdot\mathbf{n}\right)^3 f_2(\mathbf{v}_1, \mathbf{x}, \mathbf{v}_2, \mathbf{x}+\mathrm{d}\mathbf{n}) d\mathbf{n} \tag{3.32}$$

being $\mathbf{G} = \left(\mathbf{V}_1 + \mathbf{V}_2\right)/2$ the velocity of the center of mass.
The Enskog equations are not closed, since the equation for a given moment depends on higher order moments. As for the dilute case, the solution of the set of hydrodynamic equations, togheter with the constitutive relations, is obtained using the Chapman-Enskog method. The procedure is exactly the same described above, which adopts the expansion of the fields in terms of their gradients, with the distribution function determined perturbatively [40]. The Chapman-Enskog solution at the first order in the spatial gradient for the Enskog equations leads to the following constitutive relations:

$$\sigma_{ij} = p\delta_{ij} - 2\eta\left(\dot{\varepsilon}_{ij} - \frac{1}{3}\delta_{ij}\nabla\cdot\mathbf{u}\right) - \gamma\left(\nabla\cdot\mathbf{u}\right)\delta_{ij}, \tag{3.33}$$

$$\mathbf{q} = -\kappa\nabla T - \mu\nabla\rho. \tag{3.34}$$

with the hydrostatic pressure computed as

$$p = \rho T\left[1 + \frac{1+e_n}{3}\pi n \mathrm{d}^3 g_0(n)\right]. \tag{3.35}$$

The hydrostatic pressure deriving from the Enskog equation differs from that deriving from the Boltzmann equation due to the presence of the radial distribution function in the two-particle distribution function. We introduce the solid volume fraction (or concentration), ν, the fractional, local volume occupied by the spheres, which is defined as $\nu = \pi n \mathrm{d}^3/6$. Then, the pressure can be rewritten as

$$p = \rho T\left[1 + 2\left(1+e_n\right)\nu g_0(\nu)\right], \tag{3.36}$$

being $\rho = \nu\rho_p$.
The expressions for the shear viscosity η, the thermal conductivity κ, the coefficient of the

density gradient μ and the additional bulk viscosity γ have been derived by Garzó and Dufty [40] using a lowest order expansion in Sonine polynomials, and are given by

$$\eta = \tilde{\eta}_{(e_n=1)}\eta^* \tag{3.37a}$$

$$\kappa = \tilde{\kappa}_{(e_n=1)}\kappa^* \tag{3.37b}$$

$$\mu = \frac{T}{\rho}\tilde{\kappa}_{(e_n=1)}\mu^* \tag{3.37c}$$

$$\gamma = \tilde{\eta}_{(e_n=1)}\gamma^* \tag{3.37d}$$

where $\tilde{\eta}_{(e_n=1)}$ and $\tilde{\kappa}_{(e_n=1)}$ are the low density values of the shear viscosity and the thermal conductivity in the elastic limit, respectively, expressed in Eq. (3.24). The collisional rate of dissipation of fluctuating energy is also determined by

$$\Gamma = \frac{144}{5\sqrt{\pi}}\frac{\rho}{d}\nu T^{3/2}\zeta^* \tag{3.38}$$

Finally, the auxiliary functions η^*, κ^*, μ^*, γ^* and ζ^* are reported in Appendix A, as function of the radial distribution function g_0. The radial distribution function depends only on the density number, or equivalently, on the volume fraction ν. Various forms of the radial distribution function have been used. Garzó and Dufty [40] adopted the Carnahan and Starling [25] approximation, which reads

$$g_0 = \frac{2-\nu}{2\left(1-\nu\right)^3}. \tag{3.39}$$

This expression was determined numerically by Carnahan and Starling for a fluid of identical hard spheres at contact.
Eqs. (3.36) and (3.37) are rewritten with the following notation

$$p = 4\rho GFT \tag{3.40}$$

$$\eta = \frac{8}{5\sqrt{\pi}}d\rho GJT^{1/2} \tag{3.41a}$$

$$\kappa = \frac{4}{\sqrt{\pi}}d\rho GMT^{1/2} \tag{3.41b}$$

$$\mu = \frac{25}{128}\sqrt{\pi}\frac{d}{\nu}NT^{3/2} \tag{3.41c}$$

$$\gamma = \frac{4}{3\sqrt{\pi}}d\rho GQT^{1/2} \tag{3.41d}$$

where

$$G = \nu g_0 \tag{3.42a}$$

$$F = \frac{1}{4G} + \frac{1+e_n}{2} \tag{3.42b}$$

$$J = \frac{25\pi\eta^*}{768\nu G} \tag{3.42c}$$

$$M = \frac{25\pi\kappa^*}{512\nu G} \tag{3.42d}$$

$$N = \mu^* \tag{3.42e}$$

$$Q = \frac{5\pi\gamma^*}{128\nu G}. \tag{3.42f}$$

3.1.5. Friction in kinetic theories

Some kinetic theories have been revised in order to take into account the role of interparticle friction. When the particles are frictional, the collisions are characterized by an impulse having a normal and a tangential component [60], and tangential forces and grains rotation are the consequence. Walton [124] proposed that impacts can be modeled in terms of three coefficients: the normal coefficient of restitution, e_n, the tangential coefficient of restitution, e_t, and the interparticle friction coefficient, μ. The normal and the tangential coefficients of restitution relate, respectively, the normal and the tangential component of the relative particle velocities before and after the collision. Considering two colliding spheres of diameters d_1 and d_2 and masses m_1 and m_2, with centers located at $\mathbf{x}_1$ and $\mathbf{x}_2$, the unit normal along the line joining the centers of the two spheres is $\mathbf{n} = (\mathbf{x}_1 - \mathbf{x}_2) / |\mathbf{x}_1 - \mathbf{x}_2|$. Before the collision, the traslational velocities of the spheres are denoted as $\mathbf{v}_1$ and $\mathbf{v}_2$, and the angular velocities as $\boldsymbol{\omega}_1$ and $\boldsymbol{\omega}_2$. The corresponding post-collision velocities are denoted by primes. The velocities before and after the collision are related by

$$\mathbf{J} = m_1 \left(\mathbf{v}_1' - \mathbf{v}_1\right) = m_2 \left(\mathbf{v}_2' - \mathbf{v}_2\right),$$
$$-\mathbf{n} \times \mathbf{J} = 2\frac{I_1}{d_1} \left(\boldsymbol{\omega}_1' - \boldsymbol{\omega}_1\right) = 2\frac{I_2}{d_2} \left(\boldsymbol{\omega}_2' - \boldsymbol{\omega}_2\right)$$

being $\mathbf{J}$ the impulse imparted on the first particle by the second, and $I_i = m_i d_i^2/10$ the moment of inertia about the center of a homogeneous sphere. In the case of frictional contacts, the relative velocity $\mathbf{g}$ of the point of contact reads

$$\mathbf{g} = (\mathbf{v}_1 - \mathbf{v}_2) - \left(\frac{d_1}{2}\boldsymbol{\omega}_1 + \frac{d_2}{2}\boldsymbol{\omega}_2\right) \times \mathbf{n}.$$

The usual normal coefficient of restitution e_n characterizes the incomplete restitution of the normal component of $\mathbf{g}$, and is defined by Eq. (3.1). In collisions that involve sliding, the tangential and normal components of the impulse are related by the interparticle friction coefficient,

$$|\mathbf{J} \times \mathbf{t}| = \mu \left(\mathbf{J} \cdot \mathbf{n}\right). \tag{3.43}$$

Finally, the tangential coefficient of restitution is defined in analogy with the normal one, using the tangential component of the relative velocities:

$$\mathbf{n} \times \mathbf{g}' = -e_t \left(\mathbf{n} \times \mathbf{g}\right). \tag{3.44}$$

In Walton's model, friction and tangential restitution are mutually exclusive properties of the contact point. The collision can be sliding or sticking depending on the angle between $\mathbf{g}$ and $\mathbf{n}$, γ, defined by:

$$\cot \gamma = \frac{\mathbf{g} \cdot \mathbf{n}}{\mathbf{g} \times \mathbf{n}}.$$

If the incident angle γ is less than a threshold value, γ_0, the point of contact is sliding and Eq. (3.43) holds; on the other hand, for greater values of the incident angle, the contact point is sticking and Eq. (3.44) replaces Eq. (3.43). The limit incident angle which distinguishes between sliding or sticking collision, γ_0, is computed as

$$(1 + e_t) = -\frac{7}{2} \left(1 + e_n\right) \mu \cot \gamma_0.$$

When the particles are frictionless (as for the Standard Kinetic Theory) the tangential component of the collisional impulse vanishes and the tangential coefficient of restitution

does not play any role. In the case of frictional particles, the coefficient of tangential restitution ranges between -1 and 1. The case $e_t = 1$ corresponds to smooth particles, that is, the tangential velocity and, thus, the angular velocities of colliding particles do not change [9]. When $e_t = -1$, the tangential component of this velocity reverses completely and the spheres are said to be perfectly rough [26].

Basically two approaches have been proposed in the literature to account for the presence of friction in the framework of kinetic theory. The first approach is the most rigorous, although the most onerous from a computational point of view. It introduces the angular momentum and the spin for each particle. Then, the standard hydrodynamic equations for translational degree of freedoms (i.e., density, velocity and granular temperature) are supplemented by the additional equations for the rotational degrees of freedom: the conservation of the angular momentum for the angular velocity field and an evolutive equation for the spin energy -through a granular spin temperature- or the spin energy must be included in the granular temperature [23]. This approach has been employed in Goldstein and Shapiro [47], Jenkins and Richman [57], Lun [80], Lun and Savage [81].

The second approach has been derived in the case of slightly frictional grains, i.e. small values of μ, and assumes that the effect of the tangential contact in collisions can be absorbed in a renormalized restitution coefficient. For small values of μ, Jenkins and Zhang [60] suggested that hydrodynamic equations for frictional grains are reduced to those for translational degree of freedoms by introducing an effective restitution coefficient,

$$e_{\text{eff}} = e_n - \frac{1}{2}a_1 + \frac{1}{2}a_2\frac{b_1}{b_2} \tag{3.45}$$

where

$$a_1 = \frac{\mu}{\mu_0}\left[\pi\mu_0\left(1 - \frac{2}{\pi}\arctan\mu_0\right) + \frac{2\mu_0^2}{1+\mu_0^2}\left(1 - \frac{2\mu}{\mu_0}\right)\right], \tag{3.46a}$$

$$a_2 = \frac{5}{2}\frac{\mu}{\mu_0}\left[\frac{\pi}{2}\mu_0\left(1 - \frac{2}{\pi}\arctan\mu_0\right) + \frac{\mu_0^2 - \mu_0^4}{\left(1+\mu_0^2\right)^2}\right], \tag{3.46b}$$

$$b_1 = \left(\frac{\mu}{\mu_0}\right)^2\frac{\mu_0^2}{1+\mu_0^2}, \tag{3.46c}$$

$$b_2 = \frac{1}{2}\frac{\mu}{\mu_0}\left[\frac{\pi}{2}\mu_0\left(1 - \frac{2}{\pi}\arctan\mu_0\right) + \frac{\mu_0^2}{1+\mu_0^2}\right], \tag{3.46d}$$

and

$$\mu_0 = \frac{7}{2}\frac{(1+e_n)}{(1+e_t)}\mu. \tag{3.47}$$

The expressions for pressure (3.40), shear viscosity, thermal conductivity, coefficient of the density gradient and the bulk viscosity (3.41) remain unchanged, and the additional dissipation of kinetic energy due to friction is taken into account by replacing e_n with e_{eff} in all the coefficients appearing in Appendix A.

3.2. Extended Kinetic Theory

In order to test the predictions of Standard Kinetic Theory, Lois et al. [76] and Mitarai and Nakanishi [87] performed numerical simulations on granular systems of inelastic disks. The

simulations performed by Lois et al. [76] concern steady, homogeneous shearing flows of frictionless disks, whereas steady flows of frictional disks down inclines have been analyzed by Mitarai and Nakanishi [87]. The numerical results show that the rate of collisional dissipation is overpredicted by the Standard Kinetic Theories. The Extended Kinetic Theory takes into account the fact that, when repeated collisions induce correlated motion among the particles, the rate at which energy is dissipated decreases by the factor L (correlation length) [11]:

$$\Gamma = \frac{144}{5\sqrt{\pi}} \frac{\rho}{L} \nu T^{3/2} \zeta^*. \tag{3.48}$$

L is the length of a chain of contacting (if soft) or chattering (if rigid) particles, employed in place of the diameter of the spheres. The idea is that enduring contacts (or reapeted collisions) between the grains reduce the collisional dissipation between them, while still permitting the transfer of momentum and energy. Consequently, the rate of dissipation is modified, but the stresses are not.
Jenkins [53] assumes that the spheres are forced into contact along the principal compressive axis of the shearing flow and that the random motion of the spheres acts to destroy this order. Then the magnitude and direction of the vector $\mathbf{L}$ of chain length is determined by the simple balance

$$2L^* \dot{\varepsilon}_{ij} L_j + \frac{LT^{1/2}}{d^2} L_i = 0, \tag{3.49}$$

where L^* is a function of the concentration and the particle properties. When L is equal to one diameter, the molecular chaos assumption is valid and the Extended Kinetic Theory reduces to the Standard Kinetic Theory.
Different expressions of L^* have been proposed, on the basis of experimental and numerical results on inclined granular flows and shearing flows. The first form proposed for L^* was

$$L^* = \frac{1}{2} c G^{\alpha}, \tag{3.50}$$

where $G = \nu g_0$, being g_0 the radial distribution function, and c a constant of order one. The power of G, α, has been chosen equal to $1/2$ by Jenkins [52, 53] to provide a good agreement with the results of numerical simulations. Subsequently Jenkins and Berzi [54] proposed to use $\alpha = 1/3$ obtaining a relatively good fit with the physical experiments of Pouliquen [102] on the steady and fully developed flows of glass spheres on inclined planes. The presence of an additional material parameter, c, whose physical meaning is not well defined, represents a weakness of the theory.
Recently, Berzi [11] has suggested an expression for L^* on the basis of previous results of numerical simulations of simple shear flows performed by Mitarai and Nakanishi [88]:

$$L^* = \left(\frac{JG}{18\nu\zeta^*} \right)^{1/2} \left[\frac{2\,(1-e)}{15} \left(g_0 - g_{0,\mathrm{f}} \right) + 1 \right]^{3/2}, \tag{3.51}$$

where $g_{0,\mathrm{f}}$ is the value of g_0 at the freezing point, $\nu = 0.49$, i.e., the lowest value of the volume fraction for which a transition to an ordered state is first possible [118]. This expression has been derived in the case of steady, shearing flows, and has to be proven to be valid also in other flow conditions.
Finally, it is important to notice that the Extended Kinetic Theory is a phenomenological extension of kinetic theory, which aims at incorporating the role of pre-collisional velocity correlations when the molecular chaos assumption is violated. As a matter of fact, this improvement is not based in any kinetic description.

4. Constitutive approach*

The main goal of this thesis is to develop a general, physically sounded rheological model for granular flows, in the framework of continuum mechanics. The theory aims to reproduce the mechanical behavior of granular flows in the different flow regimes and, in particular, to deal with the phase transition from a solid-like to a fluid-like state and vice versa. The constitutive model is based on the main assumption that the energy of the system is dissipated thorugh two mechanisms of interaction between particles: the enduring contacts among grains, which are involved in force chains, and the inelastic, nearly instantaneous collisions. In Section 4.1, the "hydrodynamic" balance equations of the continuum mechanics are introduced for the case of "discontinuum" granular materials. In Section 4.2, the constitutive approach, based on the distinction between enduring contacts between grains and nearly instantaneous collisions, is generally derived. Finally, in Section 4.3 the steady state condition of a granular material under plane shear conditions is analyzed.

4.1. A peculiar continuum medium

Despite the fact that granular material is a discontinuous medium, its behavior is commonly described by the continuum approach. A continuum mechanical model is mainly composed of two parts. The first component includes the field equations, which are generally derived from the conservation laws of mass, momentum and energy. These are applied to a finite arbitrary volume, called a control volume. This control volume is fixed in time and space with flow allowed to occur across the boundaries. Then, the macroscopic description of the system consists of a set of time-evolution equations for the "hydrodynamic fields" of the continuum, which usually are the density, the velocity and the temperature related to the energy. The set of partial differential equations has to be supplemented by "constitutive equations" providing a closed description in terms of the fields alone. The second component of a continuum mechanics model contains the constitutive equations, which describe the material characteristics.
For a generic continuum medium, the mass balance reads:

$$\frac{D\rho}{Dt} + \rho\nabla \cdot \mathbf{u} = 0, \tag{4.1}$$

where ρ is the density of the material and $\mathbf{u}$ the local velocity. Here and in what follows, D/Dt denotes the material derivative and is defined as $D/Dt = \partial/\partial t + \mathbf{u} \cdot \nabla$, where $\partial/\partial t$ is the local time derivative.
The momentum balance equation, in absence of external forces, is given by:

$$\rho\frac{D\mathbf{u}}{Dt} = -\nabla \cdot \boldsymbol{\sigma}. \tag{4.2}$$

In continuum mechanics, the stress tensor, $\boldsymbol{\sigma}$, represents the manner in which force is internally trasmitted. Each component of the stress tensor, σ_{ij}, represents the force in the

*mainly based on D. Berzi, C. di Prisco, and D. Vescovi. Constitutive relations for steady, dense granular flows. *Physical Review E*, 84:031301, 2011

i-direction on a surface with inward pointing normal unit vector in the j direction.
Considering $\mathcal{E}$ to be the internal specific energy of the system (energy per unit mass), the energy balance can be written as

$$\rho \frac{D\mathcal{E}}{Dt} = -\nabla \cdot (\mathbf{u} \cdot \boldsymbol{\sigma}) - \nabla \cdot \mathbf{q} - \Gamma \tag{4.3}$$

That is, the convected time rate of change of internal energy, $\rho D\mathcal{E}/Dt$, is equal to the rate that surface stresses do work on the system, $-\nabla \cdot (\mathbf{u} \cdot \boldsymbol{\sigma})$ [109], less the sum of the diffused energy, which is given by the divergence of the flux of energy, $\mathbf{q}$, and the rate of dissipation Γ. Equations (4.1)-(4.3) contain several unknonws, $\mathbf{u}$, $\boldsymbol{\sigma}$, ν, $\mathcal{E}$, $\mathbf{q}$ and Γ, while only five equations are available. Then, this set of partial differential equations has to be supplemented by the constitutive relations for the stress tensor $\boldsymbol{\sigma}$, the energy flux $\mathbf{q}$ and the rate of dissipation Γ.

As previously stated, granular materials are not actually continuum media but are composed of many discrete particles. An hydrodynamic description of this medium has to incorporate the micro-mechanical properties of the single grain and an averaging process over the number of particles which composes the material. Then, a definition of the macroscopic variables appearing into Eqs. (4.1)-(4.3), ρ, $\mathbf{u}$ and $\mathcal{E}$, has to be provided. However, in contrast to conventional hydrodynamics, the applicability of granular hydrodynamics is often questionable given that, typically, there is no separation of scale between microscopic and macroscopic motion [2].
At the microscopic level, each particle is characterized by its shape, dimension, material properties and so on. For the sake of simplicity, in this thesis an assembly of identical spheres, of diameter d and density ρ_p is considered. The density of the continuum medium can be computed as the product as the particle density and the solid concentration (or volume fraction), ν, defined as the fractional, local volume occupied by the spheres:

$$\rho = \rho_p \nu. \tag{4.4}$$

Each grain moves with its proper velocity $\mathbf{v}$, and the macroscopic flow velocity of the grain system can be defined as the average over the single particle velocity:

$$\mathbf{u} = \langle \mathbf{v} \rangle . \tag{4.5}$$

Here, $\langle\ \rangle$ represents average over the microscopic scales.
The difference between the velocity of a particle and the macroscopic velocity is the fluctuating velocity:

$$\mathbf{V} = \mathbf{v} - \mathbf{u}. \tag{4.6}$$

The internal energy $\mathcal{E}$ can be defined as the sum of two contributions [63, 64]:

$$\mathcal{E} = \mathcal{E}_\mathrm{h} + \mathcal{E}_\mathrm{k}. \tag{4.7}$$

where $\mathcal{E}_h$ is the specific true thermal energy of the material and $\mathcal{E}_\mathrm{k}$ is the kinetic specific energy. The specific thermal energy $\mathcal{E}_\mathrm{h}$ is given by $k_B T_\mathrm{h}/m$, where k_B is the Boltzmann's constant, m the grain mass and T_h the true thermal temperature. For a grain of 1 mm diameter moving with a typical velocity of 1 cm/s at room temperature, $\mathcal{E}_\mathrm{h}$ is at least ten orderds of magnitude less than the specific kinetic energy [2, 50], so that $\mathcal{E} \cong \mathcal{E}_\mathrm{k}$.
As suggested by Savage [109], the specific kinetic energy of the particles can be expressed as

$$\mathcal{E}_\mathrm{k} = \frac{1}{2} \langle \mathbf{v} \cdot \mathbf{v} \rangle , \tag{4.8}$$

and then subdivided into two parts

$$\mathcal{E}_{\mathrm{k}} = \mathcal{E}_{\mathrm{k,m}} + \mathcal{E}_{\mathrm{k,f}} \tag{4.9}$$

where

$$\mathcal{E}_{\mathrm{k,m}} = \frac{1}{2}\left|\mathbf{u}\right|^2 \tag{4.10}$$

is the mean kinetic energy associated with the local mean velocity $\mathbf{u}$, and

$$\mathcal{E}_{\mathrm{k,f}} = \frac{1}{2}\left\langle\left|\mathbf{V}\right|^2\right\rangle \tag{4.11}$$

is the "pseudo-thermal" energy associated with deviations of the motion of individual particles from the mean flow, here called fluctuating kinetic energy.
Then, the energy equation (4.3) becomes

$$\rho\frac{D}{Dt}\left(\mathcal{E}_{\mathrm{k,m}} + \mathcal{E}_{\mathrm{k,f}}\right) = -\nabla\cdot\left(\mathbf{u}\cdot\boldsymbol{\sigma}\right) - \nabla\cdot\mathbf{q} - \Gamma. \tag{4.12}$$

Taking the vector product of $\mathbf{u}$ and the momentum equation (4.2) yields

$$\rho\frac{D\mathcal{E}_{\mathrm{k,m}}}{Dt} = -\mathbf{u}\cdot\nabla\cdot\boldsymbol{\sigma}.$$

Then, Eq. (4.12) reduces to

$$\rho\frac{D\mathcal{E}_{\mathrm{k,f}}}{Dt} = -\boldsymbol{\sigma} : \nabla\mathbf{u} - \nabla\cdot\mathbf{q} - \Gamma. \tag{4.13}$$

Finally, assuming the stress tensor to be symmetric, $\sigma_{ij} = \sigma_{ji}$, $\nabla\mathbf{u}$ can be replaced by its symmetric part, and Eq. (4.13) can be expressed as

$$\rho\frac{D\mathcal{E}_{\mathrm{k,f}}}{Dt} = -\boldsymbol{\sigma} : \dot{\boldsymbol{\varepsilon}} - \nabla\cdot\mathbf{q} - \Gamma, \tag{4.14}$$

which represents the balance of the fluctuating kinetic energy. The strain rate tensor, $\dot{\boldsymbol{\varepsilon}}$, is classically defined as the symmetric part of the the gradient of the velocity

$$\dot{\boldsymbol{\varepsilon}} = \frac{1}{2}\left(\nabla\mathbf{u} + \nabla^t\mathbf{u}\right). \tag{4.15}$$

Note that, for a continuum medium, the symmetry of the stress tensor is ensured by the conservation of angular momentum of the macroscopic flow field. In granular materials, macroscopic sources of rotation, which lead to additional rotational degrees of freedom, are caused by the microscopic dissipation of energy. Models based on higher order gradients of the strain tensor and micropolar Cosserat medium, in which the stress tensor is not symmetric, have been recently developed [8, 89, 90, 121].

4.2. Constitutive relations

At the micro-scale level, the two possible dissipative mechanisms of interaction among soft grains are enduring contacts among grains involved in force chains, and inelastic, nearly instantaneous collisions. When the latter mechanism prevails, which is when the density of the medium is low to moderate, the stress tensor shows a strain rate-dependent behavior. Whereas, when the force chains developed along the system span the entire domain, the stress tensor becomes strain rate-independent. This latter condition can occur only if the

material is dense enough, and is defined as quasi-static condition. The model proposed in this thesis is based on the assumption that, in granular flows, the energy of the system is dissipated throughout the two mechanisms said above: enduring contacts among particles involved in force chains (quasi-static contribution) and collisions (collisional contribution). Then, the material behaves like a solid when the first mechanism prevails. On the contrary, when the energy is totally dissipated by collisions, the deformations of the system are rapid and the material flows like a granular gas.

Figure 4.1.: Mechanisms of interaction between particles: enduring contacts among grains, which are involved in force chains (a), and inelastic collisions (b).

The existence of force chains is related to the friction of the particles and to the concentration. In absence of interparticle friction (frictionless particles), force chains are inhibited, and the quasi-static contribution vanishes. Also, in the case of frictional particles, if the concentration is lower than a critical threshold, the grains can interact only through collisions. Considering the two dissipation mechanisms, we assume that the rate of energy dissipation Γ in Eq. (4.3) is given by the sum of two terms:

$$\Gamma = \Gamma_{\mathrm{qs}} + \Gamma_{\mathrm{col}} \tag{4.16}$$

where Γ_{qs} is the rate at which energy is dissipated by enduring contacts, and Γ_{col}, the energy dissipated by collisions. Here and in what follows, the subscripts "qs" (quasi-static) and "col" (collisional) refer to quantities associated with enduring, frictional contacts of particles involved in force chains (soil skeleton) and nearly instantaneous collisions, respectively.
We assume to subdivide also the the energy flux and the granular stress tensor into the sum of two terms:

$$\mathbf{q} = \mathbf{q}_{\mathrm{qs}} + \mathbf{q}_{\mathrm{col}}, \tag{4.17}$$

$$\boldsymbol{\sigma} = \boldsymbol{\sigma}_{\mathrm{qs}} + \boldsymbol{\sigma}_{\mathrm{col}}. \tag{4.18}$$

We suppose that

$$0 = -\boldsymbol{\sigma}_{\mathrm{qs}} : \dot{\boldsymbol{\varepsilon}} - \nabla \cdot \mathbf{q}_{\mathrm{qs}} - \Gamma_{\mathrm{qs}}, \tag{4.19}$$

so that enduring contacts among particles in force chains do not contribute to the transport of kinetic fluctuating energy. Then, the balance of kinetic fluctuating energy (4.14) reduces to

$$\rho \frac{D\mathcal{E}_{\mathrm{k},f}}{Dt} = -\boldsymbol{\sigma}_{\mathrm{col}} : \dot{\boldsymbol{\varepsilon}} - \nabla \cdot \mathbf{q}_{\mathrm{col}} - \Gamma_{\mathrm{col}}. \tag{4.20}$$

As a consequence of this last assumption, the quasi-static energy flux and rate of energy dissipation do not appear into the conservation equations, and are not required to be defined in order to solve the problem.

4.2.1. Collisional contribution

The constitutive relations for the collisional stress tensor, energy flux and rate of energy dissipation are taken from the kinetic theory of granular gases. The kinetic fluctuating energy can be expressed in terms of the granular temperature T, using Eq. (3.7) into Eq. (4.11),

$$\mathcal{E}_{\mathrm{k,f}} = \frac{3}{2}T \tag{4.21}$$

so that Eq. (4.20) becomes

$$\frac{3}{2}\rho\frac{DT}{Dt} = -\boldsymbol{\sigma}_{\mathrm{col}} : \dot{\boldsymbol{\varepsilon}} - \nabla \cdot \mathbf{q}_{\mathrm{col}} - \Gamma_{\mathrm{col}}. \tag{4.22}$$

This equation describes the evolution of the granular temperature and has the same shape and meaning of the balance of fluctuating energy derived by kinetic theory and given by Eq. (3.10).

The kinetic theory proposed by Garzó and Dufty [40] for the collisional stress tensor and energy flux is adopted. Then, $\boldsymbol{\sigma}_{\mathrm{col}}$ and $\mathbf{q}_{\mathrm{col}}$ are entirely defined by Eqs. (3.33)-(3.34). For the collisional rate of energy dissipation, Γ_{col}, we use Eq. (3.48) as proposed by Jenkins [52, 53] in the Extended Kinetic Theory. There, as already mentioned, L is the correlation length whose form is given by Eq. (3.49).
In order to take into account the role played by the friction during collisions, the approach suggested by Jenkins and Zhang [60] is here followed. The additional dissipation of kinetic energy due to friction is incorporate by replacing the coefficient of normal restitution appearing in the constitutive relations, with an effective coefficient of restitution, e_{eff}, that depends on the normal coefficient of restitution e_n, the tangential coefficient of restitution in a sticking collision, e_t, and the Coulomb friction coefficient, μ, characterizing sliding collisions. The expression of the effective coefficient of restitution is given by Eq. (3.45). From this point onward, the symbol e is used to denote the effective coefficient of restitution.
The resulting kinetic theory here considered differes from the standard one described in Section 3.1. Indeed, assumptions of dilute systems (VII), frictionless particless (III), and molecular chaos (VIII) are overcome: the kinetic theory of Garzó and Dufty [40] was derived from the Enskog equation, then is even valid for moderate dense systems; the introduction of an effective coefficient of restitution makes the theory applicable to frictional grains; the Extended Kinetic Theory, throughout the correlation length L, accounts for the correlated motion of particles.

In this work, two further modifications to the kinetic theory are added.

1. A function f_r, which takes into account the influence of the particle stiffness on the contact duration during collisions, is introduced, allowing to overcome the assumption of rigid particles (V). The functional f_r has been suggested by Hwang and Hutter [49] and reads

$$f_r = \left[1 + 2\frac{d}{s}\left(\frac{\rho_p T}{E}\right)^{1/2}\right]^{-1}. \tag{4.23}$$

There, E is the Young's modulus of the particles and s is the mean separation distance among particles. At equilibrium, the latter can be identified as the mean free path (mean distance traveled by a particle between two successive collisions). In the context of classic kinetic theories [26],

$$s = \frac{\sqrt{2}}{12}\frac{d}{G}, \tag{4.24}$$

being $G = \nu g_0$ and g_0 the radial distribution function. The constitutive relations of $\boldsymbol{\sigma}_{\text{col}}$, $\mathbf{q}_{\text{col}}$ and Γ_{col} are all multiplied by f_r. When the particles are very rigid, i.e., when E is large enough, f_r tends to 1 and the particle stiffness does not affect the collisional contribution.

2. A different radial distribution function is proposed on the basis of recent numerical results on plane shear flows of frictionless particles [27, 28, 88, 123].
As stated before, for frictionless particles, momentum is exchanged only through collisions [122], and the constitutive model reduces to the collisional contribution. From the constitutive relation for the (collisional) pressure provided by the kinetic theory, (3.40), and the expressions of G and F, Eqs. (3.42a) and (3.42b),

$$g_0 = \frac{1}{2\nu(1+e_n)}\left(\frac{p}{\nu\rho_p T} - 1\right), \tag{4.25}$$

so that the radial distribution function can be obtained from the numerical (measured) values of pressure, concentration and granular temperature. For small concentrations, g_0 obeys the Carnahan and Starling's expression [25],

$$g_{0,\text{cs}} = \frac{2-\nu}{2\,(1-\nu)^3}, \tag{4.26}$$

whereas Torquato's [118] proposed, on the basis of numerical results on elastic particles,

$$g_{0,\text{t}} = \begin{cases} g_{0,\text{cs}} & \text{if } \nu < 0.49, \\ \dfrac{(2-0.49)}{2\,(1-0.49)^3}\dfrac{(\nu_\text{s}-0.49)}{(\nu_\text{s}-\nu)} & \text{otherwise.} \end{cases} \tag{4.27}$$

Here, ν_s represents the densest possible disordered configuration of identical spheres, and depends on the flow configuration and the particles properties. ν_s coincides with the random close packing concentration, $\nu_\text{rcp} = 0.636$, defined as the densest possible disordered packing of identical spheres [117], (i) in static condition and (ii) in the case of frictionless particles. In dynamic conditions, ν_s is expected to be different from ν_rcp if the particles are frictional, and to depend on the interparticle friction.
Fig. 4.2 shows the radial distribution function obtained from the numerical simulations of Mitarai and Nakanishi [88] and Chialvo and Sundaresan [27] on homogeneous plane shear flows and the present SS-DEM simulations of inhomogeneous plane shear flows (described in Chapter 6), using different values of the (normal) coefficient of restitution. Eq. (4.27) fits well the numerical results in the case of nearly elastic particles (Fig. 4.2(a)), while underestimates the data for dense flows of particles when $e \leq 0.95$ (Fig. 4.2(b)). In the latter case, as in Vescovi et al. [123], we propose to use the following expression of g_0:

$$g_0 = f g_{0,\text{cs}} + (1-f)\,\frac{2}{(\nu_\text{s}-\nu)}, \tag{4.28}$$

where f is a function of the concentration which makes g_0 equal to the Carnahan and Starling's expression when the concentration is less than a limit value, ν_m:

$$f = \begin{cases} 1 & \text{if } \nu < \nu_\mathrm{m} \\ \dfrac{\nu^2 - 2\nu_\mathrm{m}\nu + \nu_\mathrm{s}\left(2\nu_\mathrm{m} - \nu_\mathrm{s}\right)}{2\nu_\mathrm{s}\nu_\mathrm{m} - \nu_\mathrm{m}^2 - \nu_\mathrm{s}^2} & \text{otherwise} \end{cases} \tag{4.29}$$

The quadratic expression for f when $\nu \geq \nu_\mathrm{m}$ ensures that the first derivative of g_0 is continuous. The radial distribution function depends on two parameters: ν_s and ν_m. In the framework of this thesis, ν_m has been estimated only for steady, shear flows of inelastic spheres, and is equal to 0.4, whereas, as mentioned before, ν_s is affected by the interparticle friction coefficient μ (see discussion in Section 4.3.1).

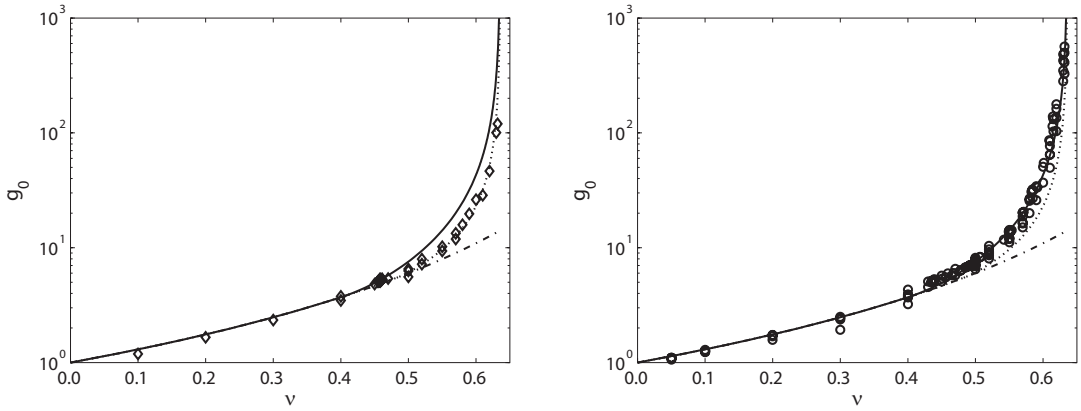

(a) (b)

Figure 4.2.: Numerical (symbols) radial distribution function (after Mitarai and Nakanishi [88], Chialvo and Sundaresan [27] and present SS-DEM simulations) as a function of the concentration for: (a) $e = 0.98$ and 0.99; (b) $0.5 \leq e \leq 0.95$. Also shown are Eq. (4.28) (solid line) and the expressions of Carnahan and Starling (Eq. 4.26, dot-dashed line) and Torquato (Eq. 4.27, dotted line).

Finally, the form of the coefficient L^*, appearing in the correlation length L (3.49), is slightly modified with respect to that proposed by Berzi [11] and expressed by Eq. (3.51). Here, L^* is taken to diverge always at ν_rcp, independently of the interparticle friction coefficient. Then, Eq. (3.51) is replaced by

$$L^* = \left(\frac{JG}{18\nu\zeta^*}\right)^{1/2} \left[\frac{2\left(1-e\right)}{15}\left(\tilde{g}_0 - \tilde{g}_{0,\mathrm{f}}\right) + 1\right]^{3/2}, \tag{4.30}$$

where

$$\tilde{g}_0 = \tilde{f} g_{0,\mathrm{cs}} + \left(1 - \tilde{f}\right) \frac{2}{\left(\nu_\mathrm{rcp} - \nu\right)}, \tag{4.31}$$

and

$$\tilde{f} = \begin{cases} 1 & \text{if } \nu < \nu_\mathrm{m} \\ \dfrac{\nu^2 - 2\nu_\mathrm{m}\nu + \nu_\mathrm{rcp}\left(2\nu_\mathrm{m} - \nu_\mathrm{rcp}\right)}{2\nu_\mathrm{rcp}\nu_\mathrm{m} - \nu_\mathrm{m}^2 - \nu_\mathrm{rcp}^2} & \text{otherwise} \end{cases} \tag{4.32}$$

with $\tilde{g}_{0,\mathrm{f}} = \tilde{g}_0(0.49)$, the value of $\tilde{g}_0$ at the freezing point ($\nu_\mathrm{f} = 0.49$).
The new forms of the radial distribution function and of L^* have been recently derived

[123] on the basis of numerical results on plane shear flows of frictionless spheres. We will show in Section 5.3 that these two modifications to the kinetic theory allow to notably improve the theoretical predictions of the numerical data in the collisional regime.

4.2.2. Quasi-static contribution

The quasi-static component of the stress tensor is modeled by using the "critical state" theory introduced in soil mechanics fifty years ago and still largely adopted [10, 39, 93, 110]. Since the pioneering works of Roscoe et al. [106] and Schofield and Wroth [110], the critical state concept has been introduced as a certain attractor state, independent on the initial arrangement, characterized by the capability of a granular material of developing unlimited shear strains without any change in the concentration [16]. At the critical state, an ideal mechanism of yielding is assumed to develop within the specimen: the external work is totally dissipated by frictional processes at the contact level (disregarding both crushing and damage); the micro-structure does not evolve and, consequently, the concentration, remains constant.

In geomechanics, the deformation of a continuous body is commonly defined by the strain, which describes a deformation in terms of relative displacement of a material point $\mathbf{x}$ (which is not necessary a grain). Considering a point, $\mathbf{x}$, in an undeformed continuum medium, if the body is deformed, the point $\mathbf{x}$ will be moved to $\mathbf{x}'$, where

$$\mathbf{x}' = \mathbf{x} + \mathbf{s}.$$

Here, $\mathbf{s}$ is the displacement of the point, with the component s_i describing the displacements in the x_i direction over time, i.e. $x_i' = x_i + s_i(x_i, t)$. The strain tensor is defined as

$$\boldsymbol{\varepsilon} = \frac{1}{2}\left(\nabla\mathbf{s} + \nabla^t\mathbf{s}\right). \tag{4.33}$$

The strain rate tensor describes the rate of change of the strain of the continuum medium:

$$\dot{\boldsymbol{\varepsilon}} = \frac{\partial\boldsymbol{\varepsilon}}{\partial t}.$$

Here and in what follows, the dot represents a time derivative. Being the local velocity $\mathbf{u}$ the time derivative of the local displacement, $\dot{\mathbf{s}} = \mathbf{u}$, the strain rate tensor takes the usual form of the symmetric component of the gradient of the velocity, as given by Eq. (4.15).
In the context of soil mechanics, the strain is finite and the strain rate is zero (and the granular temperature is ignored). On the other hand, in the context of granular flows, the strain is infinite and the strain rate is finite, different from zero (as is the granular temperature). The critical state represents the boundary between them, and can be interpreted as a limit condition for the steady state, for which the strain is infinite and both the strain rate and the granular temperature vanish.

Soil mechanics studies the behaviour of soils (i.e., granular materials) in quasi-static conditions, i.e., when the deformations are extremely slow and the assumption of small strains applies. In this framework, geomechanics approaches focus mainly on the initiation of the deformation of soils under loading and on the coupling between strain, stress, concentration, and possibly other microstructural properties. Usually, such models do not predict what happens when continuous quasi-static flow is imposed on the material [38].
In order to study and predict the movements and failure of a soil mass, the relationships between stresses and strains up to and beyond failure have to be defined. The soil response

is often described with elasto-plastic or elasto-viscoplastic constitutive models, where soils are assumed to undergo both elastic and plastic deformation when subject to loading. In standard elasto-plastic models, the constitutive relations relate the stress rate tensor, $\dot{\boldsymbol{\sigma}}$, to the strain rate tensor (incremental relationships). Then, the stress rate tensor, which represents the increment of $\boldsymbol{\sigma}$ in the time (i.e., loading), is computed as

$$\dot{\boldsymbol{\sigma}} = \mathbf{E} : \dot{\boldsymbol{\varepsilon}},$$

where $\mathbf{E}$ is the fourth order stiffness tensor. The total strain rate tensor is assumed to be the sum of an elastic and a plastic part

$$\dot{\boldsymbol{\varepsilon}} = \dot{\boldsymbol{\varepsilon}}^{\mathrm{el}} + \dot{\boldsymbol{\varepsilon}}^{\mathrm{pl}},$$

where the superscripts "el" and "pl" stand for elastic and plastic, respectively. The threshold which divides elastic and plastic behaviors is the curve in the stress space known as yield locus $\mathcal{F}$, or yield surface [92]. When the stress state of an element of soil lies within the yield locus, it is considered to be elastic and, then, to undergo recoverable and reversible deformations. On the other hand, if the stress state lies on the yield surface and remains on it during the stress increment, plastic (irreversible) strains occur. The elastic response is related to the stress rate tensor by

$$\dot{\boldsymbol{\sigma}} = \mathbf{E}^{\mathrm{el}} : \dot{\boldsymbol{\varepsilon}}^{\mathrm{el}}$$

being $\mathbf{E}^{\mathrm{el}}$ the fourth order tensor containing the tangential elastic stiffness moduli. This linear relationship ensures that the elastic strain rate automatically vanishes in steady conditions, i.e., at constant stress. The plastic strain rate is defined through the flow rule:

$$\dot{\boldsymbol{\varepsilon}}^{\mathrm{pl}} = \dot{\lambda}\mathbf{m},$$

where $\dot{\lambda}$ is the plastic multiplier which determines the magnitude of $\dot{\boldsymbol{\varepsilon}}^{\mathrm{pl}}$, while $\mathbf{m}$ specifies the plastic flow direction. Usually, the second order tensor $\mathbf{m}$ is derived as the stress gradient of the plastic potential function $\mathcal{G}$:

$$\mathbf{m} = \frac{\partial \mathcal{G}}{\partial \boldsymbol{\sigma}}.$$

The flow rule is said associated if the plastic potential coincides with the yield surface, $\mathcal{G} = \mathcal{F}$, and, consequently, the plastic strain rates are directed perpendicular to the yield surface. The elasto-plastic theory is completed with the consistency law, from which the plastic multiplier is determined. The consistency law forces the stress states to remain on the yield surface $\mathcal{F}$ during plastic deformations, and is expressed as $\dot{\mathcal{F}} = 0$. As a consequence, according to elasto-plastic model, the stress state can never overstep the yield locus.

Elasto-plasticity is based on two main assumptions: (i) unrecoverable deformations take place instantaneously and (ii) no role is played by the rate of external loading. Although elasto-plasticity has been proven to be a powerful tool for capturing most features of the inelastic response of soils, the assumption of rate-independence prevents some important experimental evidences to be reproduced, as well as any dependence of the material behavior on the loading rate. To overcome this intrinsic limitations of standard elasto-plasticity, the theory of elasto-viscoplasticity was purposely introduced.

In the context of the elasto-viscoplasticity, a finite amount of time is required for irreversible (viscoplastic) strains to develop. As a result, the time variable actively contributes

to the global material response, which is in turn determined by the interaction between the intrinsic material rate-sensitiveness and the external loading rate. The total strain rate is decomposed into an elastic component $\dot{\boldsymbol{\varepsilon}}^{\mathrm{el}}$ and a viscoplastic component $\dot{\boldsymbol{\varepsilon}}^{\mathrm{vp}}$,

$$\dot{\boldsymbol{\varepsilon}} = \dot{\boldsymbol{\varepsilon}}^{\mathrm{el}} + \dot{\boldsymbol{\varepsilon}}^{\mathrm{vp}}.$$

The viscoplastic strain rate evolves via a flow rule different from that of elasto-plasticity,

$$\dot{\boldsymbol{\varepsilon}}^{\mathrm{vp}} = \tilde{\gamma}\Phi(\mathcal{F})\frac{\partial \mathcal{G}}{\partial \boldsymbol{\sigma}}. \tag{4.34}$$

There, $\tilde{\gamma}$ is the fluidity parameter and $\Phi(\mathcal{F})$ is the viscous nucleus, function of the yield surface $\mathcal{F}$ [98]. This flow rule ensures that viscoplastic strains can happen also in absence of stress increments (i.e., without loading), and the viscous nucleus describes the time dependence of the material mechanical response. Finally, in the elasto-viscoplastic model, the stress state is allowed to lie outside the yield surface when viscoplastic strains develop (the consistency law does not apply).

Usually, the yield locus is assumed to be described by the Mohr-Coulomb criterion, which, for three-dimensional stress states, reads

$$\mathcal{F} = \frac{1}{2}(\sigma_3 - \sigma_1) + \frac{1}{2}(\sigma_3 + \sigma_1)\sin\phi. \tag{4.35}$$

There, ϕ is the internal friction angle and σ_1 and σ_3 are the major and minor principal stresses, respectively*. The yield condition $\mathcal{F} = 0$ describes an angular yield surface in the principal stress space. The Mohr-Coulomb criterion assumes that the "failure" of the material (said the initiation of the motion) occurs in the form of plastic sliding on rupture plains within the granular material element, when $\mathcal{F} = 0$. On the rupture plain, the Mohr-Coulomb criterion can be rewritten in terms of normal stress, σ, and shear stress, τ:

$$\mathcal{F} = \tau - \sigma\tan\phi, \tag{4.36}$$

where σ and τ are related to the principal stresses: $\sigma = (\sigma_1 + \sigma_3)/2$, $\tau = (\sigma_1 - \sigma_3)/2$. Then, the Mohr-Coulomb criterion asserts than, on the sliding planes, the shear component of the stress equals the frictional resistance of the material.

When a soil element reaches the limit condition in which it continues to (plastically) deform indefinitely without further change in stresses and volume, it is said to have reached the critical state [110]. Then, the critical state "locus" is defined as a non-evolving state reached after a progressive increase in strain, at a vanishingly small strain rate, and does not depend on the initial arrangement of the granular material. A granular material reaches the critical state when two conditions are simultaneously fulfilled:

- the stress state lies on the yield surface ($\mathcal{F} = 0$);
- in the "compression" plane [92], defined by the volumetric variable void ratio e_v (the ratio of the volume of voids to the volume of solid particles, related to the

*The (three) principal stresses are defined as the normal stresses which act on the principal planes. The principal planes are the three orthogonal planes in which there are zero shear stresses (i.e., the stress tensor is a diagonal matrix and the elements on the diagonal are the principal stresses). The principal stresses of the stress tensor are the eigenvalues of the stress tensor, and their direction vectors are the principal directions or eigenvectors.

concentration by the relation $\nu = 1/(1 + e_v)$) and the pressure $p = \mathrm{tr}\boldsymbol{\sigma}/3$, the following relation occurs

$$e_v = \Gamma - \lambda \log p. \tag{4.37}$$

The constants Γ and λ are intrinsic material properties, and are not affected by the stress state and the loading history.

Note that, in principle, the critical state is not necessary associated to a Mohr-Coulomb criterion.
A fundamental characteristic of the behavior of granular materials is the dilatancy. The dilatancy is defined as the change in volume associated with distorsion of granular materials. In principle, deformations in granular materials are always accompanied by volumetric changes, and when granular material is stressed, a shear motion occurs between neighboring grains, which generates a bulk expansion, i.e., dilatation [125]. The volumetric response of a granular material under loading is different depending on the initial state of the sample: dense samples dilate, whereas loose samples contract. This feature of granular materials has been revealed using both triaxial tests and shearing tests. At the critical state, the dilatancy vanishes, given that the material undergoes deformations without volume changes. Considering a conventional experiment of triaxial compression (but the same effect is obtained in shear tests) on a sample of sand, loose samples contract, as previously stated, and the critical state is reached when the volume change is gradually ceased, whereas dense samples expand and approach the critical state after strain softening has occured [92]. The stress-strain curve for dense and loose sands merge together at the critical state.
Independently of the mechanism which leads the granular material to the critical state (triaxial compression, shear tests, etc.), soils fall in a purely frictional manner at the critical state [92] if the Mohr-Coulomb criterion is adopted. Consequently, the critical state line represents the Mohr-Coulomb failure envelope in the stress space.

A constitutive model adopting the critical state theory and employing the Mohr-Coulomb yield surface, has to satisfy the Mohr-Coulomb criterion on the shear stress-normal stress plane when the granular material is in the condition of developing unlimited strains without any change in the concentration. Here, the critical state is considered as a non-evolving state reached after a progressive increase in strain, at negligible strain rates. Also, it is interpreted as a limit condition for the steady state at vanishingly small strain rate, by employing the granular temperature, as an additional state variable for the system [122].
This work focuses on the behavior of granular materials under steady conditions. In this case, the quasi-static component of the stress tensor can be easily defined by the definition of critical state and Mohr-Coulomb criterion, without further assumptions on the form of the stresses. It is important to notice that the interpretation of the constitutive approach in the light of standard viscoplasticity can be seen as a first step towards an evolving constitutive model capable of describing the mechanical behavior of granular material under both solid-like and fluid-like conditions.

4.3. Steady, plane shear flows of granular materials

A collection of identical spheres, of diameter d and density ρ_p, sheared under steady conditions, is considered. Here and in the following, x and y are taken to be the flow and the shearing directions, respectively, and variations along the transversal direction z are

ignored. Fig. 4.3 shows a sketch of the flow configuration.

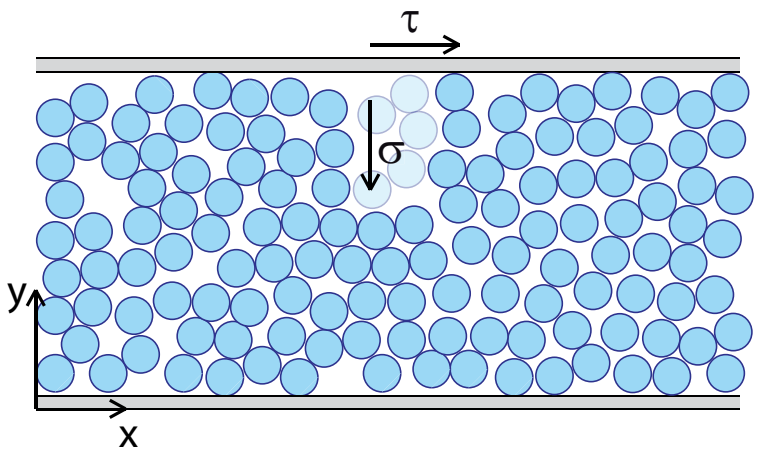

Figure 4.3.: Plane shear flow configuration of a collection of identical spheres.

In this simple configuration, the flow is assumed to be one-dimensional, such that only the horizontal velocity component u is nonzero, $\mathbf{u} = (u, 0)$, and the flow variables vary only in the y-direction ($\partial X/\partial x = 0$, for each variable X).
At the steady state, the mass balance equation, (4.1), is automatically satisfied, and the divergence of the velocity is zero, $\nabla \cdot \mathbf{u} = 0$. The momentum balance equation, in absence of external forces, (4.2), reduces to

$$\frac{\partial \tau}{\partial y} = 0, \tag{4.38a}$$

$$\frac{\partial \sigma}{\partial y} = 0, \tag{4.38b}$$

respectively in the x and y-direction. Here, τ and σ are the shear and the normal stress, corresponding to the components $-\sigma_{xy}$ and σ_{yy} of the stress tensor $\boldsymbol{\sigma}$.
By employing the constitutive relations (4.18), the normal and the shear stresses read, respectively

$$\sigma = \sigma_{\mathrm{qs}} + \sigma_{\mathrm{col}}, \tag{4.39}$$

$$\tau = \tau_{\mathrm{qs}} + \tau_{\mathrm{col}}. \tag{4.40}$$

Finally, the fluctuating energy equation (4.22) reduces to a balance between the fluctuating energy produced through the collisional shear work and the sum of collisional energy diffusion (divergence of the energy flux) and dissipation:

$$\tau_{\mathrm{col}} \frac{\partial u}{\partial y} = \frac{\partial q_{\mathrm{col}}}{\partial y} + \Gamma_{\mathrm{col}}, \tag{4.41}$$

where q_{col} is the vertical component of the energy flux, $q_{y,\mathrm{col}}$, and the y subscript is removed for simplicity.
The set of three differential equations (4.39)-(4.41) in the unknown ν, u, T, σ_{qs}, τ_{qs}, σ_{col}, τ_{col}, q_{col} and Γ_{col} is closed when providing the constitutive relations for the quasi-static

stresses and the collisional contributions.

As stated in Section 4.2.1, the constitutive relations for the collisional stresses, energy flux and rate of dissipation of fluctuating energy are taken from the kinetic theory of granular gases derived by Garzó and Dufty [40] (Section 3.1.4), and modified as described in Section 4.2.1: accounting for the role of the particle stiffness on the contact duration during collisions (through the function f_r defined by Eq. (4.23)) and using the definition of the radial distribution function given in Eq. (4.28). Using the equation for the stress tensor (3.33), applied to shearing flows, together with the relations for the pressure (3.40) and for the shear viscosity (3.41a), and introducing the function f_r, the collisional normal and shear stresses can be written as:

$$\sigma_{\text{col}} = \rho_p f_1 f_r T, \tag{4.42}$$

$$\tau_{\text{col}} = \rho_p d f_2 f_r T^{1/2} \frac{\partial u}{\partial y}. \tag{4.43}$$

The collisional rate of dissipation of fluctuating energy, Γ_{col}, is that proposed by Jenkins [52, 53] in the Extended Kinetic Theory, Eq. (3.48), multiplied by the function f_r:

$$\Gamma_{\text{col}} = \rho_p \frac{f_3}{L} f_r T^{3/2}. \tag{4.44}$$

The collisional energy flux q_{col} is obtained by multiplying Eq. (3.34) by f_r:

$$q_{\text{col}} = -\rho_p d \left(f_4 T^{1/2} \frac{\partial T}{\partial y} + f_5 T^{3/2} \frac{\partial \nu}{\partial y} \right) f_r. \tag{4.45}$$

Functions f_j, $j = 1, \cdots, 5$ are solely dependent on the concentration and can be easily derived from the original expressions of $\boldsymbol{\sigma}_{\text{col}}$, $\mathbf{q}_{\text{col}}$ and Γ_{col}, (3.33), (3.34) and (3.48):

$$f_1 = 4\nu G F, \tag{4.46}$$

$$f_2 = \frac{8}{5\sqrt{\pi}} \nu G J, \tag{4.47}$$

$$f_3 = \frac{12}{\sqrt{\pi}} \left(1 - e^2\right) \nu G \left(1 + \frac{3}{32} c^*\right), \tag{4.48}$$

$$f_4 = \frac{4}{\sqrt{\pi}} \nu G M, \tag{4.49}$$

$$f_5 = \frac{25}{128} \sqrt{\pi} \frac{N}{\nu}. \tag{4.50}$$

G is the product of ν and the radial distribution function g_0, as in (3.42a), and the new expression of g_0 is given by Eq. (4.28). The radial distribution function is assumed to diverge when the concentration approaches a critical value, ν_{s}. The critical value ν_{s} represents the maximum concentration that a disordered collection of identical spheres can achieve, and is affected by the mechanical properties of the particles. At the steady state, under shearing, when the concentration reaches ν_{s}, a shear rigidity develops, then ν_{s} is here called the 'shear rigidity concentration'. Functions F, J, M and N are defined by Eqs. (3.42b), (3.42c), (3.42d) and (3.42e), respectively, and c^* is computed as

$$c^* = 32(1 - e)\left(1 - 2e^2\right)\left[81 - 17e + 30e^2(1 - e)\right]^{-1}, \tag{4.51}$$

as reported in Appendix A.
In Eq. (4.44), L is the correlation length, accounting for the decrease in the rate of collisional energy dissipation due to the correlated motion of particles that is likely to occur

when the flow is dense [52, 53, 54]. As stated in Section 4.2.1, L has been introduced by Jenkins [52] in the Extended Kinetic Theory, and its generic form is given by Eq. (3.49). In the case of planar shearing flows, Eq. (3.49) yields

$$\frac{L}{d} = \max\left(1, L^* \frac{d}{T^{1/2}} \frac{\partial u}{\partial y}\right), \tag{4.52}$$

where the coefficient L^* is a function of the concentration and the particle properties. Several expressions of L^* have been proposed in the literature. Here, the form derived by Berzi [11] on the basis of numerical results on simple shear flows of spheres obtained by Mitarai and Nakanishi [88] is adopted and slightly modified, as described in Section 4.2.1. Such an expression, given by Eq. (4.30), has been proved to be valid in the case of steady, shearing flows, and can be rewritten in terms of functions f_2 and f_3 as

$$L^* = \left(\frac{f_2}{f_3}\right)^{1/2} \left[\frac{2\,(1-e)}{15}\,(\tilde{g}_0 - \tilde{g}_{0,\mathrm{f}}) + 1\right]^{3/2}, \tag{4.53}$$

where $\tilde{g}_0$ is given by Eq. (4.31) and $\tilde{g}_{0,\mathrm{f}}$ is the value of $\tilde{g}_0$ at the freezing point, $\nu = 0.49$ [118]. Function $\tilde{g}_0$ is defined in a manner similar to g_0 but replacing ν_s with $\nu_\mathrm{rcp} = 0.636$, such as the correlation length diverges at the random close packing concentration, independently of the interparticle friction coefficient.
In all the relations, e is the effective coefficient of restitution (e_eff), whose expression is given by (3.45).

At the steady state, the quasi-static static component of the shear stress is assumed to be proportional to the quasi-static component of the normal stress through the tangent of the internal friction angle at the critical state:

$$\tau_\mathrm{qs} = \sigma_\mathrm{qs} \tan\phi. \tag{4.54}$$

Eq. (4.54) represents the critical state theory of soil mechanics, which, in the case of shearing flows, collapse on the Mohr-Coulomb criterion (4.36) in the plane shear stress-normal stress. Here, the internal friction angle, ϕ, is a function of both the interparticle friction coefficient, μ, and the shearing contraints [34].
For dimensional reasons, the quasi-static component of the normal stress must obey

$$\sigma_\mathrm{qs} = f_0 \frac{K}{d}, \tag{4.55}$$

where the particle stiffness K is equal to $\pi d E/8$ in the case of linear elastic contacts [62], with E the Young's modulus, whereas f_0 is solely a function of the concentration [16, 122]. As anticipated, the quasi-static component of stresses is required to vanish when the concentration is below the critical threshold which allows the force chains to develop. Furthermore, the present constitutive model assumes that friction supports force chains, and the quasi-static contribution must disappear whenever interparticle friction does not play any role, i.e., when the particles are frictionless.
Then, to be consistent with physical observations on granular packings, the function f_0 vanishes when the concentration is equal to the random loose packing value, ν_rlp, defined as the minimum concentration at which a disordered packing exists [117]. In other words, at the random loose packing, the granular material undergoes a phase transition to a purely collisional regime.
Also, f_0 is taken to diverge when the concentration approaches the shear rigidity concentration, ν_s, here considered as the maximum concentration that a disordered configuration

of identical spheres can achieve, under steady, shearing conditions. This assumption must be revised in view of very recent results of numerical simulations, but it does not affect the qualitative behavior of the model. Therefore,

$$f_0 = \begin{cases} a\dfrac{(\nu - \nu_{\mathrm{rlp}})}{(\nu_{\mathrm{s}} - \nu)} & \text{if and only if } \nu > \nu_{\mathrm{rlp}} \text{ and } \nu_{\mathrm{rlp}} < \nu_{\mathrm{s}} \\ 0 & \text{otherwise} \end{cases} \tag{4.56}$$

where a is a dimensionless material coefficient [16].
According to the model, the response of the material is governed only by collisions (collisional regime) when

$$\nu < \nu_{\mathrm{rlp}}. \tag{4.57}$$

By substituting Eqs. (4.42), (4.43), (4.55) and (4.54) into (4.39) and (4.40), the expressions for the total stress in steady, shearing flows read

$$\begin{cases} \sigma = \dfrac{K}{d} f_0 + \rho_p f_1 f_r T & \text{(4.58a)} \\ \tau = \dfrac{K}{d} f_0 \tan\phi + \rho_p d f_2 f_r T^{1/2} \dfrac{\partial u}{\partial y}. & \text{(4.58b)} \end{cases}$$

Function f_r can be rewritten as function of σ and ν, eliminating the dependence on the granular temperature. By using Eq. (4.58a),

$$T = \frac{\sigma - f_0 K/d}{\rho_p f_1 f_r}. \tag{4.59}$$

And also, from Eq. (4.59) and Eq. (4.23),

$$\frac{1}{f_r} - 2\frac{d}{s}\sqrt{\frac{\pi}{8 f_1}\left(\frac{\sigma d}{K} - f_0\right)}\frac{1}{\sqrt{f_r}} - 1 = 0, \tag{4.60}$$

that gives

$$f_r = \frac{2}{2 + \mathcal{A} + \sqrt{\mathcal{A}^2 + 4\mathcal{A}}}, \tag{4.61}$$

where, from the definition of the mean separation distance s, (4.24),

$$\mathcal{A} = \frac{36\pi G^2}{f_1}\left(\frac{\sigma d}{K} - f_0\right). \tag{4.62}$$

As expected, f_r tends to one as K tends to infinity.
It is important to notice that taking into account the role of particle stiffness on the duration of a collision, the collisional contributions σ_{col}, τ_{col}, q_{col} and Γ_{col} depend not only on the concentration, the granular temperature and the shear rate, $\partial u/\partial y$, as in classic kinetic theories, but also on the ratio between the normal stress and the particle stiffness $\sigma/(K/d)$ (which can now be considered as a measure of how stiff is a particle).

The idea of adding collisional and quasi-static (frictional) contributions in the granular stresses has been previously proposed by Johnson and Jackson [63, 64]. However, Johnson and Jackson did not take into account the role of particle stiffness on the frictional component of the normal stress, so that the constitutive relation for the latter was not physically based [16]. Moreover, for the collisional contribution to the stresses, they used

a kinetic theory developed for dilute flows, that does not take into account the breaking of the molecular chaos assumption [26], at high concentrations. Hence, they were unable to explain the variation of the ratio of shear to normal stress with concentration observed in numerical simulations on simple shear flows [30]. Similar considerations apply also to the theory developed by Savage [109], who assumed a plastic behavior and the presence of gaussian fluctuations of the strain rate and stresses in the planar flow of a dense granular material, and obtained constitutive relations very similar to those of Johnson and Jackson [63, 64].

4.3.1. Model parameters

The model parameters which affect the constitutive relations for the stresses, (4.58), the collisional energy flux, (4.45), and rate of dissipation of fluctuating energy, (4.44), can be subdivided into (i) micro-mechanical parameters, characteristics of the single particle (i.e., ρ_p, d, K and e); (ii) macro-mechanical parameters, characteristics of the "continuum" medium (i.e., ν_{rlp}, ν_{s}, $\tan\phi$ and a). As previously mentioned, micro and macro-mechanical parameters are related to each other. In particular, the concentration at which the shear rigidity develops ν_{s}, the random loose packing ν_{rlp}, the critical friction angle ϕ and the effective coefficient of restitution e are affected by the interparticle friction coefficient μ.

The effective coefficient of restitution, e, depends on μ, e_n and e_t through the relation Eq. (3.45) proposed by Jenkins and Zhang [60]. Foerster et al. [37] developed an experimental apparatus to measure those quantities from the dynamics of the flights of colliding spheres. Lorenz et al. [77] employed the same apparatus, slightly modified, to measure the three coefficients for several materials. A table summarizing the measured impact properties for a variety of spheres is available at the Cornell University web page: `http://grainflowresearch.mae.cornell.edu/impact/impact.html`.

The dependence of the shear rigidity concentration on the interparticle friction coefficient in the cases of steady, shearing flows has been studied by Chialvo et al. [28] by performing numerical simulations of simple, shear flows of spheres. The shear rigidity concentration is identified with the critical concentration defined by Chialvo et al. [28]. For frictionless particles, that is, $\mu = 0$, ν_{s} coincides with the random close packing, $\nu_{\mathrm{rcp}} = 0.636$ (densest possible disordered packing of identical spheres in static conditions, [117]), whereas in the case of frictional particles, ν_{s} is a decreasing function of μ.

Also the concentration at the random loose packing decreases with increasing interparticle friction coefficient, as theoretically demostrated by Song et al. [117] and numerically proved by Silbert [115]. In the case of frictionless particles, ν_{rlp} equals the random close packing concentration, and, consequenlty, $\nu_{\mathrm{s}}(\mu = 0) = \nu_{\mathrm{rlp}}(\mu = 0) = \nu_{\mathrm{rcp}}$. Then, the quasi-static stresses vanish automatically according to Eq. (4.56), satisfying the assumption that force chains can develop only in presence of friction. Measured values of $\nu_{\mathrm{s}}(\mu)$ [28] and $\nu_{\mathrm{rlp}}(\mu)$ [115] are reported in Tab. 4.1.

In the case of steady and homogeneous shear flows, the tangent of the critical friction angle can be interpreted as the yield stress ratio, i.e., the asymptotic value reached by τ/σ for vanishing small shear rate, $\partial u/\partial y$. This typical rate-independent behavior of frictional granular material, in such a simple shear flow configuration, will be discussed in details in Section 5. Nevertheless, the critical friction angle can be easily obtained by performing numerical simulations of homogeneous, steady shear flows of frictional spheres, by impos-

ing the shear rate to vanish and measuring the constant-value asymptote reached by the stress ratio τ/σ. These numerical experiments have been performed by Chialvo et al. [28], and the measured values of $\tan\phi$ for different values of the interparticle friction angle μ are summarized in Tab. 4.1.

Table 4.1.: Measurements of the shear rigidity concentration ν_s, the random loose packing concentration ν_{rlp} and the tangent of the critical friction angle $\tan\phi$ for different values of the interparticle friction coefficient μ. The data of ν_s and $\tan\phi$ have been obtained by Chialvo et al. [28] by performing 3D DEM numerical simulations of simple shear flows of identical spheres, and the values of ν_{rlp} have been extrapolated by Silbert [115] by performing 3D numerical simulations on soft-spheres packings.

μ	0	0.001	0.01	0.1	0.2	0.3	0.5	1	10
ν_s	0.636	–	–	0.613	–	0.596	0.598	0.581	–
ν_{rlp}	0.639	0.638	0.634	0.614	0.595	–	0.574	0.556	0.544
$\tan\phi$	0.105	–	–	0.268	–	0.357	0.382	0.405	–

The unique model parameter which needs to be inferred by numerical simulations or experiments is the constant a appearing in the function f_0 (4.56) in the quasi-static component of the normal stress. Experimental investigations on the critical state of identical spheres are though rare. To our knowledge, only Wroth [129] performed experiments on the critical state of 1 mm stainless steel spheres ($\rho_p = 7.79$ kg/m^3, $K = 8.25 \cdot 10^7$ Pa m) using a shear cell [94]. The experiments confirm that the ratio of τ_{qs} to σ_{qs} is constant and that f_0 is a unique function of the concentration. In Fig. 4.4(a) the theoretical expression of Eq. (4.56), with $\nu_s = 0.619$, $\nu_{rlp} = 0.598$ and $a = 1.8 \cdot 10^{-6}$, obtained from linear regression, is drawn. The data of Fig. 4.4(a) are plotted in terms of f_0 against void ratio e_v in Fig. 4.4(b).

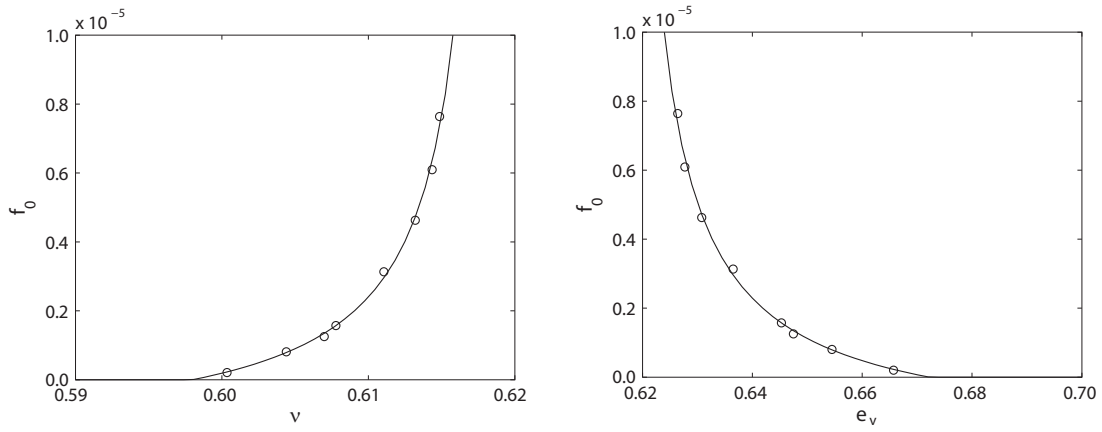

(a) (b)

Figure 4.4.: Experimental (circles, after [129]) and theoretical (solid line) coefficient f_0 for steel spheres as a function of (a) concentration and (b) void ratio.

For stainless steel spheres, Lorenz et al. [77] found that $\mu = 0.099 \pm 0.008$; the obtained value of the shear rigidity concentration, 0.619, is very similar to that measured by Chialvo et al. [28] at $\mu = 0.1$ (0.613). On the other hand, the random loose packing concentration

is lower than that estimated by Silbert [115]. The fact that the $\nu_{\rm rlp}$ obtained by Silbert [115] exceeds the shear rigidity concentration for $\mu = 0.1$, suggests that that value is not completely reliable, and here the value 0.598 for $\nu_{\rm rlp}$ deduced by the experiments of Wroth [129] is adopted.

4.4. Conclusions

A costitutive model, based on a continuum mechanics approach, has been developed, in which both standard geotechnical constitutive models, based on the critical state theory, and kinetic theories of granular gases are merged. Both enduring contacts among particles involved in force chains and non-instantaneous collisions are considered. In particular, the steady state condition of a granular material under plane shear has been analyzed. The energy and the total stress are defined as the linear sum of a quasi-static and a collisional component, accounting, respectively, for the force chains and the collisions.
The enduring contacts among particles in force chains are assumed not to contribute to the transport of kinetic fluctuating energy. Then, the quasi-static energy flux and rate of energy dissipation do not appear into the conservation equations. We have assumed that: (i) friction supports force chains, and the quasi-static contribution must disappear whenever interparticle friction does not play any role, i.e., when the particles are frictionless; (ii) the quasi-static component of the stress vanishes when the particle concentration is less than the random loose packing, that represents the lower limit for the existence of a disordered granular packing [117].
In the collisional contribution, both the role of particle stiffness and the correlated motion among the particles have been accounted for. For modeling the latter, we have adopted a recently suggested expression [11] for the correlation length in the dissipation rate of fluctuating energy, which depends only on the coefficient of restitution. The particle stiffness is introduced through the function f_r, which multiplies the collisional contributions and tends to one when the particles are rigid. Also, we have proposed an expression for the radial distribution function which is a combination of the Carnahan and Starling's [25] at small concentration, and diverges as the concentration approaches the shear rigidity like the Torquato's [118] but, unlike the latter, its derivative is continuous in the entire range of concentration.
The application of the model to homogeneous and non homogeneous shear flows of inelastic spheres will be described in the following Chapters.

5. Simple shear flows of granular materials*

In this Chapter, the theoretical model proposed in Chapter 4 is applied to the steady, homogeneous shear flows of a mixture of identical spheres, usually called simple shear flows. Section 5.1 is devoted to the description of the equations governing simple shear flows, and the constitutive relations derived from the model; then a critical discussion on the salient properties of the theory is proposed in Section 5.2 and, finally, in Section 5.3 the comparison with experimental and numerical results found in literature is illustrated.

5.1. Simple shear flow configuration and governing equations

This Section focuses on the steady, simple shear flows of an assembly of identical, dry spherical particles of diameter d and density ρ_p (Fig. 5.1).

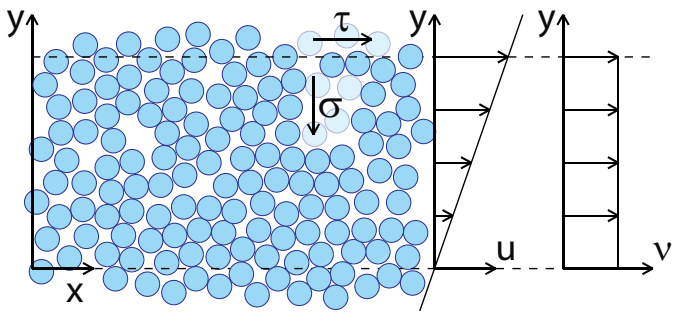

Figure 5.1.: Simple shear flow configuration of a collection of identical spheres.

Simple shear flows are characterized by homogeneous shearing, then all the variables are constant along the flow field and the horizontal velocity is linearly distributed along the shearing direction, y. The kinematic variable which affects the problem is then the shear rate, $\dot{\gamma} = \partial u/\partial y$, that remains constant along y. The momentum balances indicate that both the normal and the shear stresses are constant, as stated by Eqs. (4.38a)-(4.38b); also, the divergence of the collisional energy flux can be neglected in the fluctuating energy equation (4.41), $\partial q_{\mathrm{col}}/\partial y = 0$. Consequently, Eq. (4.41) reduces to

$$\tau_{\mathrm{col}}\dot{\gamma} = \Gamma_{\mathrm{col}}. \tag{5.1}$$

Hence, the energy produced by the work of the collisional shear stress is entirely dissipated in collisions.
By substituting the constitutive relationships for the collisional shear stress, (4.43), and the collisional rate of dissipation of fluctuating energy, (4.44), into Eq. (5.1), the granular temperature results an algebraic function of the shear rate:

$$T = d^2 f_6 \dot{\gamma}^2, \tag{5.2}$$

*mainly based on D. Vescovi, C. di Prisco, and D. Berzi. From solid to granular gases: the steady state for granular materials. *International Journal for Numerical and Analytical Methods in Geomechanics*, 37:2937-2951, 2013

with

$$f_6 = \frac{L}{d}\frac{f_2}{f_3}. \tag{5.3}$$

Using Eq. (5.2) and the expression of L^* (4.53), the correlation length, (4.52), can be written as

$$\frac{L}{d} = \max\left[1, \frac{2\,(1-e)}{15}\,(\tilde{g}_0 - \tilde{g}_{0,\mathrm{f}}) + 1\right], \tag{5.4}$$

as inferred in [11]. Here, $\tilde{g}_0$ is the radial distribution function where the shear rigity concentration has been replaced by the random close packing value, $\nu_{\mathrm{rcp}} = 0.636$, Eq. (4.31). Then, the correlation length does not depend on the interparticle friction through the shear rigidity concentration, and diverges at $\nu_{\mathrm{rcp}} = 0.636$, unlike the other kinetic function f_1, f_2, f_3 and f_r which diverge at ν_{s}. The validity of this assumption is confirmed by numerical experiments, as will be shown in the upcoming Section 5.3.

By introducing Eq. (5.2) into Eqs. (4.58a) and (4.58b), the expressions for the total stresses in steady, simple shear flows read

$$\begin{cases} \sigma = \dfrac{K}{d} f_0 + \rho_p d^2 f_1 f_r f_6 \dot{\gamma}^2, & \text{(5.5a)} \\ \tau = \dfrac{K}{d} f_0 \tan\phi + \rho_p d^2 f_2 f_r f_6^{1/2} \dot{\gamma}^2. & \text{(5.5b)} \end{cases}$$

Here, functions f_0, f_1 and f_2 are given by Eqs. (4.56), (4.46) and (4.47), respectively. The coefficient f_r is defined by Eq. (4.23), and by using Eq. (5.2), it reads

$$f_r = \left[1 + 6G\left(\pi f_6 \frac{\rho_p d^3 \dot{\gamma}^2}{K}\right)^{1/2}\right]^{-1}. \tag{5.6}$$

In Eq. (5.6), f_r depends on the concentration and the shear rate, but, as already stated, it can be rewritten as a function of the ratio between the normal stress and the particle stiffness, $\sigma/(K/d)$, by using Eq. (4.61).
Eqs. (5.5) represent an extension in a four dimensional space of the critical state condition to nonzero values of $\dot{\gamma}$ (or T) [122]. A graphical illustration of such a locus is reported in Fig. 5.2, where the different lines in the $\tau - \sigma - e_v$ space correspond to different values of T. In other words, the critical state is here interpreted as a particular steady state for which the granular temperature vanishes as well as the shear rate. The material parameter values employed to obtain the curves and used in the following Section 5.2, unless differently stated, coincide with those of 1 mm stainless spheres reported in Section 4.3.1: $d = 10^-3$ m, $\rho_p = 7.79$ kg/m^3, $K = 8.25 \cdot 10^7$ Pa m, $\nu_{\mathrm{s}} = 0.619$, $\nu_{\mathrm{rlp}} = 0.598$, $a = 1.8 \cdot 10^{-6}$, $e = 0.83$ (as computed using Eq. 3.45 with the impacts coefficients evaluated by Lorenz et al. [77] for stainless steel spheres: $\mu = 0.1$, $e_n = 0.95$ and $e_t = 0.32$) and $\tan\phi = 0.268$ (as estimated by Chialvo et al. [28] for particles having interparticle friction coefficient $\mu = 0.1$). An alternative way of writing Eqs. (5.5) is the following:

$$\begin{cases} 1 - \dfrac{K}{\sigma d} f_0 - \dfrac{\gamma_1^2}{\gamma_2^2}\left(\dfrac{\tau}{\sigma} - \tan\phi\right) = 0, & \text{(5.7a)} \\ \dfrac{\tau}{\sigma} - \tan\phi - \dfrac{t_m^2}{\gamma_1^2}\dot{\gamma}^2 = 0 & \text{(5.7b)} \end{cases}$$

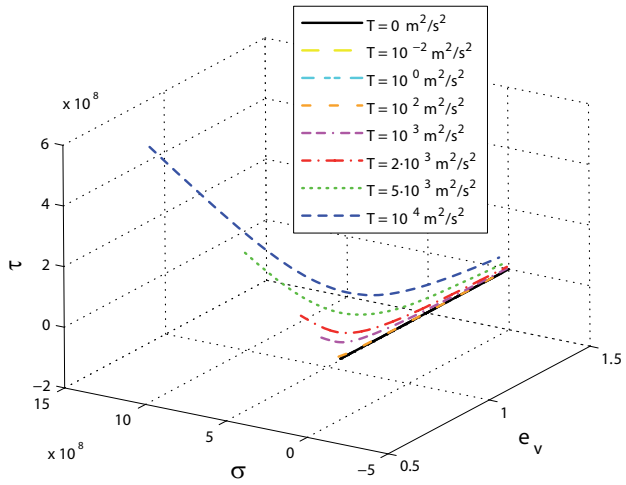

Figure 5.2.: Evolution of the steady state locus in the space shear stress-normal stress-void ratio as a function of the granular temperature T.

where $t_m = d\left(\rho_p \nu/\sigma\right)^{1/2}$ is the microscopic time scale associated with the rearrangement of particles [44], and

$$\gamma_1 = \left[\frac{\nu}{f_r\left(f_2 f_6^{1/2} - \tan\phi f_1 f_6\right)}\right]^{1/2}, \tag{5.8a}$$

$$\gamma_2 = \left[\frac{\nu}{f_1 f_r f_6}\right]^{1/2}. \tag{5.8b}$$

Eqs. (5.7) provide

$$\dot{\gamma} = \frac{\gamma_1}{t_m}\left(\frac{\tau}{\sigma} - \tan\phi\right)^{1/2}, \tag{5.9}$$

which can be interpreted in the viscoplastic framework. According to the definition of the viscoplastic strain rate tensor, Eq. (4.34), the viscoplastic shear rate reads

$$\dot{\gamma}^{\mathrm{vp}} = \tilde{\gamma}\Phi\left(\mathcal{F}\right)\frac{\partial \mathcal{G}}{\partial \tau}. \tag{5.10}$$

Eq. (5.10) coincides with Eq. (5.9) if an associated flow rule is adopted, i.e., $\mathcal{G} = \mathcal{F}$, and the yield locus, $\mathcal{F}$, is defined by the Mohr-Coulomb criterion (4.36),

$$\mathcal{F} = \tau - \sigma\tan\phi. \tag{5.11}$$

Then, the the viscous nucleus, $\Phi\left(\mathcal{F}\right)$, and the fluidity parameter, $\tilde{\gamma}$, are given by

$$\Phi\left(\mathcal{F}\right) = \left(\frac{\mathcal{F}}{\sigma}\right)^{1/2}, \tag{5.12}$$

$$\tilde{\gamma} = \frac{\gamma_1}{t_m}. \tag{5.13}$$

Note that the fluidity parameter is not constant, unlike commonly assumed in the literature.
The French research group GDR-MiDi [44] has suggested that dense granular materials

obey to a local, phenomenological rheology that can be expressed in terms of two relations between three non-dimensional quantities, if the particles are rigid: the concentration ν, the stress ratio τ/σ and the inertial number I. The inertial number represents the ratio between the microscopic time scale $t_m = d\left(\rho_p \nu/\sigma\right)^{1/2}$, associated with the transversal motion of a particle submitted to a normal stress σ, and the macroscopic time scale, $t_M = 1/\dot{\gamma}$, associated with the motion parallel to the flow [15], then it sounds

$$I \equiv \frac{t_m}{t_M} = d\dot{\gamma}\left(\frac{\rho_p \nu}{\sigma}\right)^{1/2}. \tag{5.14}$$

Despite the notable results obtained in modeling many different configurations of dense granular flows [12, 13, 14, 66, 97], the GDR MiDi rheology does not apply when there is an additional time scale associated with the particle velocity fluctuations [53], whose intensity is provided by the granular temperature; in fact, the role of the latter can not be disregarded in regions of thickness some diameters close to the boundaries (free surface, rigid and/or erodible bottom) [70, 116]. Moreover, when the particles are soft, i.e., have a finite stiffness, another dimensionless quantities plays a role: the ratio between the normal stress and the particle stiffness $\sigma/(K/d)$. Using Eqs. (5.9), (5.7a) and the definition of the inertial number (5.14), the constitutive relationships in terms of ν, τ/σ, I and $\sigma/(K/d)$ can be derived:

$$\frac{\tau}{\sigma} = \tan\phi + \left(f_2 f_6^{1/2} - \tan\phi f_1 f_6\right) f_r \frac{I^2}{\nu}, \tag{5.15a}$$

$$I = \left[\frac{\nu}{f_1 f_6 f_r}\left(1 - \frac{K}{\sigma d} f_0\right)\right]^{1/2}. \tag{5.15b}$$

As mentioned in the previous Chapter, the response of granular materials is governed only by collisions, i.e., the steady flow is in the collisional regime, when the concentration is lower than the random loose packing (condition 4.57). In terms of stress ratio, using Eqs. (5.5) and considering that the quasi-static contributions disappear when $\nu < \nu_{\mathrm{rlp}}$ ($f_0 = 0$), the threshold between the two regimes is the stress ratio value associated with the random loose packing concentration

$$\left(\frac{\tau}{\sigma}\right)_{\mathrm{rlp}} = \frac{f_{2,\mathrm{rlp}}}{f_{1,\mathrm{rlp}} f_{6,\mathrm{rlp}}^{1/2}}, \tag{5.16}$$

where the subscript rlp denotes functions evaluated at $\nu = \nu_{\mathrm{rlp}}$. $\left(\frac{\tau}{\sigma}\right)_{\mathrm{rlp}}$ is not affected by $\sigma/(K/d)$, but depends only on the material parameters d, ν_{rlp}, ν_{s} and e. By employing the material parameters adopted in this Section, $\left(\frac{\tau}{\sigma}\right)_{\mathrm{rlp}} = 0.294$. Then, the collisional regime condition Eq. (4.57), in simple shear flows, is equivalent to

$$\frac{\tau}{\sigma} > \left(\frac{\tau}{\sigma}\right)_{\mathrm{rlp}}. \tag{5.17}$$

5.2. Critical discussion of the model

In this Section, the aforementioned constitutive relationship is theoretically discussed. First, a phase diagram is introduced in Section 5.2.1. Then, steady, simple shear flows can be physically and/or numerically simulated (i) by imposing the normal stress, and measuring the concentration (or alternatively the void ratio) and the shear stress as functions of the shear rate (pressure-imposed); (ii) by imposing the concentration (void ratio),

and measuring the normal and shear stress as functions of the shear rate (concentration-imposed); (iii) by imposing the stress ratio, and measuring the concentration and the shear rate as functions of the normal stress (stress ratio-imposed). The results of the three configurations are equivalent, if dimensionless quantities are employed [30]. Pressure-imposed, concentration-imposed and stress ratio-imposed flow configurations are analyzed in Sections 5.2.2, 5.2.3 and 5.2.4, respectively.

5.2.1. Phase diagram

From (5.5a), since the second term on the right-hand-side is always positive, it must be

$$1 - \frac{K}{d\sigma} f_0 \geq 0. \tag{5.18}$$

By substituting Eq. (4.56) into Eq. (5.18), for positive values of f_0, we obtain

$$\nu \leq \nu_{\mathrm{cs}} \tag{5.19}$$

where

$$\nu_{\mathrm{cs}} = \frac{a\nu_{\mathrm{rlp}}}{a + \sigma d/K} + \frac{\nu_{\mathrm{s}}}{1 + a(\sigma d/K)^{-1}} \tag{5.20}$$

is the concentration at the critical state. ν_{cs} represents the maximum concentration that can be achieved under steady conditions, for a fixed value of σ, when the shear rate vanishes.
Fig. 5.3 shows the qualitative phase diagram in the concentration-normal stress plane. For large values of $\sigma d/K$, ν_{cs} approaches ν_{s}; on the other hand, ν_{cs} tends to ν_{rlp} when $\sigma d/K$ is small. Then, the range of coexistence of quasi-static and collisional stresses depends on the imposed normal stress. As a consequence, considering a fixed value of σ, the simple shear flow can be in the purely collisional regime or in the regime where both collisions and force chains coexist, depending on the value of the shear rate.

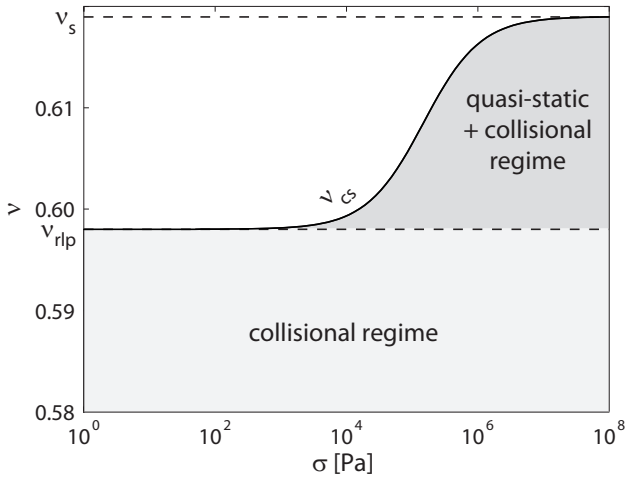

Figure 5.3.: Phase diagram for steady, simple shear flow of inelastic spheres in the $\sigma - \nu$ plane. Eq. (5.20) (solid line) is plotted by using $d = 1$ mm, $\nu_{\mathrm{rlp}} = 0.598$, $\nu_{\mathrm{s}} = 0.619$, $a = 1.8 \cdot 10^{-6}$ and $K = 8.25 \cdot 10^{7}$ Pa m.

Analogously, Fig. 5.4 depicts the qualitative phase diagram in the concentration-interparticle friction plane for the steady, simple shear flow of inelastic spheres, i.e., $e < 1$ and

$\nu_{\mathrm{rlp}} < \nu_{\mathrm{s}} < \nu_{\mathrm{rcp}}$, for an imposed value of the normal stress.

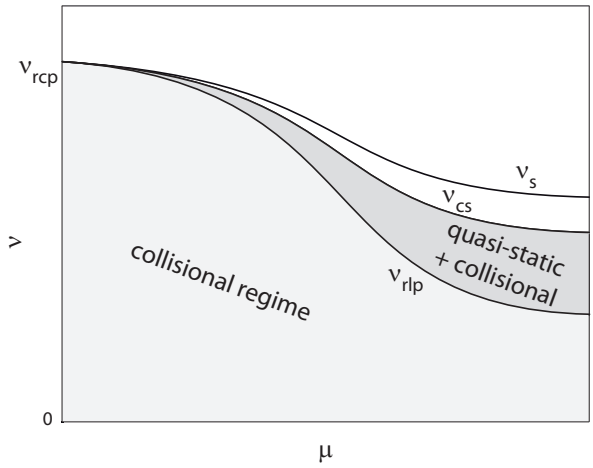

Figure 5.4.: Phase diagram in the $\mu - \nu$ plane for a fixed value of σ.

For a given value of the interparticle friction μ, the concentration decreases as the shear rate increases (as already mentioned, the maximum value is when $\dot{\gamma} = 0$, i.e., at the critical state, when the collisional stresses vanish). For small values of μ, ν_{rlp} is very close to ν_{s}, so that the quasi-static stresses are almost zero: the maximum concentration therefore coincides with ν_{s} and the steady, simple shear flow is always in the collisional regime. At larger μ, ν_{rlp} is lower than ν_{s}: the concentration at the critical state is ν_{cs}, and quasi-static and collisional stresses coexist in the range between $\nu_{\mathrm{rlp}} \leq \nu \leq \nu_{\mathrm{cs}}$. At the value of $\dot{\gamma}$ which corresponds to a concentration equal to ν_{rlp}, the quasi-static stresses vanish and the material undergoes a phase transition to the collisional regime. The range of coexistence of quasi-static and collisional stresses depends on the ratio $\sigma d/K$, which affects the value of ν_{cs}. In particular, for small values of $\sigma d/K$, i.e., small values of the total normal stress or large values of the particle stiffness, ν_{cs} approaches ν_{rlp}, as already mentioned, thus reducing the range of influence of quasi-static stresses (force chains) on the flow.

5.2.2. Pressure-imposed flows

As is common in the geotechnical community, pressure-imposed flows can be considered as a mixed-control test (i.e., both kinematic and loading quantities are imposed).
Pressure-imposed flows are obtained by keeping constant the normal stress σ and computing the concentration and the shear stress as functions of the shear rate. In this flow configuration, the concentration is obtained by solving Eq. (5.5a), once σ and $\dot{\gamma}$ are known, where the coefficient f_r is evaluated by using Eq. (4.61). Then, the shear stress is computed with Eq. (5.5b) as a function of the concentration and the shear rate. Fig. 5.5(a) and 5.5(b) show respectively the concentration and the stress ratio as functions of the shear rate for four different values of normal stress.
Depending on the imposed normal stress, the term related to the force chains can be relevant or not. In Fig. 5.5(a), the solid line is obtained for a large value of the imposed normal stress ($\sigma = 10^7$ Pa). In this case, the maximum concentration is equal to the shear rigidity concentration, and the flow is very dense at small values of the shear rate.

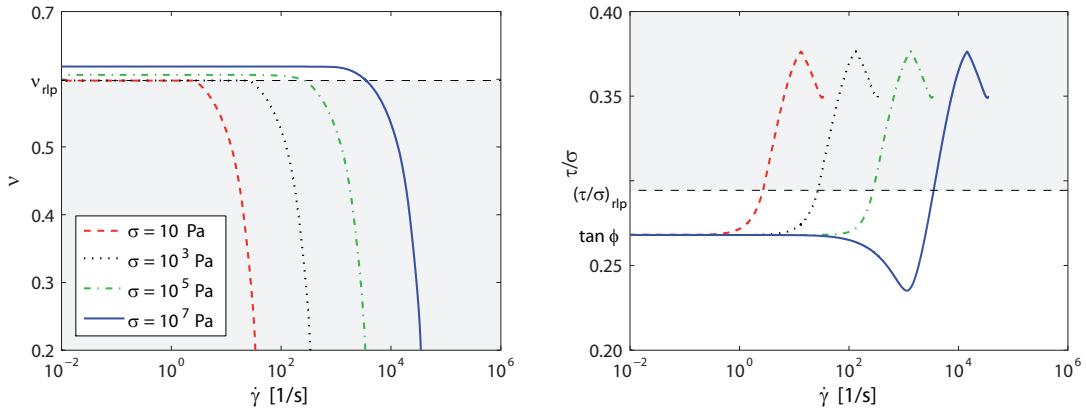

(a) (b)

Figure 5.5.: Theoretical (a) concentration and (b) stress ratio versus shear rate for 1 mm stainless spheres, at different values of the applied normal stress. The light gray regions represent the collisional regime, satisfying conditions Eqs. (4.57) and (5.17).

On the contrary, the dashed line represents a small value of the normal stress ($\sigma = 10$ Pa). The maximum concentration is equal to the random loose packing and the flow is in the collisional regime for almost each value of the shear rate, i.e., the flow is (almost completely) governed only by the collisions. The collisional regime, $\nu < \nu_{\rm rlp}$, is pointed out in Fig. 5.5(a) by the light gray region.
Fig. 5.5(b) shows the stress ratio as a function of the shear rate. Here, the collisional regime is characterized by the fulfillment of condition (5.17), represented by the light gray region. For vanishing values of the shear rate, the stress ratio approaches the constant value $\tan\phi$, for each value of the imposed normal stress. In Fig. 5.5(b), in the purely collisional regime all the curves exhibit a peak. The presence of a decreasing dependence of the stress ratio on the shear rate in the purely collisional regime is confirmed by numerical simulations on unbounded shear flows [88]. If the applied normal stress is sufficiently large (solid line in Fig. 5.5b) the present theory predicts an additional reduction in the stress ratio occurring when both collisional and quasi-static stresses coexist (i.e., when $\nu > \nu_{\rm rlp}$). There, the steady flow is characterized by the condition

$$\frac{\tau}{\sigma} < \tan\phi. \tag{5.21}$$

The condition for the occurrence of a minimum for $\dot\gamma \neq 0$ and $\tau/\sigma < \tan\phi$, when both quasi-static and collisional stresses coexist, (Fig. 5.5b) can be derived from Eq. (5.9). Indeed, for the shear rate being a real number,

$$\frac{\tau/\sigma - \tan\phi}{f_r\left(f_2 f_6^{1/2} - \tan\phi f_1 f_6\right)} > 0. \tag{5.22}$$

Hence, the condition (5.21) can occur if and only if

$$f_2 f_6^{1/2} - f_1 f_6 \tan\phi < 0, \tag{5.23}$$

given that f_r is always positive. Eq. (5.23) gives

$$\nu > \nu^*, \tag{5.24}$$

where ν^* is the value of concentration satisfying

$$\frac{f_2}{f_1 f_6^{1/2}} - \tan\phi = 0. \tag{5.25}$$

ν^* depends on the shear rigidity concentration ν_s, the critical friction angle ϕ and the effective coefficient of restitution e. In the case of stainless steel spheres, using the values of the model parameters reported in Section 5.1, ν^* is equal to 0.6074.
If ν_{cs} is larger than ν^*, the material exhibits a non-monotonic dependence of the stress ratio on the shear rate in the whole range of concentration between ν^* and ν_{cs}. In contrast, if $\nu_{cs} < \nu^*$, the stress ratio monotonically increases with $\dot{\gamma}$. By using Eq. (5.20), the condition $\nu_{cs} > \nu^*$ corresponds to

$$\sigma > \sigma^*, \tag{5.26}$$

where

$$\sigma^* = a\frac{(\nu^* - \nu_{rlp})}{(\nu_s - \nu^*)}\frac{K}{d}. \tag{5.27}$$

The dependence of ν_{cs} on σ and the values of ν and σ satisfying conditions (5.24) and (5.26) are depicted in Fig. 5.6.

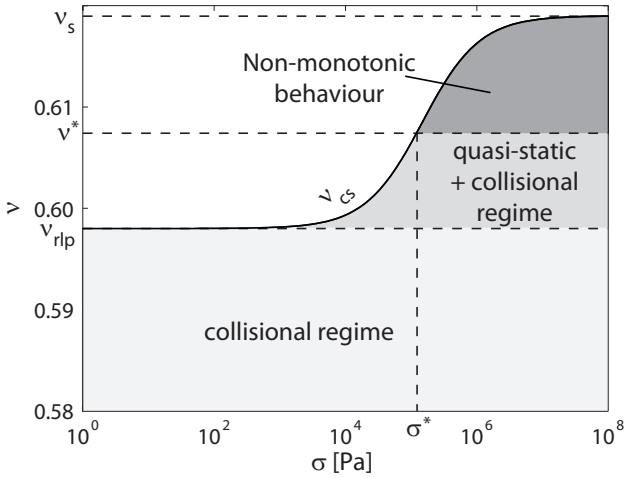

Figure 5.6.: Concentration at the critical state (solid line) attained in the steady, simple shear flow of 1 mm stainless steel spheres as a function of the applied normal stress. The dark gray area represents the range of existence of the non-monotonic dependence of τ/σ on $\dot{\gamma}$ when both collisional and quasi-static stresses coexist.

For $\nu > \nu^*$, the above mentioned viscoplastic interpretation (Eq. 5.10) still holds, if the fluidity parameter is allowed to be an imaginary number. The dependence of the fluidity parameter on the concentration for different values of σ is depicted in Fig. 5.7. The gray area represents the range of concentration for which $\tilde{\gamma}$ is imaginary. This condition cannot be *a priori* excluded but it must be further investigated by using either experimental or numerical tests on pressure-imposed flows. In fact, this unexpected trend could be a misleading consequence of the use of unphysical constitutive parameters as well as of having assumed e to be constant, i.e., independent on both σ and the relative velocity among colliding particles.

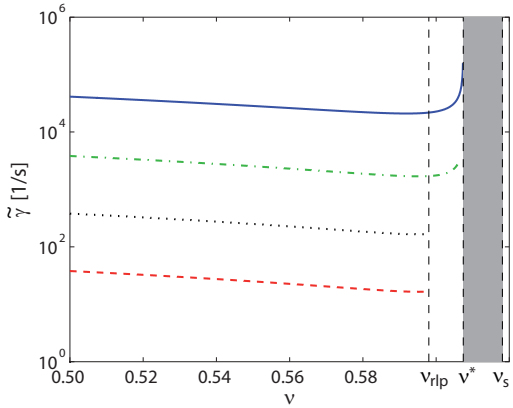

Figure 5.7.: Fluidity parameter as a function of the concentration for different values of the normal stress. The curves refer to different values of the imposed normal stress (see legend in Fig. 5.5).

Finally, Fig. 5.8 shows the same results but in terms of the dimensionless variables; then, the theoretical relations of Eqs. (5.15a)-(5.15b) between the stress ratio μ, the concentration ν and the inertial number I are plotted. Here, the different ratios $\sigma/(K/d)$ are obtained by using the usual particles properties ($d = 1$ mm, $K = 8.25 \cdot 10^7$ Pa m) and the four values of σ employed in Fig. 5.5.

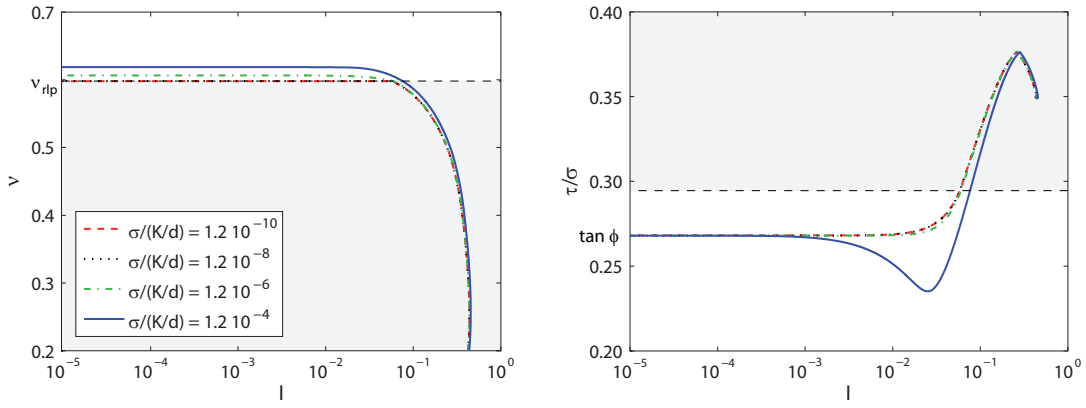

(a) (b)

Figure 5.8.: Theoretical (a) concentration and (b) stress ratio versus inertial number for 1 mm stainless spheres, at different values of the ratio between the normal stress and the particle stiffness. The light gray regions represent the collisional regime, satisfying conditions Eqs. (4.57) and (5.17).

For small values of $\sigma/(K/d)$, all the distinctive features observed by da Cruz et al. [30] on numerical simulations on disks are present in Fig. 5.8:

(i) at the lowest values of I, the collisional components of the stresses are negligible, so that the stress ratio is approximately constant and equal to $\tan\phi$, a substantially rate-independent regime (Fig. 5.8b);

(ii) in that regime, the concentration (Fig. 5.8a) shows the tendency to saturate towards ν_{cs}, lying between the random loose packing and the shear rigidity;

(iii) at the largest values of I, the quasi-static components of the stresses vanish, and the stress ratio is predicted by classical kinetic theories in the dense limit [58].

Fig. 5.8(b) shows that, for $\sigma/(K/d) < 10^{-5}$, $\sigma/(K/d)$ does not substantially affect the curves since, for the granular material here considered, the values of ν_{rlp} and ν_s are very close. For larger values of the ratio between the normal stress and the particle stiffness, the stress ratio presents a non-monotonic dependence on the inertial number (similarly to the shear stress), in the regime where both collisional and quasi-static stresses coexist, corresponding to the fulfillment of condition (5.21).

da Cruz et al. [30] also investigated the influence of the interparticle friction on the τ/σ-I and ν-I curves. As stated in Section 4.3.1, the interparticle friction affects the critical friction angle [30] and the values of ν_{rlp} and ν_s [62, 117]. In particular, for frictionless particles ($\mu = 0$), $\tan\phi = 0$ and $\nu_{rlp} = \nu_s = \nu_{rcp} = 0.636$ [36, 117]. Then, the quasi-static contributions vanish and the theoretical model reduces to the kinetic theory of granular gases, where the two modifications described in Section 4.2.1 are applied.
Fig. 5.9 shows the results of the present theory in the case of frictionless spheres. Here, the (collisional) material parameters employed are: $d = 10^-3$ m, $\rho_p = 7.79$ kg/m^3, $K = 8.25 \cdot 10^7$ Pa m, $\nu_s = 0.636$ and $e = 0.7$.

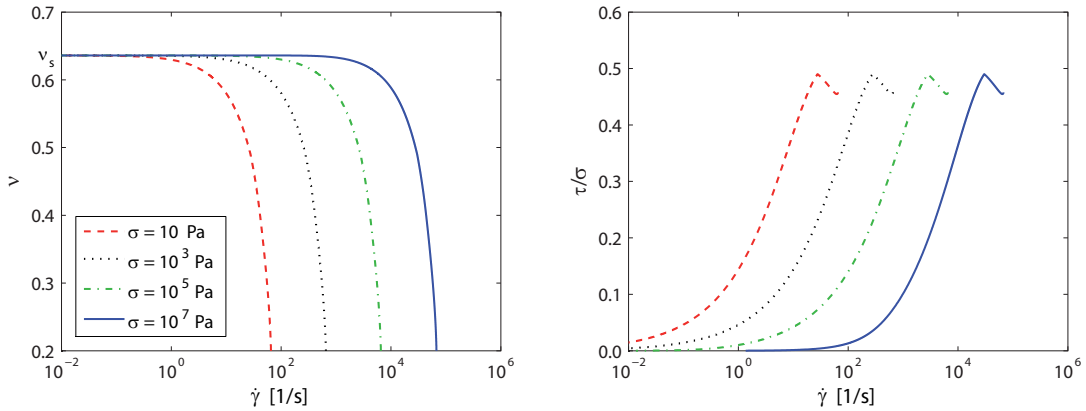

Figure 5.9.: Theoretical (a) concentration and (b) stress ratio versus shear rate at different values of the applied normal stress, when frictionless particles are used (purely collisional model with $d = 1$ mm, $K = 8.25 \cdot 10^7$ Pa m, $\nu_s = 0.636$ and $e = 0.7$).

The comparison of Fig. 5.9 with Fig. 5.5 allows to emphasize some key predictions of the theory: (i) the value of the concentration for $\dot{\gamma} \to 0$ would be independent of σ in a purely collisional model; (ii) a purely collisional model cannot predict the asymptotic approach of the stress ratio to the critical friction angle for $\dot{\gamma} \to 0$ [30].
Plotting the same results in terms of inertial number (Fig. 5.10), all the curves collapse except that obtained for a large value of $\sigma/(K/d)$. The ratio between the normal stress and the particle stiffness affects the function f_r appearing in the collisional contributions, which takes into account the influence of the particle stiffness on the contact duration

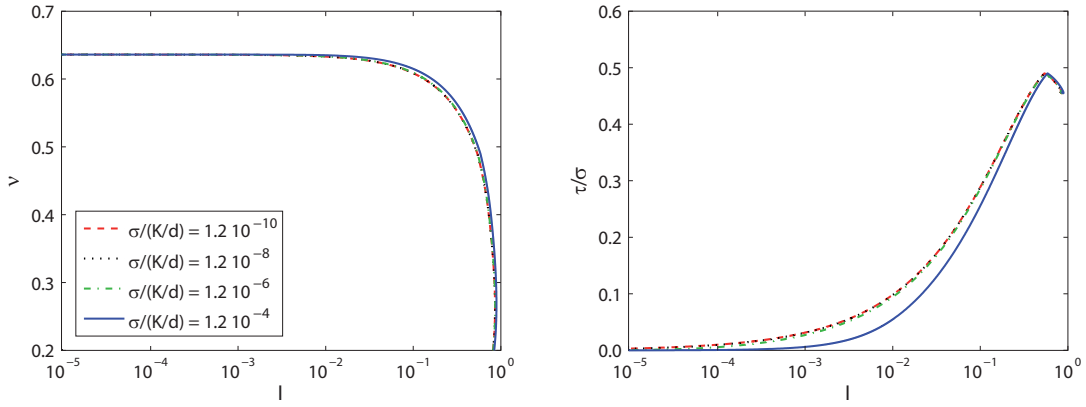

(a) (b)

Figure 5.10.: Theoretical (a) concentration and (b) stress ratio versus inertial number at different values of the ratio between the normal stress and the particle stiffness, when frictionless particles are used (purely collisional model with $d = 1$ mm, $K = 8.25 \cdot 10^7$ Pa m, $\nu_s = 0.636$ and $e = 0.7$).

during collisions. By using Eqs. (4.23), (5.2) and the definition of the inertial number (5.14), f_r can be rewritten as

$$f_r = \left[1 + 2\left(\frac{\pi}{8}\right)^{1/2} \frac{d}{s} \nu^{-1/2} f_6^{1/2} I \left(\frac{\sigma d}{K}\right)^{1/2}\right]^{-1}. \tag{5.28}$$

For dense flows, the dimensionless mean separation distance s/d and f_6 are of order 10^{-1}, while ν and I are of order unity. The second member on the right-hand-side of Eq. (5.28) is therefore negligible if $\sigma/(K/d)$ is lower than 10^{-5}. On the other hand, when $\sigma/(K/d) > 10^{-5}$ (solid line in Fig. 5.10), the collision time influences the material response and the stress ratio curve differs from the others.

5.2.3. Concentration-imposed flows

In this Section, the steady state condition in concentration-imposed flows is discussed.
As was already mentioned, the concentration-imposed flow is a kinematic-control test where stresses are computed as a function of the two kinematic variables: concentration and shear rate. In this configuration, from Eq. (5.5), the stress ratio is given by

$$\frac{\tau}{\sigma} = \frac{\frac{K}{d} f_0 \tan\phi + \rho_p d^2 f_2 f_r f_6^{1/2} \dot{\gamma}^2}{\frac{K}{d} f_0 + \rho_p d^2 f_1 f_r f_6 \dot{\gamma}^2} \tag{5.29}$$

where the function f_r is evaluated by using Eq. (5.6) as a function of the shear rate and of the imposed concentration.
Figs. 5.11(a) and Fig. 5.11(b) show the results in terms of stress ratio versus shear rate and normal stress versus shear rate, respectively, for different values of the concentration. Fig. 5.11(a) highlights the difference between the purely collisional regime and the regime where both quasi-static and collisional stresses coexist. Indeed, when the concentration is lower than the random loose packing (collisional regime), the stress ratio is constant

(curve with $\nu = 0.595$), whereas, for $\nu > \nu_{\mathrm{rlp}}$, τ/σ is affected by the shear rate.
Moreover, when the concentration is lower/greater than ν^*, the stress ratio is an increasing/decreasing function of $\dot{\gamma}$, as a consequence of condition (5.24). The limit case is $\nu = \nu^*$, where the stress ratio is constant and equal to $\tan\phi$ for all values of shear rate.
Fig. 5.11(b) shows that, at low shear rates, there is an evident separation between the two flow regimes. When $\nu < \nu_{\mathrm{rlp}}$, i.e., in the collisional regime, the normal stress continuously decreases for decreasing shear rate values, and σ scales quadratically with $\dot{\gamma}$; whereas, when $\nu > \nu_{\mathrm{rlp}}$, the normal stress approaches a constant value for $\dot{\gamma} \longrightarrow 0$. When $\nu > \nu_{\mathrm{rlp}}$ and $\dot{\gamma}$ is vanishingly small, the term relates to force chains (quasi-static contribution) dominates the material response. As the shear rate increases, all the curves collapse, independently of the imposed concentration.

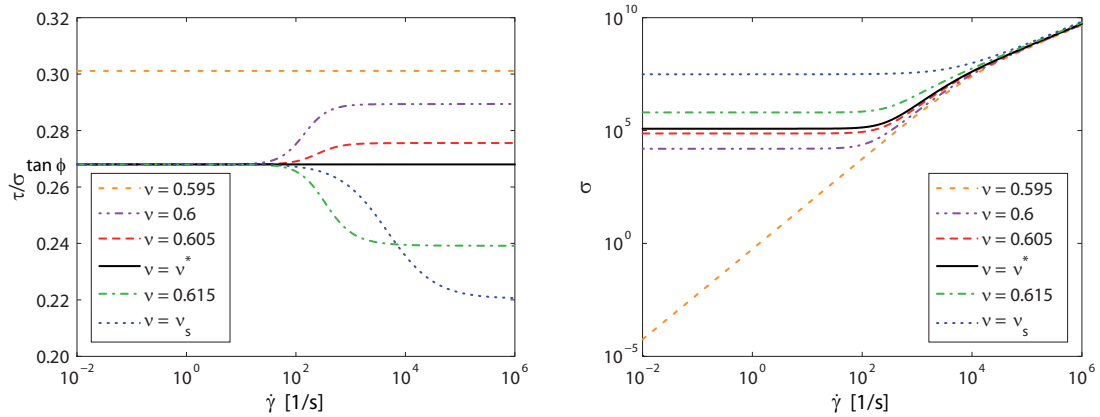

Figure 5.11.: Theoretical (a) stress ratio and (b) normal stress versus shear rate for 1 mm stainless steel spheres, at different values of concentration.

5.2.4. Stress ratio-imposed flows

The stress ratio-imposed flows are finally discussed in this Section. A stress ratio-imposed flow is obtained by keeping constant the stress ratio τ/σ, by varying the normal stress and measuring the shear rate and the concentration; then, it is a load-control test.
When $\nu > \nu_{\mathrm{rlp}}$, by using Eqs. (5.29) and (5.5a), the relation between the concentration and the normal stress reads

$$f_0 \left[1 + \frac{f_1 f_6 \left(\tan\phi - \dfrac{\tau}{\sigma} \right)}{f_1 f_6 \dfrac{\tau}{\sigma} - f_2 f_6^{1/2}} \right] = \frac{d}{K}\sigma \tag{5.30}$$

and the shear rate is given by

$$\dot{\gamma} = \sqrt{\frac{\sigma - \dfrac{K}{d} f_0}{\rho_p d^2 f_1 f_r f_6}}, \tag{5.31}$$

where f_r is evaluated by using Eq. (4.61).
In the purely collisional regime ($\nu < \nu_{\mathrm{rlp}}$), the concentration is imposed by the stress ratio through

$$\frac{f_2}{f_1 f_6^{1/2}} = \frac{\tau}{\sigma} \tag{5.32}$$

and it does not depend on the normal stress. Then, the shear rate reduces to

$$\dot{\gamma} = \sqrt{\frac{\sigma}{\rho_p d^2 f_1 f_r f_6}}. \tag{5.33}$$

The threshold between the two regimes is the stress ratio value associated with the random loose packing concentration, $(\tau/\sigma)_{\mathrm{rlp}}$, defined by Eq. (5.16).
Figs. 5.12(a) and 5.12(b) depict concentration and shear rate versus normal stress, respectively, for different stress ratio values. The curves of Fig. 5.12(a) represent the iso-stress ratio lines in the phase diagram of Section 5.2.1 (Fig. 5.3).

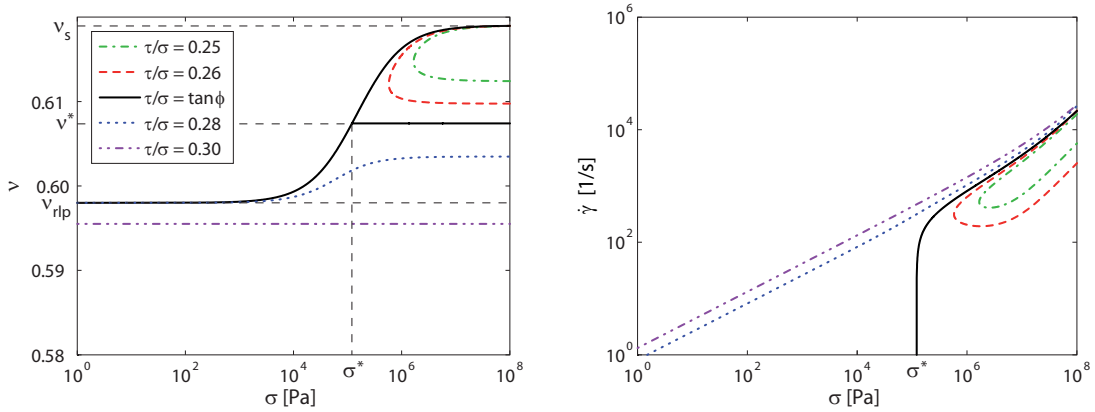

Figure 5.12.: Theoretical (a) concentration and (b) shear rate versus normal stress for 1 mm stainless steel spheres, at different values of the stress ratio.

The solid lines of Fig. 5.12(a) represent the limit case $\tau/\sigma = \tan\phi$. From Eq. (5.29), by imposing $\tau/\sigma = \tan\phi$, we obtain:

$$\left(f_2 f_6^{1/2} - f_1 f_6 \tan\phi\right)\dot{\gamma}^2 = 0, \tag{5.34}$$

which leads to two solutions:

1. $\dot{\gamma} = 0$. It is the usual definition for critical state, where the collisional contribution vanishes and the concentration is equal to ν_{cs} (5.20).

2. $f_2 f_6^{1/2} - f_1 f_6 \tan\phi = 0$, implying a concentration independent of σ and equal to ν^* (Eq. 5.25), with the shear rate given by Eq. (5.31).

When $\sigma > \sigma^*$ (corresponding to $\nu_{\mathrm{cs}} > \nu^*$ and, together, $\tau/\sigma < \tan\phi$), the steady flow undergoes a loss of uniqueness of the solution in terms of the two kinematic variables, ν and $\dot{\gamma}$.
This loss of uniqueness of the solution characterizes also all the curves at imposed stress ratio lower than $\tan\phi$. When $\tau/\sigma < \tan\phi$, there is only a limited range of the normal stress for which the steady state is possible, and, in this range, there are always two concentrations and two shear rates for a given value of σ. The range of existence of the steady state (range of possible normal stresses) increases accordingly to the imposed stress ratio, and the minimum normal stress in Fig. 5.12(a) moves on the left and tends to σ^* as τ/σ

tends to $\tan\phi$. All the curves characterized by an imposed stress ratio lower than $\tan\phi$ are enclosed between the dark gray area of the phase diagram of Fig. 5.6.
Both the theoretical concentrations are larger than ν^*, as was predicted by Eq. (5.24), and, consequently, both the steady states belong to the regime of coexistence of quasi-static and collisional stresses. Fig. 5.13 shows the same results of Fig. 5.12 for the case of $\tau/\sigma = 0.26$ only.

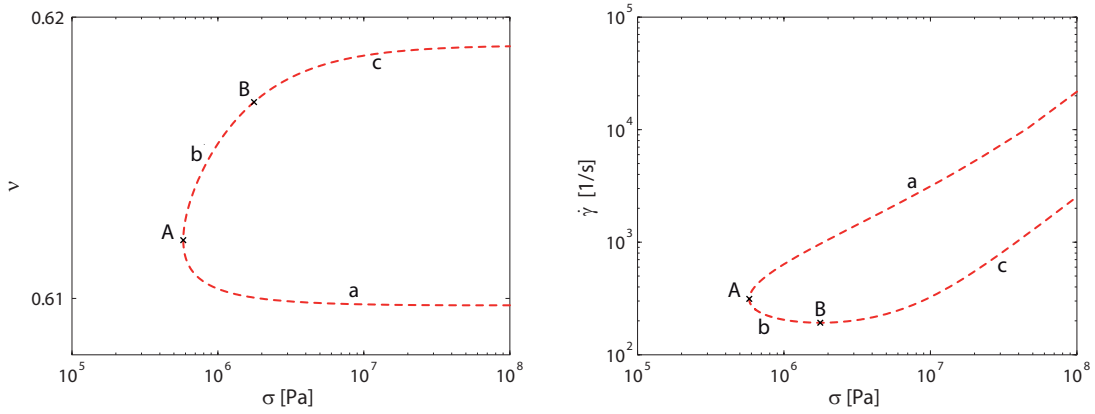

Figure 5.13.: Theoretical (a) concentration and (b) shear rate versus normal stress for $\tau/\sigma = 0.26$.

There, point A corresponds to the minimum normal stress possible at the steady state, whereas B represents the minimum shear rate. Given these two points, we can distinguish three branches of the curves:

- branch a., where an increasing normal stress induces an increasing shear rate and a decreasing concentration;
- branch b., where an increasing normal stress induces a decreasing shear rate and an increasing concentration, as commonly expected;
- branch c., where an increasing normal stress induces an increase in both shear rate and concentration.

The apparent counter-intuitive behaviour in branches a and c will require further investigations.
When $\tau/\sigma > \tan\phi$, the steady state is possible for all values of σ. Multiple solutions can still occur depending on the value of τ/σ, even in the purely collisional regime [128].
If the applied stress ratio is lower than $(\tau/\sigma)_{\mathrm{rlp}}$ (dotted line in Fig. 5.12), the solution lies in the regime of coexistence of collisions and force chains, and is characterized by an increasing shear rate, given by Eq. (5.31), and an increasing concentration (5.30), that varies between ν_{rlp} and ν^*. On the other hand, when $\tau/\sigma > (\tau/\sigma)_{\mathrm{rlp}}$, the steady state is in the collisional regime. Here the concentration is constant, as predicted by Eq. (5.32), and the shear rate is given by Eq. (5.33). The relationship between the concentration and the stress ratio in the collisional regime (5.32) is illustrated in Fig. 5.14. This shows a non-monotonic trend, which implies that, if the imposed stress ratio is in the range between the local maximum and minimum of τ/σ, there are three possible solutions in

the collisional regime (i.e., three values of concentration satisfying Eq. 5.32). The relative maximum and minimum collisional stress ratio correspond to concentrations equal to 0.49 and 0.23, respectively, employing the set of material parameter previously introduced.

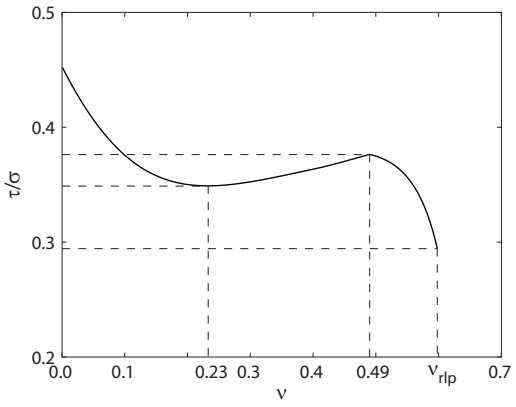

Figure 5.14.: Dependence of the stress ratio on the concentration in the purely collisional regime (5.32).

5.3. Analysis of the model using numerical and experimental results

In this Section, the present theoretical model is compared with numerical and experimental results selected from literature. First, in Section 5.3.1, the theory is validated against the experiments on incline flows of glass spheres over rigid beds obtained by Pouliquen [102]. Then, in Section 5.3.2, the theoretical model is compared with numerical simulations performed by Mitarai and Nakanishi [88] and Chialvo and Sundaresan [27] using frictionless spheres. When the particles are frictionless, the force chains can not develop and the steady flow is always in the collisional regime. The numerical data analyzed in this Section are usefull to test the collisional contributions, i.e., the modified kinetic theory. The sets of numerical simulation are obtained using nearly rigid particles; then, there is no influence of the function f_r, introduced in this work to take into account the role of stiffness during particle collisions. As a consequence, the new proposed expression of the radial distribution function is the unique modification which plays a role and can be independently tested with the support of numerical results. Finally, Section 5.3.3 is devoted to the comparison with numerical simulations obtained using frictional spheres. Chialvo and Sundaresan [27] performed 3D SS-DEM simulations using frictional but very stiff particles, as for the case of frictionless spheres, and investigated a range of concentration for which the flow is mainly in the collisional regime. These sets of numerical results allow to check the influence of the friction in the collisional terms, which in this work is accounted for through the introduction of the effective coefficient of restitution, in the form proposed by Jenkins and Zhang [60]. On the other hand, Chialvo et al. [28] performed a set of numerical simulations, using the same code as in [27], investigating the role of particle stiffness and in a wide range of concentration. In these second sets of numerical data, (i) force chains are allowed to develop, so that the definition of the quasi-static contribution can be tested; also, (ii) the range of particle stiffness investigated is large enough to check its role in the collisional contribution and to justify the introduction of the function f_r.

Several numerical simulations have been performed in the collisional regime, as well as different theoretical models have been proposed, based on the kinetic theory. As discussed in the previous Section 4.3, accordingly to the present theoretical model, the response of granular materials under steady, shearing conditions, is characterized only by collisions, i.e., the regime is purely collisional, in two cases: (i) if the particles are frictionless and (ii), for frictional particles, when the concentration is lower than the random loose packing, $\nu < \nu_{\mathrm{rlp}}$ (4.57). In the purely collisional regime, the theoretical model reduces to the collisional terms, which are here modelled using the Extended Kinetic Theory introduced by Jenkins [53], and modified as illustrated in Section 4.2.1: (i) by using a new expression of the radial distribution function, g_0 (4.28), and (ii) by taking into account the role of the particle stiffness on the contact duration during collisions through the function f_r (4.23). The modified kinetic theory here proposed will be compared, in Sections 5.3.2 and 5.3.3, with the modified kinetic theory recently proposed by Chialvo and Sundaresan [27], on the basis of their numerical results. Since the work of Chialvo and Sundaresan [27] is based on an approach similar to that of the present theory, a short summary of their model is here presented.

Accordingly to Chialvo and Sundaresan [27], and as previously discussed in Chialvo et al. [28], three flow regimes are possible in steady, simple shear flows, depending on the concentration and the shear rate: (1) a "quasi-static" regime for concentrations larger than the "critical" concentration, ν_c, in which normal and shear stresses are independent of the shear rate; (2) an "inertial" regime, for $\nu < \nu_c$, in which the normal and the shear stresses scale with the square of the shear rate: $\sigma, \tau \sim \dot{\gamma}^2$; (3) an "intermediate" regime occurring in a narrow range of concentration around ν_c in which $\sigma, \tau \sim \dot{\gamma}^{\alpha}$ with $0.5 \leq \alpha \leq 1$. Also, when the particles are very rigid, i.e., when $K \longrightarrow \infty$, only the inertial regime can be observed.

In this thesis, only two flows regime are considered possible: the collisional regime, for concentrations lower than the random loose packing, and the regime of coexistence of collisional and quasi-static contributions, for $\nu > \nu_{\mathrm{rlp}}$. In both the approches, the development of force chains which span the whole domain is related to a given value of the concentration. The critical concentration introduced and measured by Chialvo et al. [28] is related to the random close packing and the shear rigidity concentration which appear in the present model. Also, the intermediate regime of Chialvo et al. [28] is here considered as a particular case of the collisional regime or of the coexistence regime, depending only on the concentration, when the particle stiffness is large enough to influence the collisional terms through the function f_r. This difference between the two approches, together with the relationships between ν_c, ν_{rlp} and ν_{s}, will be pointed out in the upcoming Section 5.3.3, in the case of frictional spheres, given that, in the case of frictionless spheres, only the collisional regime can be observed and all the limit concentrations collapse on the random close packing concentration.

For both the cases of frictionless and frictional particles, the authors in [27] focused on the inertial regime (i.e., concentration lower than the critical value and large values of the particle stiffness) and proposed corrections to the kinetic theory of Garzó and Dufty [40] on the basis of 3D SS-DEM simulations of simple shear flows. Their modifications can be summarized as:

1. they propose a new definition of the radial distribution function;
2. they define a different expression of the correlation lenght,
3. they adopt a new expression of the effective coefficient of restitution, as a function of the interparticle friction coefficient, different from that of Jenkins and Zhang [60];

4. they introduce of a correction for the constitutive relation of the (collisional) shear stress;

5. they assume that the normal and the shear stress are unaffected by the interparticle friction coefficient; then, the effective friction coefficient appears only in the costitutive relation of the collisional rate of dissipation of fluctuating energy, $\Gamma_{\rm col}$.

In the case of frictionless particles and at concentration lower than 0.49, the model of Chialvo and Sundaresan [27] recover the Standard Kinetic Theory of Garzó and Dufty [40], as well as the present theory. But, despite the basic forms of the corrections used to achieve the improved performance all are similar to that of this thesis, the two models produces very different results. The comparison of the two models will be discussed in the following, with the support of the numerical data. But it is important to notice that a weakness of the model proposed by Chialvo and Sundaresan [27] is its limitation to the case of simple, shear flows. The extension to non homogeneous flows is prevented by the lack of the definition of the collisional energy flux, whose divergence can not be neglected in the energy balance, when non homogeneous flows are considered.

5.3.1. Comparison with experimental results on inclined planes

In this Section, the present theoretical model is compared with the experimental results on the steady and fully developed flows of glass spheres on inclined planes performed by Pouliquen [102]. In that flow configuration, the stress ratio is constant along the flow cross-section and equal to the tangent of the angle of inclination of the plane [54]. If the flow is thick enough (say, depth greater than ten diameters), the influence of the boundaries can be neglected and both the inertial number and the concentration are also constant along the cross-section of the flow [54, 70]. The incline flow configuration works therefore as a rheometer [44] and provides values of τ/σ and I that can be compared with those derived from the present theory for pressure-imposed flows.
Pouliquen [102] measured the particle depth-averaged velocity, V, and the depth, h, for different angles of inclination of the plane, θ (ranging from 22° to 28°). As shown by GDR-MiDi [44], the experimental values of the inertial number and the stress ratio correspond to $I = 5V/\left[2\left(\cos\theta\right)^{1/2} h^{3/2}\right]$ and $\tau/\sigma = \tan\theta$, respectively.
Fig. 5.15 shows the comparison of the present theory with the results inferred from the experiments of Pouliquen, in term of stress ratio against the inertial number. The experimental values reported on Fig. 5.15 (symbols) have been obtained by averaging all the data reported by Pouliquen [102] with depths greater than ten diameters. The line represents Eq. (5.15a). The model parameters which affect the theory are chosen in agreement with the experiments: Pouliquen measured the angle of repose for glass sphere, which gives $\tan\phi = 0.38$. This value of the critical friction angle corresponds, accordingly to Tab. 4.1, to an interparticle friction angle equal to $\mu = 0.5$, from which the random loose packing and the shear rigidity can be estimated, as in Tab. 4.1: $\nu_{\rm rlp} = 0.574$, $\nu_{\rm s} = 0.598$. Then, the glass density and stiffness are adopted, $\rho_p = 2500$ kg/m^3, $K = 70 \cdot 10^9$ Pa m; Jenkins [53] and Jenkins and Berzi [54] suggested to use $e = 0.6$ for dense flows of glass spheres; $a = 1.8 \cdot 10^{-6}$ is employed as for steel spheres. Finally, in the experiments of Pouliquen, $\sigma/(K/d)$ is of order 10^{-8}, then the term f_r is about one, as shown in Section 5.2.2, and does not influence the collisional contributions.

The agreement between the theoretical and the experimental results is remarkable, especially because there is no tuning of the model parameters. It is also worth emphasizing

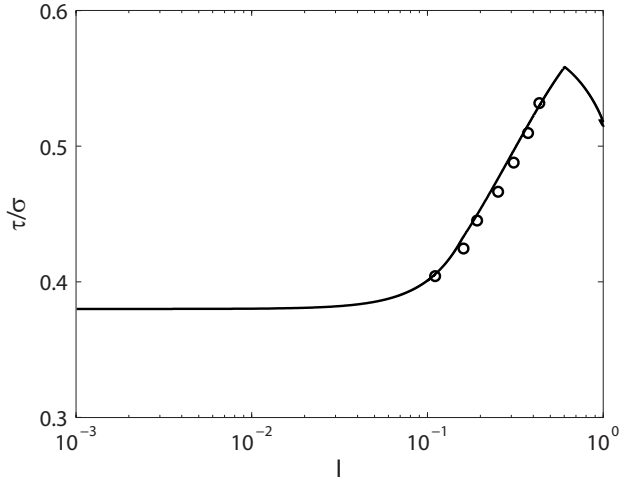

Figure 5.15.: Predicted (line, Eq. 5.15a with $\sigma/(K/d) = 10^{-8}$) and measured (symbols, [102]) values of the stress ratio versus the inertial number for glass spheres ($\rho_p = 2500$ kg/m^3, $K = 70 \cdot 10^9$ Pa m, $\tan\phi = 0.38$, $\nu_{\mathrm{rlp}} = 0.574$, $\nu_{\mathrm{s}} = 0.598$, $e = 0.6$, $a = 1.8 \cdot 10^{-6}$).

that the constitutive relation for the frictional component of the normal stress holds, in principle, for steel spheres. As already stated, the theories of Johnson and Jackson [63, 64] and Savage [109] would predict a constant stress ratio, independent of the inertial number, in contrast with the experiments.

5.3.2. Comparison with numerical simulations of frictionless, hard spheres

In this Section, the numerical results obtained by Mitarai and Nakanishi [88] and Chialvo and Sundaresan [27] on frictionless spheres are compared with the present theory.
When the particles are frictionless, the steady flow is in the collisional regime and, in simple shear flows, the governing equations can be summarized as

$$\frac{T}{d^2\dot{\gamma}^2} = f_6, \tag{5.35}$$

$$\frac{\sigma}{\rho_p d^2\dot{\gamma}^2} = f_1 f_r f_6, \tag{5.36}$$

$$\frac{\tau}{\sigma} = \frac{f_2}{f_1 f_6^{1/2}}. \tag{5.37}$$

The model parameters which affect Eqs. (5.35)-(5.37) are the shear rigidity concentration, ν_{s}, and the coefficient of restitution, e. For frictionless particles, $\nu_{\mathrm{s}} = \nu_{\mathrm{rcp}} = 0.636$ (see Tab. 4.1) and the (effective) coefficient of restitution coincides with the normal coefficient of restitution. Then, no model parameters are to be set.
Mitarai and Nakanishi [88] performed Event-Driven simulations of simple shear flows of hard spheres, whereas Chialvo and Sundaresan [27] used a Soft-Spheres Discrete Element Method code with a linear spring-dashpot model. In both works, the Lees-Edwards [73] boundary conditions were implemented in the shearing direction, in order to allow for the system to remain homogeneous during the shearing. In the ED numerical simulations performed by Mitarai and Nakanishi [88], the spheres are hard, while Chialvo and Sundaresan [27] employed a finite but very high value of K, such as the finite stiffness plays

no role ($K/(\rho_p d^3\dot{\gamma}^2) \longrightarrow \infty$). According to Eq. (5.6), the function f_r, which represents the first modification to the kinetic theory introduced in this work, is equal to 1 and does not affect the system. Then, this two sets of numerical simulations can be used to validate the second modification here proposed, i.e., the new expression of the radial distribution function g_0 (4.28). Also, the form of the correlation length [11], which, in simple shear flows, is given by Eq. (5.4), can be tested.

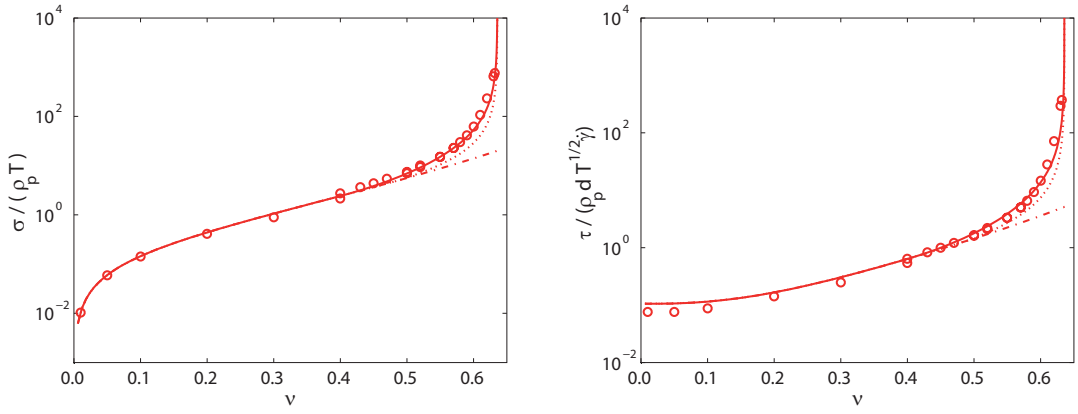

(a) (b)

Figure 5.16.: Numerical (symbols, after Mitarai and Nakanishi [88] and Chialvo and Sundaresan [27]) quantities $\sigma/(\rho_p T)$ (a) and $\tau/\left(\rho_p d T^{1/2}\dot{\gamma}\right)$ (b) as functions of the concentration for $e = 0.70$ and $\mu = 0$, compared with the theoretical expression of f_1 and f_2 (solid lines, Eqs. 4.46 and 4.47). The dot-dashed lines and the dotted lines represent the present theory when the radial distribution function is that proposed by Carnahan and Starling [25], (4.26), and Torquato [118], (4.27), respectively.

To check the validity of the proposed expression of the radial distribution function, Eq. (4.28), we consider the constitutive relations of the collisional stresses, which, for plane shear flows, are given by Eqs. (4.42)-(4.43). Here, f_1 and f_2 are solely functions of the concentration through g_0 and are expressed by Eqs. (4.46) and (4.47), respectively. In the collisional regime, when $f_r = 1$, f_1 and f_2 can be rewritten as

$$f_1 = \frac{\sigma}{\rho_p T}, \tag{5.38}$$

$$f_2 = \frac{\tau}{\rho_p d T^{1/2}\dot{\gamma}}. \tag{5.39}$$

By using Eqs. (5.38)-(5.39), f_1 and f_2 can be inferred by the numerical simulations once σ, T, τ and $\dot{\gamma}$ are measured. Figs. 5.16(a) and 5.16(b) depict, respectively, the quantities $\sigma/(\rho_p T)$ and $\tau/\left(\rho_p d T^{1/2}\dot{\gamma}\right)$ as functions of the concentration, where σ, T, τ and $\dot{\gamma}$ are those measured by Mitarai and Nakanishi [88] and Chialvo and Sundaresan [27], when $e = 0.70$, together with the theoretical expressions of f_1 and f_2, Eqs. (4.46) and (4.47), with g_0 given by Eq. (4.28) (solid lines). Also plotted in Fig. 5.16, are the predictions of the present theory if the Carnahan and Starling's [25] (4.26) (dot-dashed lines) and the Torquato's [118] (4.27) (dotted lines) expressions of g_0 are employed.
The agreement between the numerical data and the theoretical expressions of f_1 and f_2 is remarkable when Eq. (4.28) is used for g_0. Similar agreement is obtained for other

values of the coefficient of restitution. The comparison of Eqs. (4.46) and (4.47) with the measured quantities $\sigma/(\rho_p T)$ and $\tau/\left(\rho_p d T^{1/2}\dot{\gamma}\right)$ for other values of the coefficient of restitution is reported in Appendix B. If the Carnahan and Starling's form [25] of g_0 is used into the theoretical functions f_1 and f_2, the asymptotic behavior of both $\sigma/(\rho_p T)$ and $\tau/\left(\rho_p d T^{1/2}\dot{\gamma}\right)$ is not reproduced. Also, the numerical data are underpredicted at large concentrations ($\nu > 0.49$), if the Torquato's expression [118] is adopted.

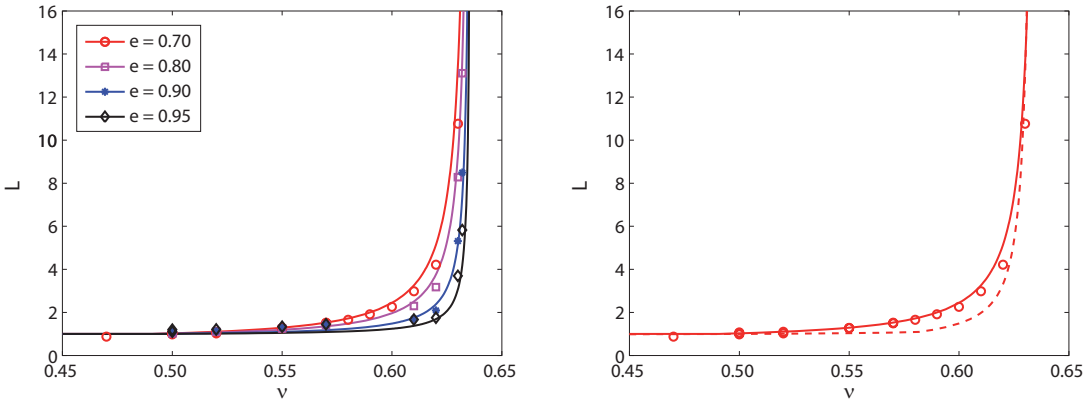

(a) (b)

Figure 5.17.: (a) Numerical (symbols, after Mitarai and Nakanishi [88] and Chialvo and Sundaresan [27]) and theoretical (lines, Eq. 5.4) correlation length as a function of the concentration, for different values of the coefficient of restitution, when $\mu = 0$. (b) Same as in Fig. 5.17(a) for the case $e = 0.7$. The dashed line represents the theory of Chialvo and Sundaresan [27].

For simple shear flows, when $f_r = 1$, using the definition of the collisional rate of dissipation of fluctuating energy, Γ_{col}, Eq. (4.44), into the energy balance, Eq. (5.1), gives for the correlation length

$$L = \frac{f_3 T^{3/2}}{\tau\dot{\gamma}}. \tag{5.40}$$

In Fig. 5.17(a) the quantity $f_3 T^{3/2}/(\tau\dot{\gamma})$ is plotted as a function of the concentration, where τ and T are those measured by Mitarai and Nakanishi [88] and Chialvo and Sundaresan [27] in their numerical simulations, while f_3 is evaluated from the expression (4.48), using Eq. (4.28) and the measured values of the concentration. There, the solid lines represent the theoretical expression of the correlation length, Eq. (5.4). The theoretical correlation length is in quantitatively agreement with the numerical results. Fig. 5.17(b) depicts, for comparison, the correlation length obtained from the modification of the kinetic theory suggested by Chialvo and Sundaresan [27] when $e = 0.7$.

The dimensionless quantities $T/\left(d^2\dot{\gamma}^2\right)$ and $\sigma/\left(\rho_p d^2\dot{\gamma}^2\right)$, obtained from the numerical simulations of Mitarai and Nakanishi [88] and Chialvo and Sundaresan [27], are shown in Fig. 5.18(a) and 5.18(b), respectively, for different values of the coefficient of restitution. The lines represent Eqs. (5.35) and (5.36), with the radial distribution function given by Eq. (4.28) and the correlation lenght given by Eq. (5.4). For all the values of the coefficient of restitution, the scaled normal stress shows a decreasing behavior at low concentrations ($\nu < 0.2$), then σ increases with ν and diverges at the random close packing concentration (Fig. 5.18(b)). Also the scaled granular temperature presents a non-monotonic behavior:

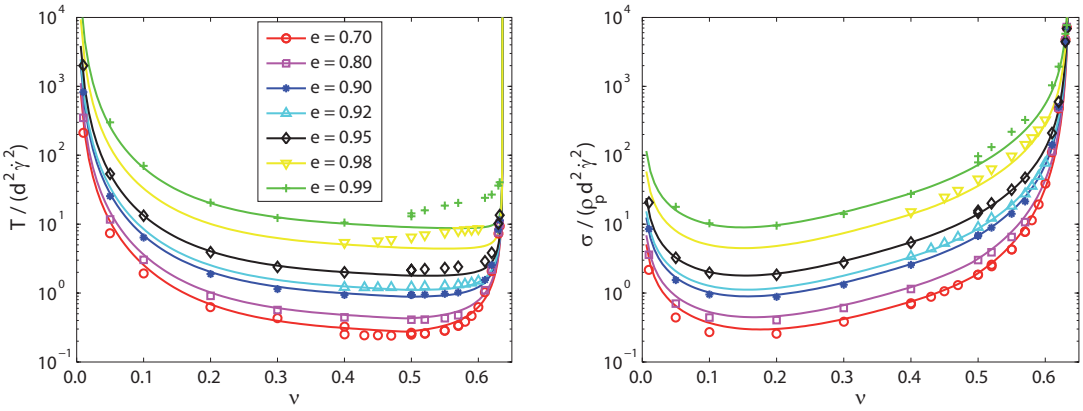

Figure 5.18.: Numerical (symbols, after Mitarai and Nakanishi [88] and Chialvo and Sundaresan [27]) and theoretical (lines, Eqs. 5.35 and 5.36) scaled granular temperature (a) and normal stress (b) as functions of the concentration, for different values of the coefficient of restitution, when $\mu = 0$.

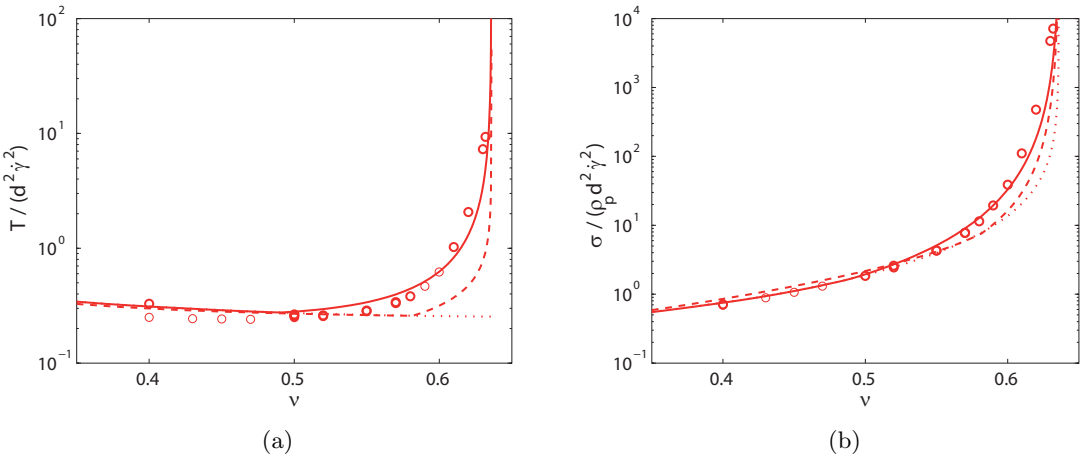

Figure 5.19.: Same as in Fig. 5.18 for the case $e = 0.7$. The dotted line represents the present theory when $L = 1$, while the dashed line the theory of Chialvo and Sundaresan [27].

it drops at very small ν, continues to decreases with the concentration and then becomes an increasing function at large values of ν (Fig. 5.18(a)).
Except for large coefficients of restitution ($e > 0.95$), $T/\left(d^2\dot{\gamma}^2\right)$ and $\sigma/\left(\rho_p d^2\dot{\gamma}^2\right)$ are well predicted by kinetic theory in the entire range of concentration, if the expressions (4.28) for g_0 and (5.4) for L are adopted. The poor agreement in the case of nearly elastic particles, although rather unexpected, is clearly limited to concentrations larger than 0.49. This is an indication that, for nearly elastic particles, Eq. (4.28) is not accurate. Replacing Eq. (4.28) with Eq. (4.27) would allow a good fitting also for the case of nearly elastic particles ($e > 0.95$). In most realistic cases, though, the coefficient of restitution is lower than 0.95, so that this discrepancy is not crucial.
Figs. 5.19(a) and 5.19(b) depict, for the case $e = 0.7$, the comparison of the theory

with (i) the predictions of the present theory if the breaking of the molecular chaos is not accounted for (i.e., $L = 1$) and (ii) the predictions from the theory of Chialvo and Sundaresan [27]. All the models collapse at low concentration, where the radial distribution function is well predicted by the Carnahan and Starling [25] expression, Eq. (4.26). If the role of correlated motion among particles is disregarded (i.e., $L = 1$), the granular temperature results a monotonically decreasing function of the concentration (dotted line), in complete contrast with the numerical measurements (Fig. 5.19(a)). This disagreement in T generates underpredictions of the normal stress, according to the constitutive relation for σ, Eq. (4.42) (Fig. 5.19(b)). The model of Chialvo and Sundaresan [27] underpredicts the normal stress and, mostly, the granular temperature, at large concentrations. Using the proposed g_0, Eq. (4.28), in the Extended Kinetic Theory, and the expression of the correlation length derived by Berzi [11], Eq. (5.4), allows to notably improve the prediction of T and σ, in the whole range of concentration. The comparisons of the numerical data and the theories when using different values of the coefficient of restitution confirm the best agreement of the proposed model.

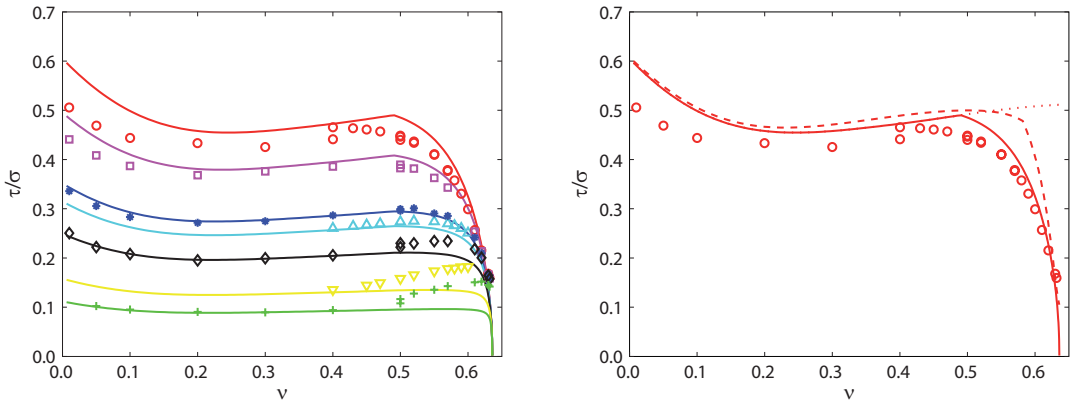

Figure 5.20.: (a) Numerical (symbols, after Mitarai and Nakanishi [88] and Chialvo and Sundaresan [27]) and theoretical (lines, Eq. (5.37)) stress ratio as a function of the concentration, for different values of the coefficient of restitution (see legend in Fig. 5.18), when $\mu = 0$. (b) Same as in Fig. 5.20(a) for the case $e = 0.7$. The dotted line represents the present theory when $L = 1$, while the dashed line the theory of Chialvo and Sundaresan [27].

Finally, in Fig. 5.20(a) the measured values of the stress ratio are compared with the theoretical predictions Eq. (5.37). The theoretical curves are in very good agreement with the numerical data in the range of coefficient of restitution 0.7-0.95, capturing the non-monotonic trend and the close-packed limit of τ/σ. When $e > 0.95$, the stress ratio is underpredicted as well as the scaled granular temperature and the scaled normal stress. The present theory reproduces betten than the theory in [27] the behavior of τ/σ, as can be observed in Fig. 5.20(b) for the case $e = 0.7$. In particular, Fig. 5.20(a) indicates that there is no need to modify the constitutive relation of the shear stress of kinetic theory, at least if the particles are sufficiently inelastic [11]. The presence of the correlation length into the energy dissipation rate makes the predicted stress ratio a decreasing function of the concentration in the dense regime, whereas using $L = 1$ produces an increase of the

stress ratio (dotted line in Fig. 5.20(b)). The overprediction of τ/σ at very low concentration ($\nu < 0.2$) for $e = 0.7$, common to both the theories, is at present puzzling.

5.3.3. Comparison with numerical simulations of frictional spheres

The comparison of the present theoretical model with numerical results for frictional spheres is discussed in this Section. Here, two sets of simulations will be analyzed. In both the works, concentration-imposed, steady, simple shear flows of frictional spheres are performed using the same 3D SS-DEM code, but considering differently the role of the particles stiffness. In [27], the range of concentration investigated is such that the flows are mostly in the collisional regime. Also, as for the frictionless spheres, Chialvo and Sundaresan [27] employed a very high values of K, disregarding the role of particle stiffness. These numerical results are useful to check the role of interparticle friction in the collisional contribution. On the other hand, Chialvo et al. [28] analyzed the role of particle stiffness on the different flows regimes and investigated a large range of imposed concentration. Then, the numerical simulations carried out in [28] allows to investigate (i) the validity of the function f_r in the collisional terms, (ii) the form of the quasi-static contribution to the stresses.

Frictional, hard spheres and collisional regime

The governing equations for steady, simple shear flows of frictional particles can be written as

$$\frac{T}{d^2\dot{\gamma}^2} = f_6, \tag{5.41}$$

$$\frac{\sigma}{\rho_p d^2\dot{\gamma}^2} = f_1 f_r f_6 + f_0 \frac{K}{\rho_p d^3\dot{\gamma}^2}, \tag{5.42}$$

$$\frac{\tau}{\sigma} = \frac{f_0 \dfrac{K}{\rho_p d^3\dot{\gamma}^2} + f_1 f_r f_6}{f_0 \dfrac{K}{\rho_p d^3\dot{\gamma}^2} \tan\phi + f_2 f_r f_6^{1/2}}, \tag{5.43}$$

The equations for the scaled normal stress and the stress ratio, Eqs. (5.42)-(5.43), reduce to those valid in the collisional regime, Eqs. (5.36)-(5.37), only when $\nu < \nu_{\mathrm{rlp}}$, i.e., $f_0 = 0$. In principle, if $\nu > \nu_{\mathrm{rlp}}$, the dimensionless quantities $\sigma/\left(\rho_p d^2\dot{\gamma}^2\right)$ and τ/σ are not solely functions of the concentration, but depend also on the dimensionless particle stiffness $K/\left(\rho_p d^3\dot{\gamma}^2\right)$, whereas the scaled granular temperature, $T/\left(d^2\dot{\gamma}^2\right)$, depends only on the concentration through the function f_6.
Chialvo and Sundaresan [27] performed 3D SS-DEM simulations of steady, simple shear flows of frictional spheres. The aim of the authors was to investigate the behavior of the granular material in the 'inertial' regime. According to them, the 'inertial' regime can be observed using very hard particle, characterized by stiffness $K \longrightarrow \infty$. Conversely, in the present theory, only two flow regimes are supposed to be possible: the collisional regime ($\nu < \nu_{\mathrm{rlp}}$) and the regime of coexistence of collisional and quasi-static contributions ($\nu > \nu_{\mathrm{rlp}}$). The transition among the two regimes is governed solely by the concentration. The numerical simulations in [27] have been performed: using large values of $K/\left(\rho_p d^3\dot{\gamma}^2\right)$ (for which, acconding to Eq. (5.6), the function f_r tends to one); setting the tangential coefficient of restitution, e_t, equal to 1; varying the normal coefficient of restitution

($e_n = 0.7, 0.8, 0.9, 0.95, 0.99$) and the interparticle friction angle ($\mu = 0.1$ and 0.5). Hence, according to Tab. 4.1, here we use: (1) for $\mu = 0.1$: $\nu_s = 0.613$, $\tan\phi = 0.268$, $\nu_{rlp} = 0.598$; (2) for $\mu = 0.5$: $\nu_s = 0.598$, $\tan\phi = 0.382$, $\nu_{rlp} = 0.585$. Also, $a = 1.8 \cdot 10^{-6}$ is adopted, as for steel spheres, and the effective coefficient of restitution is computed using Eq. (3.45), with $e_t = 1$ and the choosen values of e_n and μ. Finally, the data have been obtained for concentrations lower than 0.61, for the case $\mu = 0.1$, and lower than 0.585 for the case $\mu = 0.5$; then, just a few measurements lie in the narrow window of the regime of coexistence of collisional and quasi-static contributions, i.e., $\nu_{rlp} < \nu < \nu_s$, in both the sets of simulations. As a consequence, the most of the data are in the collisional regime, where the present theory reduces to the modified kinetic theory.

(1) Slightly frictional particles

Fig. 5.21 shows the measured dimensionless quantities $T/\left(d^2\dot{\gamma}^2\right)$ and $\sigma/\left(\rho_p d^2\dot{\gamma}^2\right)$, obtained from the numerical simulations of Chialvo and Sundaresan [27] when using $\mu = 0.1$, for different values of the normal coefficient of restitution. The lines represent the present theory, Eqs. (5.41) and (5.42) with g_0 and L given by Eqs. (4.28) and (5.4), respectively.

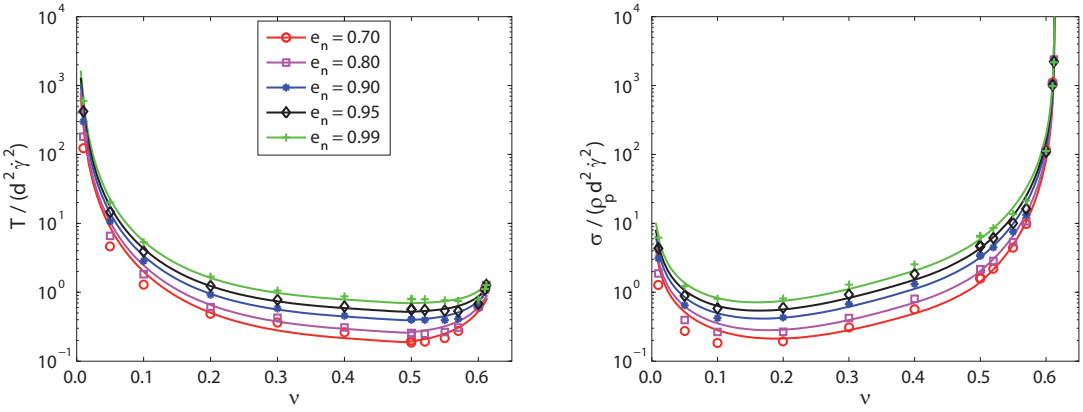

Figure 5.21.: Numerical (symbols, Chialvo and Sundaresan [27]) and theoretical (lines, Eqs. 5.41 and 5.42) scaled granular temperature (a) and normal stress (b) as functions of the concentration, for different values of the normal coefficient of restitution, when $\mu = 0.1$ and $e_t = 1$.

The trends of both $T/\left(d^2\dot{\gamma}^2\right)$ and $\sigma/\left(\rho_p d^2\dot{\gamma}^2\right)$ are similar to the case of frictionless spheres, and both the variables diminish with increasing interparticle friction coefficient. The theory predicts extremely well the measurements of the scaled granular temperature and the scaled normal stress, for all the values of the normal coefficient of restitution (for the largest value of the normal coefficient of restitution, $e_n = 0.99$, the effective coefficient of restitution is equal to 0.87). It is important to notice that there is no tuning of the model parameters. The disagreement between the theory and the data in the dilute regime, $\nu < 0.2$, quantitatively increases with the interparticle friction coefficient.
In Fig. 5.22(a) the stress ratio is plotted as a function of the concentration, for different values of the normal coefficient of restitution. Here, the symbols represent the numerical measurements of Chialvo and Sundaresan [27] and the lines Eq. (5.43), with $f_r = 1$.

The stress ratio is well predicted for $e_n = 0.7$ and 0.8 ($e = 0.58$ and 0.68, respectively), but slightly underestimated for larger values of e_n, especially at large concentrations. Nevertheless, the theory is able to reproduce the change of concavity of τ/σ which occurs, independently of the coefficient of restitution, at the freezing point, $\nu_f = 0.49$. Whereas, the modified kinetic theory of Chialvo and Sundaresan [27] predicts a larger value of concentration at which the decrease in τ/σ starts to occur, as shown in Fig. 5.22(b) for the case $e_n = 0.7$ ($e = 0.58$). At very low concentrations, $\nu < 0.2$, the measured stress ratio is strongly over predicted by both the theories when $e_n = 0.7$, as in the case of frictionless spheres.

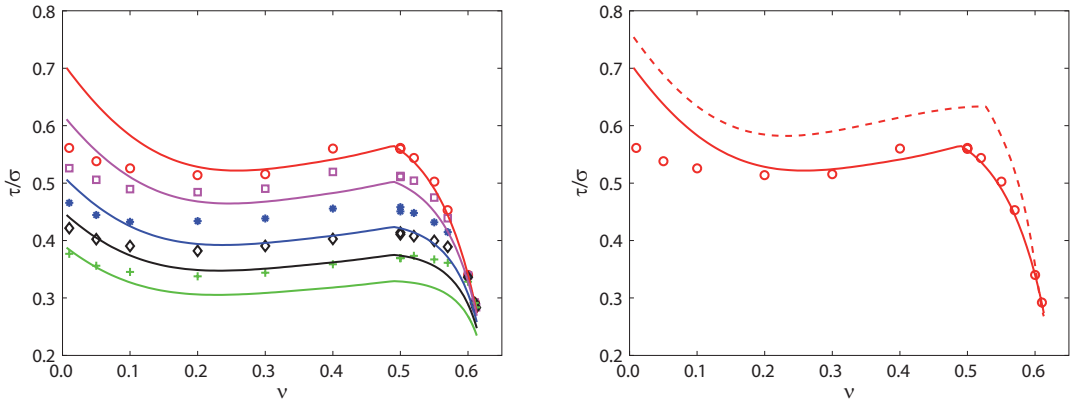

(a) (b)

Figure 5.22.: (a) Numerical (symbols, Chialvo and Sundaresan [27]) and theoretical (lines, Eq. 5.43) stress ratio as a function of the concentration, for different values of the normal coefficient of restitution (see legend in Fig. 5.21), when $\mu = 0.1$ and $e_t = 1$. (b) Same as in Fig. 5.22(a) for the case $e_n = 0.7$. The dashed line represents the theory of Chialvo and Sundaresan [27].

Finally, the measured correlation length, computed using Eq. (5.40), is illustrated in Fig. 5.23(a), for different values of the normal coefficient of restitution, together with the predictions given by Eq. (5.4). Also, a comparison with the correlation length used in the kinetic theory of Chialvo and Sundaresan [27] is depicted in Fig. 5.23(b) for the case $e_n = 0.7$. The numerical data show that the correlation length does not diverge at the shear rigidity concentration (0.613 for $\mu = 0.1$) but at the random close packing, 0.636, and is not affected by the interparticle friction. This evidence justifies the form of L given in Eq. (5.4), which depends on the concentration throughtout the function $\tilde{g}_0$, diverging at ν_{rcp}.

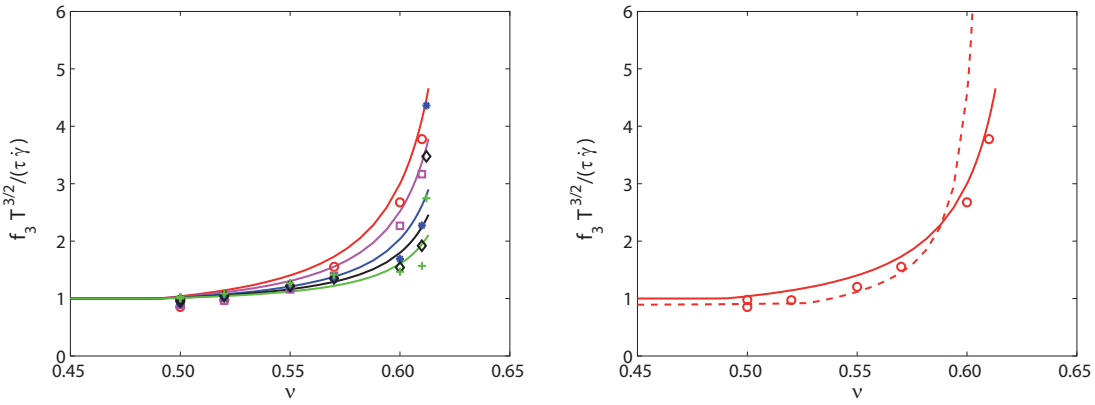

(a) (b)

Figure 5.23.: (a) Numerical (symbols, Chialvo and Sundaresan [27]) and theoretical (lines, Eq. 5.4) correlation length as a function of the concentration, for different values of the normal coefficient of restitution (see legend in Fig. 5.21), when $\mu = 0.1$ and $e_t = 1$. (b) Same as in Fig. 5.23(a) for the case $e_n = 0.7$. The dashed line represents the theory of Chialvo and Sundaresan [27].

(2) Very frictional particles

The comparison between the theoretical model and the SS-DEM results of Chialvo and Sundaresan [27] for $\mu = 0.5$ is shown in Fig. 5.24 in terms of scaled granular temperature (a), scaled normal stress (b) and stress ratio (c).
Predictions of the theory strongly disagree with the numerical results for so frictional particles. For all the values of the normal coefficient of restitution, both the granular temperature and the normal stress are underestimated at concentrations larger than 0.2, and the discrepancies amplify as the normal coefficient of restitution increases. On the other hand, the stress ratio is quite well predicted only at large concentrations ($\nu > 0.5$). The strong discrepancy between the theory and the numerical results, for all the quantities $T/\left(d^2\dot{\gamma}^2\right)$, $\sigma/\left(\rho_p d^2\dot{\gamma}^2\right)$ and τ/σ, is probably related to the effective coefficient of restitution here adopted. The effective coefficient of restitution accounts for the total energy loss during a collision, due to both inelasticity and friction, and, accordingly to the model of Jenkins and Zhang [60], it increases with the interparticle friction coefficient. The plots of scaled granular temperature (Fig. 5.24(a)) reveal that, for $\mu = 0.5$, the produced increase in the energy dissipation is too high, such that, the predicted granular temperature is lower than the measured one (for $\nu > 0.2$). The computed effective coefficients of restitution are in fact very small compared with the normal ones, such as even very elastic particles, $e_n = 0.99$, loose the 30% of their energy when collide due to the friction ($e = 0.69$), whereas for $e_n = 0.7$ we obtain $e = 0.41$. The expression of Jenkins and Zhang [60] (3.45) was derived under the assumption of slightly frictional spheres, for which the balance equations for the rotational momentum and energy can be considered satisfied in approximate ways. Evidently, this assumption does not hold for large values of the interparticle friction coefficient and it is necessary to solve the balance equations and boundary conditions for the mean spin and the rotational fluctuation energy in order to correctly account for the friction.

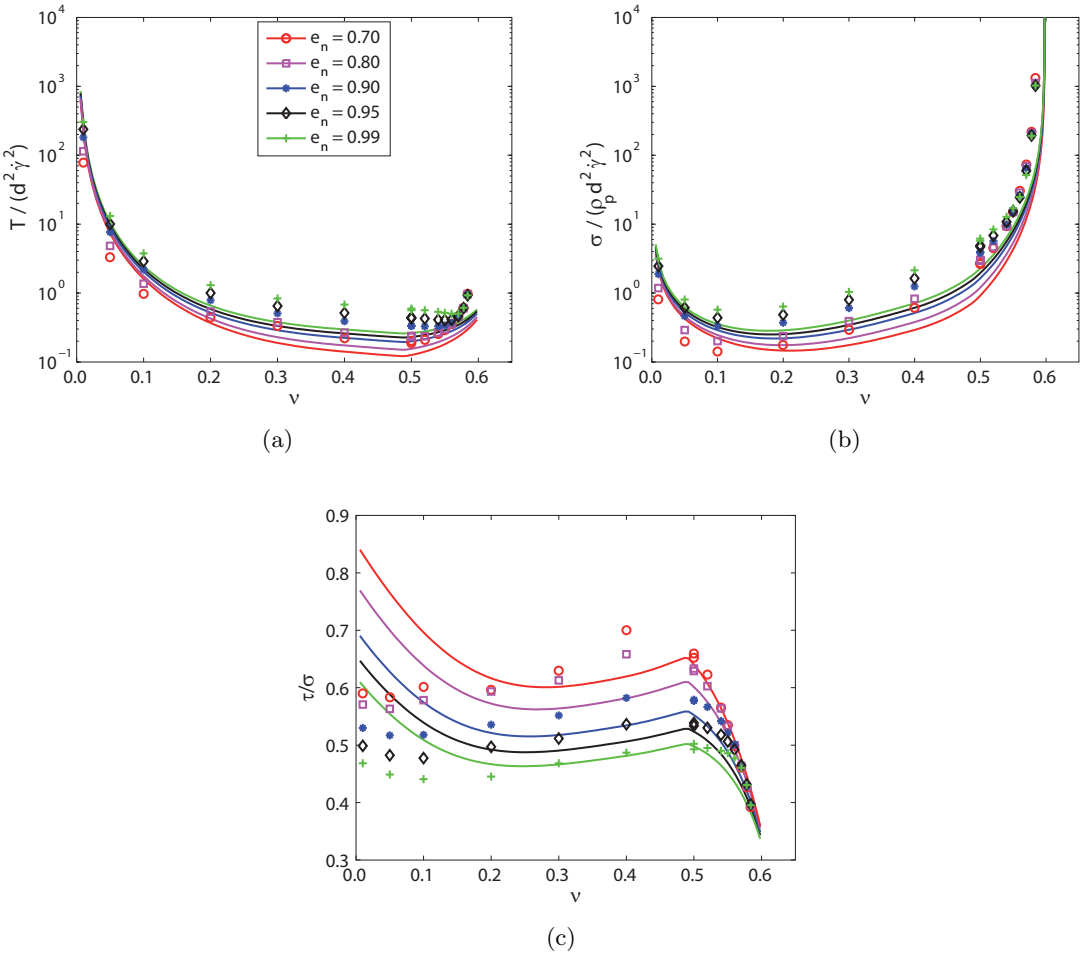

Figure 5.24.: Numerical (symbols, Chialvo and Sundaresan [27]) and theoretical (lines, Eqs. 5.41, 5.42 and 5.43) scaled granular temperature (a), normal stress (b) and stress ratio (c) as functions of the concentration, for different values of the coefficient of restitution, when $\mu = 0.5$ and $e_t = 1$.

Frictional spheres and regime of coexistence of collisional and quasi-static contributions

In this Section, the present theory is compared with the numerical simulations of concentration-imposed simple shear flows of frictional spheres, performed by Chialvo et al. [28]. The authors employed the same 3D SS-DEM code as in Chialvo and Sundaresan [27], analyzing the role of the particle stiffness over a large range of concentrations. They used spheres characterized by coefficients of normal and tangential restitution equal to $e_n = 0.7$ and $e_t = 1$, respectively, and two different values of the interparticle friction coefficient, 0.1 and 0.5. Hence, there we use: (a) for $\mu = 0.1$: $e = 0.58$, $\nu_s = 0.613$, $\tan\phi = 0.268$, $a = 1.8 \cdot 10^{-6}$, $\nu_{rlp} = 0.598$; (b) for $\mu = 0.5$: $e = 0.41$, $\nu_s = 0.598$, $\tan\phi = 0.382$, $a = 1.8 \cdot 10^{-6}$, $\nu_{rlp} = 0.585$. The particle properties, d, ρ_p and K are used to make dimensionless all the quantities.
Fig. 5.25 shows the measured scaled normal stress, $\sigma d/K$, versus the scaled shear rate, $\dot{\gamma} d\,(\rho_p d/K)^{1/2}$, at various values of the concentration for (a) $\mu = 0.1$ and (b) $\mu = 0.5$.

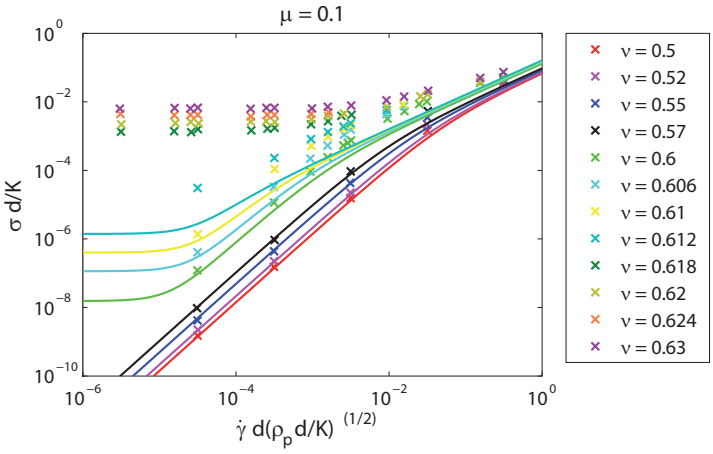

(a)

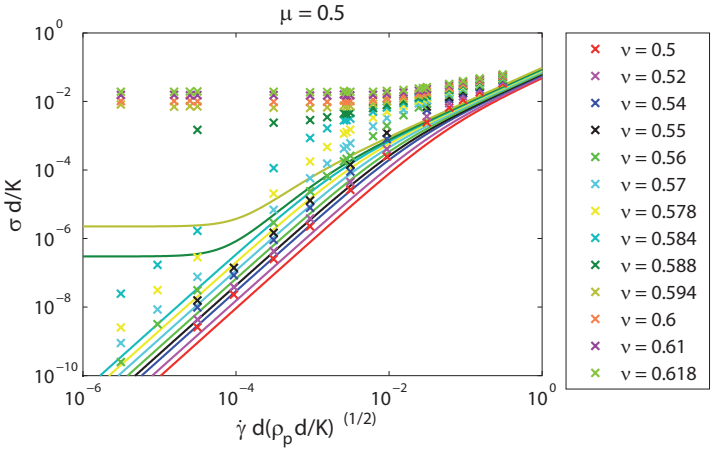

(b)

Figure 5.25.: Numerical (symbols, Chialvo et al. [28]) scaled normal stress $\sigma d/K$ as a function of the scaled shear rate $\dot{\gamma} d \left(\rho_p d/K\right)^{1/2}$ for different values of the imposed concentration, when $\mu = 0.1$ (a) and $\mu = 0.5$ (b), compared with the theoretical expression (lines, Eq. (5.44)).

The numerical measurements show that, at low shear rates, there is an evident separatrix occuring at a certain "critical value" of concentration. For concentrations lower than the critical threshold, $\sigma d/K$ continuously decreases for decreasing shear rate, and, in particular, it scales quadratically with $\dot{\gamma} \left(\rho_p d^3/K\right)^{1/2}$, whereas the scaled normal stress approaches a constant value at concentration larger than the critical threshold. As the shear rate increases, all the curves approach a shared asymptote. Considering a curve characterized by a concentration lower than the critical value, it presents a change of slope for increasing shear rate, passing from $\sigma d/K \sim \left[\dot{\gamma} \left(\rho_p d^3/K\right)^{1/2}\right]^2$ to $\sigma d/K \sim \left[\dot{\gamma} \left(\rho_p d^3/K\right)^{1/2}\right]^\alpha$ with $\alpha < 2$. On the other hand, curves characterized by concentrations greater than the critical value, show no rate dependence al low shear rates and gradually become rate-dependent for increasing shear rate. The constant values reached at vanishingly small shear rate increase with the imposed concentration. The same distinctive characteristics of concentration-imposed simple shear flows have been observed also by other authors [6, 24, 61].

As mentioned in the previous Section, Chialvo and Sundaresan [27] identified three flow regimes on the basis of the numerical results: the quasi-static regime, characterized by rate-independent normal stress; the inertial regime, where σ scales quadratically with the shear rate; and the "intermediate" regime, where $\sigma \sim \dot{\gamma}^{\alpha}$, with $\alpha < 2$. Also, the authors related the phase transition among the distinct regimes to both the concentration and the scaled shear rate.
The comparison of the proposed theoretical model with the numerical data is depicted in Figs. 5.25, where the lines represent the theoretical expression of the scaled normal stress, which, using Eq. (5.5a), reads

$$\frac{\sigma d}{K} = f_0 + f_1 f_r f_6 \frac{\rho_p d^3 \dot{\gamma}^2}{K}, \tag{5.44}$$

The comparison with the numerical results clearly points out that the proposed model exhibits several weaknesses:

1. the theory is unable to reproduce steady flows at concentrations larger than the shear rigidity concentration, whereas the numerical results show that steady, concentration-imposed flows are possible also at $\nu > \nu_{\mathrm{s}}$;

2. in the regime where force chains span the whole domain of the system ($\nu_{\mathrm{rlp}} < \nu < \nu_{\mathrm{s}}$), the scaled normal stress is underpredicted by the theory. In particular, the discrepancies increase with the friction, the imposed concentration and for decreasing shear rates;

3. when the particles are very frictional ($\mu = 0.5$, Fig. 5.25(b)), the scaled normal stress is underestimated also in the collisional regime ($\nu < \nu_{\mathrm{rlp}}$), especially at large values of the imposed concentration.

Nevertheless, the model is able to capture the characteristic features of concentration-imposed simple shear flows. In particular, if the "critical" value is interpreted as the random loose packing concentration, the collisional regime and the regime of coexistence of collisional and quasi-static contribution can be recognized in the two distinct sets of curves.
In the collisional regime ($\nu < \nu_{\mathrm{rlp}}$), as shown in Section 5.2, when the scaled particle stiffness $K/\left(\rho_p d^3 \dot{\gamma}^2\right)$ is large, function f_r does not affect the collisional contribution and the normal stress scales quadratically with the shear rate. When the scaled particle stiffness decreases, i.e., for increasing $\dot{\gamma} d \left(\rho_p d/K\right)^{1/2}$, function f_r plays a role and the normal stress is given by Eq. (5.36). As a consequence, $\sigma d/K$ scales less than quadratically with the scaled shear rate.
On the other hand, in the regime where both collisions and force chains are present ($\nu > \nu_{\mathrm{rlp}}$), for vanishingly small shear rate the collisional contribution disappears and the normal stress is given by the rate-independent quasi-static part, Eq. (4.55). Then, the theory reproduces the asymptotic behavior of the normal stress at vanishingly small shear rates. For increasing shear rates, the normal stress remains almost constant and equal to the quasi-static contribution until the collisional, rate-dependent term becomes comparable to the quasi-static one. For large enough values of the scaled shear rate, the two contributions are comparable and the resulting scaled normal stress is an increasing function of the scaled shear rate. Also, at large shear rates, the collisional contribution dominates and the curves approach the same asymptote of those of the purely collisional regime.

The reasons to the "quantitative" discrepancies between the model and the data have to be sought among the assumptions made when defining each term which affects the theory. The underprediction of the scaled normal stress in the case of very frictional particles ($\mu = 0.5$) has been highlighted in the previous Section, and is attributable to the use of a "wrong" effective coefficient of restitution.
A new interesting feature revealed by these sets of simulations concerns the role of particle stiffness in the collisions. The collisional contribution is modeled using the kinetic theory, and, as highlighted in Section 3, Standard Kinetic Theories assume several semplifications in solving the flow dynamics. In this work, the Extended Kinetic Theory proposed by Jenkins [52, 53] is adopted, then the molecular chaos hypotesis is overcome; also, the use of the effective coefficient of restitution allows to consider frictional particles. Finally, with the introduction of the function f_r here proposed, the time duration of a collision is accounted for and the collisions are no longer assumed to be instantaneous. Nevertheless, two strong assumptions still remain: binary collisions and constant coefficient of restitution. When the particle stiffness is small, two effects influence the particles motion in the collisional regime: multiple collisions occur and the time duration of each collision is finite and not negligible. If multiple particle collisions are possible, the number of collisions increases in a given time step, whereas the longer is the collision duration, the less is the number of collisions. The number of collisions affects the particle velocity fluctuations and, consequently, the granular temperature. In short, for small particle stiffness, the finite duration of the collisions produces a decrease in the granular temperature, but, at the same time, the occuring of multiple collisions generates an increase in T. Function f_r takes into account only the finite duration of the collisions, and produces a decrease in the slope of the scaled normal stress, at large scaled shear rate, which is related to the decrease in the granular temperature. The right trend of the measured normal stress is not captured in the collisional contribution at large $\dot{\gamma}\left(\rho_p d^3/K\right)^{1/2}$, where the theory underestimates the data, because the role of multiple collisions needs to be introduced. This lack in the collisional contribution affects the curves in both the purely collisional regime and the regime of coexistence of quasi-static and collisional contributions, at large values of the scaled shear rate, i.e., at small values of the dimensionless stiffness $K/(\rho_p d^3 \dot{\gamma}^2)$.
The most salient weakness of the proposed theory is the impossibility to simulate steady, shearing flows at concentrations larger than the shear rigidity. This limitation of the model is due to the expressions of the functions which affect both the collisional and the quasi-static terms. In the collisional contribution, all the functions of the concentration f_1, f_2, f_3 and f_r (except for the correlation length) involve the radial distribution function, whose expression diverges at the shear rigidity. Similarly, the function f_0 in the quasi-static stresses diverges at ν_s, as well. As a consequence, both the two contributions are defined only for concentrations lower than the shear rigidity. The theory was conceived assuming that the maximum concentration that a sheared, steady granular flow can achieve is the shear rigidity, corresponding to the densest disordered configuration of identical spheres attainable under steady, shearing conditions. The numerical results show that the simple shear flows can overcome this threshold and also ordered configurations are possible in dynamic, steady conditions. As a consequence, the model must be extended to denser flows of ordered configurations. This can be done by redefining the function f_0 in the quasi-static contribution (the data show that there is no need that it diverges). E.g., Chialvo et al. [28] obtained $f_0 \propto |\nu_s - \nu|^{2/3}$ from their SS-DEM simulations using linear contact model. A new form of f_0 will not change the physical sense of the quasi-static contribution and, in particular, its relationships with force chains and friction.
Sencondly, when the flow reaches ordered configuration, i.e., when $\nu > \nu_s$, the collisional

contribution must be defined.

All the modifications required to improve the predictions of the model do not change the distinctive features of the present theory, discussed in Section 5.2. In particular, independently of the expression of f_0, the phase diagram presented in Section 5.2.1 still holds. Just the shape of the critical state concentration, ν_{cs}, would be different, accordingly to the new definition of f_0. Moreover, the peculiar concentration ν^*, associated to the non-monotonic dependence of the stress ratio on the shear rate when $\nu > \nu_{rlp}$, is an intrinsic property of the model. The existence of ν^* is associated to two basic assumptions: (i) adding the two contributions and (ii) requiring that friction supports force chains, i.e., that the quasi-static shear stress is proportional to the quasi-static normal stress through the friction coefficient.
The quantitative improvements of the model are post-poned to future works.

5.4. Conclusions

In this Chapter, the theoretical, constitutive model has been used to solve for the steady, simple shear flow of identical, inelastic spheres. The interpretation of the constitutive relationship in the light of standard viscoplasticity is a first step towards an evolving constitutive model capable of describing the mechanical behaviour of granular material under both solid-like and fluid-like conditions. A phase diagram has been described on the plane normal stress-concentration, according to which, if the concentration is lower than the random loose packing, the grains can interact only through collisions. Also, the theory predicts the existence of a maximum "critical state" concentration, ν_{cs}, which can be achieved under steady conditions, for a fixed value of the normal stress. The critical state concentration define the range of coexistence of force chains (quasi-static terms) and collisions, and depends on the imposed normal stress.
Three flow configurations have been considered: pressure-, concentration- and stress ratio-imposed flows. Accounting for the stiffness of the particles allows to highlight the occurrence of the limit condition $\tau/\sigma < \tan\phi$, corresponding to $\nu > \nu^*$, which produces a peculiar behaviour of the variable's profiles in the three considered flow conditions. Indeed, in the pressure-imposed flow, the stress ratio curves become non-monotonic in the range of concentration between ν^* and ν_{cs}, and the fluidity parameter is imaginary. Correspondingly, in the concentration-imposed flow, the τ/σ function changes from an increasing to a decreasing dependence on the shear rate. Finally, the occurrence of the same condition generates in the stress ratio-imposed flow a loss of uniqueness of the solution for concentrations larger than the random loose packing, associated with a limited range of normal stresses at which steady state is possible.
The predictive capability of the proposed model is tested by comparing its predictions for simple shear flows against experimental and numerical results taken from the literature. We first have considered numerical results obtained in the collisional regime, in order to verify the collisional contribution (i.e., the modified kinetic theory) in absence of the quasi-static one. The comparison with numerical simulations of (nearly) hard, frictionless [88] and slightly frictional [27] spheres has shown that the kinetic theory successfully reproduces the normal stress, the granular temperature and the stress ratio, for different values of the collisional coefficient of restitution, if the proposed expression of the radial distribution function is adopted. On the other hand, when using more frictional spheres, the predictions of the kinetic theory disagree with the numerical results. This seems to be

a limit of the use of an effective coefficient of restitution, whose form was developed for slightly frictional particles, even in the case of very frictional particles.
When force chains develop, the model is able to qualitatively capture the characteristic features of concentration-imposed simple shear flows. In particular, the asymptotic behavior of the normal stress at vanishingly small shear rates and concentrations larger than the random loose packing, shown by the numerical data [28], is captured. Also, the introduction of the function f_r, which accounts for the particle stiffness in the collisional contribution, allows to predict the change of slope in the normal stress which happens at large values of the shear rate. On the other hand, the assumptions made in defining the functions of the model produce evident quantitative discrepancies between the predictions and the numerical simulations. The major limitation of the theory is the impossibility to simulate steady, shearing flows at concentrations larger than the shear rigidity, ν_s, where the particles reach an ordered configuration. The extension of the model to the case $\nu > \nu_s$ will be the subject of future works.

6. Couette flows of frictionless spheres: kinetic theory and 3D Soft-Sphere DEM simulations*

This Chapter is devoted to the study of non homogeneous shear flows of identical, frictionless and hard sphere, under steady conditions, at fixed average concentration. In the previous Chapter, the model was proven to predict very well the steady, homogeneous shear flows of an assembly of frictionless and hard spheres (Section 5.3.2), whereas the comparison with numerical results performed using frictional and soft particles (Section 5.3.3), has shown that the theory requires modifications in that case. The aim of this Chapter is to test the ability of the model to reproduce also non homogeneous steady, shear flows, in the conditions for which the homogeneous flows are well predicted.
In order to make comparisons between the theory and numerical results, 3D SS-DEM simulations have been carried out using a pre-existent code [21]. This Chapter is organized as follows. In Section 6.1 the set of differential equations deriving from the proposed theory is numerically solved with appropriate boundary conditions. Section 6.2 is devoted to describe the simulation method. Finally, the comparison between the results of the SS-DEM simulations and those obtained from the numerical integration of the equations is summarized in Section 6.3.

6.1. Couette flow configuration and governing equations

The non homogeneous shear flows of a mixture of identical, frictionless and hard sphere, under steady conditions, is known as Couette flow. In the Couette configuration, the granular material is sheared between two parallel planes, having infinite length, one at rest and the other moving at constant velocity V (Fig. 6.1). Here, x and y are taken to be the flow and the shearing directions, respectively, and variations along the transversal direction z are ignored. The granular material is an assembly of identical, frictionless spheres, having diameter d and density ρ_p. The mechanical properties of frictionless grains are described by the stiffness, K, and the (normal) coefficient of restitution, e_n. As stated in the previous Sections, in the case of frictionless particles, e_n is the unique material parameter characterizing the collision; then in this Section, the subscript n is omitted for semplicity.
The boundaries are made bumpy by gluing spheres having the same properties of the moving particles at the walls in a regular hexagonal array, where l is the distance between the edges of two adjacent spheres. The bumpiness of the wall is measured by ψ, with $\sin\psi = (1+l)/2$ [105], as depicted in the inset in Fig. 6.1. We take $y = 0$ to be at the top of the particles glued at the resting wall, and $y = H$ to be at the bottom of the particles glued at the moving wall.
For frictionless particles, momentum is exchanged only through collisions [122], and the

*based on D. Vescovi, D. Berzi, P. Richard, and N. Brodu. Plane shear flows of frictionless spheres: kinetic theory and 3D Soft-Sphere DEM simulations. *Physics of Fluids*, submitted, 2014

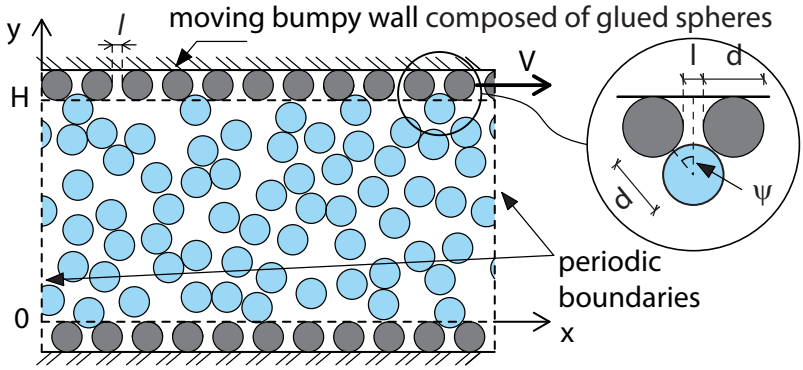

Figure 6.1.: Sketch of the constant-volume Couette flow configuration. A granular material confined between two horizontal solid planes is sheared by moving one of planes at constant velocity V (x are y are respectively the flow and shear directions). The two planes are made bumpy by gluing grains at their surface in a regular hexagonal array, where l is the distance between the edges of two adjacent spheres.

theoretical model reduces to the collisional contribution, which is modeled using the kinetic theory with the modifications described in Section 4.2.1. In this Section, only hard particles will be considered, so that the function f_r (Eq. 4.23) is equal to one and the collisions are supposed to be nearly instantaneous.
In the absence of external forces, and in steady conditions, the momentum balance trivially asserts that the normal stress and the shear stress are constant along y, as stated by Eqs. (4.38a)-(4.38b). The balance of the fluctuating energy, Eq. (4.41), reads

$$\tau u' = q' + \Gamma. \tag{6.1}$$

For semplicity, here and in what follows, the subscript "col" is omitted and a prime indicates the derivative with respect to the y direction. Also all the quantities are made dimensionless using the particle diameter d, the particle density ρ_p and the wall velocity V.
The constitutive relations for the normal stress, σ, the shear stress, τ, the rate of dissipation of fluctuating energy, Γ, and the the energy flux, q, are given by Eqs. (4.42)-(4.45), respectively, which, when $f_r = 1$, reduce to

$$\sigma = f_1 T, \tag{6.2}$$

$$\tau = f_2 T^{1/2} u', \tag{6.3}$$

$$\Gamma = \frac{f_3}{L} T^{3/2}, \tag{6.4}$$

$$q = -\left(f_4 T^{1/2} T' + f_5 T^{3/2} \nu' \right). \tag{6.5}$$

f_1, f_2, f_3, f_4 and f_5 are explicit functions of the concentration and the coefficient of restitution and are given by Eqs. (4.46)-(4.50); L is the correlation length, whose expression, according to Eq. (4.52), and using Eqs. (6.2) and (6.3), sounds

$$L = \max\left(1, L^* \frac{f_1}{f_2} \frac{\tau}{\sigma}\right), \tag{6.6}$$

with L^* expressed by Eq. (4.53).
From the constitutive relations for the shear stress (6.3) and the normal stress (6.2), we

obtain the differential equation governing the velocity,

$$u' = \frac{\tau}{\sigma}\frac{f_1}{f_2}T^{1/2}. \tag{6.7}$$

By deriving Eq. (6.2) and using Eq. (6.5), the differential equation for the concentration results

$$\nu' = \frac{Q}{T^{1/2}}\frac{f_1^2}{f_4}\left[\sigma f_{1,\nu}\left(1 - \frac{f_5 f_1}{f_4 f_{1,\nu}}\right)\right]^{-1}, \tag{6.8}$$

where $f_{1,\nu}$ represents the derivative of f_1 with respect to the concentration, which, using Eq. (4.46) with the expression of F, (3.42b), and $G = \nu g_0$, is

$$f_{1,\nu} = 1 + 2\,(1+e)\,\nu\,(2g_0 + \nu g_{0,\nu})\,,$$

being g_0 the radial distribution function, expressed by Eq. (4.28), and $g_{0,\nu}$ its first derivative with respect to ν.
Finally, using Eqs. (6.2), (6.4) and (6.7) into Eq. (6.1), the differential equation for the energy flux reads

$$q' = \sigma T^{1/2}\left[\frac{f_1}{f_2}\left(\frac{\tau}{\sigma}\right)^2 - \frac{f_3}{L f_1}\right]. \tag{6.9}$$

The constant volume condition is imposed, which corresponds to keeping constant the average concentration along the flow depth. An additional differential equation for the partial mass hold-up, defined as $M = \int_0^y \nu dz$, is introduced:

$$M' = \nu. \tag{6.10}$$

Then, the value of the average concentration, $\bar{\nu}$, along y can be implemented as a boundary condition for M.
The set of the four differential equations Eqs. (6.7)-(6.10) is numerically solved using the function 'bvp4c' implemented in MATLAB, and fixing the flow gap H. The normal stress and the shear stress are treated as parameters, so that six boundary conditions are required to solve the problem. As already mentioned, the fixed average concentration is implemented as a boundary condition for the the partial mass hold-up at the top wall ($y = H$), i.e.,

$$M_H = \bar{\nu} H, \tag{6.11}$$

while, at the resting wall ($y = 0$),

$$M_0 = 0. \tag{6.12}$$

Here and in what follows, the index represents the coordinate y at which the quantity is evaluated. The particles are allowed to slip at the bumpy walls, so that, for symmetry,

$$u_0 = u_w, \tag{6.13}$$

$$u_H = 1 - u_w, \tag{6.14}$$

where u_w is the slip velocity. The expression for the slip velocity has been proposed by Richman [105] in the case of rigid, nearly elastic semi-spheres attached to a flat wall:

$$u_w = \sqrt{\frac{\pi}{2}} h \frac{\tau}{\sigma} T_0^{1/2}, \tag{6.15}$$

with

$$h = \frac{2}{3}\frac{\left[1+\dfrac{5F_0\,(1+B)\sin^2\psi}{2\sqrt{2}J_0}\right]}{\dfrac{2\,(1-\cos\psi)}{\sin^2\psi}} + \frac{5F_0}{\sqrt{2}J_0}, \tag{6.16}$$

where $B = \pi\left[1+5/\left(8G_0\right)\right]/\left(12\sqrt{2}\right)$, and G_0, J_0 and F_0 are obtained from the corresponding expressions of G (3.42a), J (3.42c) and F (3.42b) with $\nu = \nu_0$. The bumpy walls act either as a sink or a source of fluctuating energy to the system. The two boundary conditions for the energy flux are

$$q_0 = q_w, \tag{6.17}$$

$$q_H = -q_w, \tag{6.18}$$

where Richman [105] proposed

$$q_w = \tau u_w - \sqrt{\frac{\pi}{2}}\sigma T_0^{1/2}(1-e)\frac{2\,(1-\cos\psi)}{\sin^2\psi}. \tag{6.19}$$

The results of the numerical integration will be compared with those obtained from SS-DEM simulations described in the next Section.

6.2. 3D Soft-Sphere Discrete Element Method simulations

In order to make comparisons between the theory and numerical results, 3D numerical simulations of Couette granular flows have been performed using the Soft-Sphere Discrete Element Method (SS-DEM). Section 6.2.1 presents a background information on microscale SS-DEM simulations of granular flows, whereas the numerical simulations performed in this work are described in Section 6.2.2.

6.2.1. Soft-Sphere Discrete Element Method

The Soft-Sphere Discrete Element Method (SS-DEM), is a family of numerical methods for computing the motion of large number of particles. Cundall and Strack [29] originally developed the SS-DEM for the analysis of rocks mechanics, to simulate the behavior of discontinuous materials. These methods are becoming widely accepted as an effective way of addressing engineering problems in granular and discontinuous materials, especially in granular flows and rock mechanics. In SS-DEM, the material is modeled as a finite number of discrete particles, each with its own properties. The interactions between particles are treated as dynamic processes with states of equilibrium developing when the internal forces balance.

Due to the complexity of the properties of granular materials, and the limitations of current mathematical models and computer calculation capacity, it is impossible to capture all physical features in the simulations. Therefore, only the important aspects would be considered in the Soft-Sphere Discrete Element Model. As previously stated, the granular material is considered as a collection of discrete particles which interact each other through contact forces. Since the realistic modeling of the deformations of the particles is such too complicated, the grains are assumed to be non-deformable spheres which are allowed to overlap [79].

The general SS-DEM approach involves three stages.

1. The first stage is to detect the contacts between elements.

2. In the second stage, interaction force is calculated when two particles have slightly interpenetrated. This is the kernel step in SS-DEM models and different models exist to compute the interaction force.

3. At last, Newton's equations of motion are applied and numerically integrated to compute the resulting acceleration while combining all interaction forces. The equations of motion are integrated over a small time step to relocate a new position for each particle.

This three-stage process is repeated until the whole simulation is finished. Based on the fundamental simulation flow, a large variety of modified algorithms exist and they differ mostly by the contact model and the techniques used in interaction force calculation.
In 3D SS-DEM, each grain i is a soft but stiff sphere of diameter d_i, mass m_i, moment of inertia I_i, positions $\mathbf{r}_i$, velocity $\mathbf{v}_i$ and angular velocity $\boldsymbol{\omega}_i$. For a pair of particles, the relative distance vector, $\mathbf{x}_{ij}$, the relative velocity, $\mathbf{v}_{ij}$, and the normal unit vector, $\mathbf{n}_{ij}$, are defined as

$$\begin{aligned}\mathbf{x}_{ij} &= \mathbf{x}_i - \mathbf{x}_j,\\ \mathbf{v}_{ij} &= \mathbf{v}_i - \mathbf{v}_j,\\ \mathbf{n}_{ij} &= \frac{(\mathbf{x}_i - \mathbf{x}_j)}{|\mathbf{x}_i - \mathbf{x}_j|}.\end{aligned}$$

Also, the normal relative velocity, $\mathbf{v}_{ij}^n$, and the tangential velocity at the contact point, $\mathbf{v}_{ij}^t$, in the case of small overlap, are given by

$$\begin{aligned}\mathbf{v}_{ij}^n &= (\mathbf{v}_{ij}\cdot\mathbf{n}_{ij})\,\mathbf{n}_{ij},\\ \mathbf{v}_{ij}^t &= \mathbf{v}_{ij} - \mathbf{v}_{ij}^n - \left(\frac{d_i}{2}\boldsymbol{\omega}_i + \frac{d_j}{2}\boldsymbol{\omega}_j\right)\times\mathbf{n}_{ij}.\end{aligned}$$

Note that there is no sum over repeated indices.
Two particles are in contact if their normal overlap, defined as

$$\delta_{ij}^n = \frac{d_i + d_j}{2} - \mathbf{x}_{ij}\cdot\mathbf{n}_{ij},$$

is strictly positive, $\delta_{ij}^n > 0$, and the contact point is assumed to be the center of the overlap (Fig. 6.2(a)).

In general, the force on particle i from the interaction with particle j is the sum of a normal and a tangential contribution:

$$\mathbf{F}_{ij} = \mathbf{F}_{ij}^n + \mathbf{F}_{ij}^t.$$

Although the present Section deals with frictionless particles, for which the contact force is purely normal and the grains are submitted to neither tangential forces nor torques, the general procedure is here introduced, for completeness.
As the most important step in SS-DEM, force interaction can vary, and represent different physical properties. In this work, the so called spring-dashpot model, which is schematically shown in Fig. 6.2(b), is adopted.
The forces are modeled as the sum of a linear elastic and a linear dissipative component in both the normal and the tangential direction:

$$\mathbf{F}_{ij}^n = k_n\delta_{ij}^n\mathbf{n}_{ij} - \gamma_n\mathbf{v}_{ij}^n, \tag{6.20}$$

$$\mathbf{F}_{ij}^t = -k_t\delta_{ij}^t\mathbf{t}_{ij} - \gamma_t\mathbf{v}_{ij}^t. \tag{6.21}$$

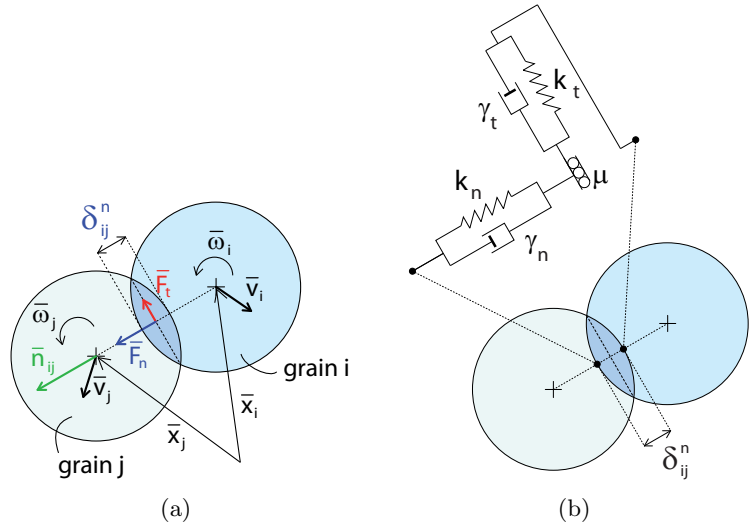

Figure 6.2.: Sketches of two particles at contact (a) and of the contact forces used (b).

Here, k_n and k_t are the normal and the tangential spring constants, and γ_n and γ_t the normal and the tangential damping coefficients, which are used to obtain an inelastic collision; δ_{ij}^t is the tangential overlap, and $\mathbf{t}_{ij}$ the tangential unit vector: $\mathbf{t}_{ij} = \mathbf{v}_{ij}^t / |\mathbf{v}_{ij}^t|$. The tangential overlap is set to zero at the initiation of a contact and its rate of change is given by the tangential relative velocity:

$$\frac{d\delta_{ij}^t}{dt} = \left|\mathbf{v}_{ij}^t\right| .$$

Note that the rigid body motion around the contact is taken into account to ensure that the tangential displacement is always in the local tangent plane of the contact.
The magnitude of δ_{ij}^t is truncated as necessary to satisfy Coulomb law, i.e,

$$\left|\mathbf{F}_{ij}^t\right| \leq \mu \left|\mathbf{F}_{ij}^n\right| ,$$

where μ is the interparticle friction coefficient. Note that the static friction coefficient is assumed to be equal to the dynamic one and that this friction coefficient depends neither on velocity nor on aging [22]. In this simplified framework, the contact surfaces are treated as a sticking contact if $|\mathbf{F}_{ij}^t| < \mu |\mathbf{F}_{ij}^n|$ and as a sliding contact if the yield criterion is satisfied, i.e., if $|\mathbf{F}_{ij}^t| = \mu |\mathbf{F}_{ij}^n|$.
Then, the total force on particle i is a combination of contact forces with other particles, with boundaries and an eventual resulting external force $\mathbf{F}_{\text{ext}}$. The resulting force $\mathbf{F}_i$ and torque $\mathbf{t}_i$ are given by

$$\mathbf{F}_i = \mathbf{F}_{\text{ext}} + \sum_{j=1, j\neq i}^{N} \mathbf{F}_{ij}, \tag{6.22}$$

$$\mathbf{t}_i = \sum_{j=1, j\neq i}^{N} \frac{d_i}{2} \mathbf{F}_{ij} \times \mathbf{n}_{ij} \tag{6.23}$$

where N is the total number of spheres. Once the forces and torques are calculated for all the particles, the Newton's equations of motion, for the translational and rotational

degrees of freedom, are integrated:

$$m_i \frac{d^2 \mathbf{x}_i}{dt^2} = \mathbf{F}_i, \tag{6.24}$$

$$I_i \frac{d\boldsymbol{\omega}_i}{dt} = \mathbf{t}_i. \tag{6.25}$$

Note that the last equation is only valid when $\delta_{ij}^n = 0$. The torque is the vector product of the lever arm and the force. But in Eq. (6.23), it is assumed that the lever arms have lengths equal to $d_i/2$ or $d_j/2$, which is true only when the grains do not overlap. The application of Eq. (6.25) will thus produce a violation of angular momentum conservation of order $\mathcal{O}\left(\delta^n/d\right)$ [83].
Eqs. (6.24) and (6.25) are ordinary differential equations (ODE) which must be numerically solved in order to update a new position for particle i. In principle, any numerical integration scheme, suitable for a large ODE system, can be implemented. In the SS-DEM code here adopted, a velocity Verlet integration scheme is implemented. The standard implementation scheme of the algorithm proposed by Verlet can be summarized as follows. For a fixed time step Δt, once the position, the velocity and the acceleration of each particle are known at time t, $\mathbf{x}_i(t)$, $\mathbf{v}_i(t)$, $\mathbf{a}_i(t)$, $\forall i = 1, \cdots, N$:

1. the velocity and the angular velocity are calculated at the intermediate time, $t+\Delta t/2$:

$$\mathbf{v}_i\left(t + \Delta t/2\right) = \mathbf{v}_i\left(t\right) + \mathbf{a}_i(t)\frac{\Delta t}{2},$$
$$\boldsymbol{\omega}_i\left(t + \Delta t/2\right) = \boldsymbol{\omega}_i\left(t\right) + \frac{\mathbf{t}_i(t)}{I_i}\frac{\Delta t}{2},$$

2. the position is calculated at time $t + \Delta t$:

$$\mathbf{x}_i\left(t + \Delta t\right) = \mathbf{x}_i(t) + \mathbf{v}_i\left(t + \Delta t/2\right)\Delta t;$$

3. the force and the torque acting on particle i at time $t+\Delta t$, $\mathbf{F}_i(t+\Delta t)$ and $\mathbf{t}_i(t+\Delta t)$, are calculated using Eqs. (6.22) and (6.23), and, consequently, the acceleration is computed: $\mathbf{a}_i(t + \Delta t) = \mathbf{F}_i(t + \Delta t)/m_i$;

4. the velocity and the angular velocity are calculated at time $t + \Delta t$:

$$\mathbf{v}_i\left(t + \Delta t\right) = \mathbf{v}_i\left(t + \Delta t/2\right) + \mathbf{a}_i(t + \Delta t)\frac{\Delta t}{2},$$
$$\boldsymbol{\omega}_i\left(t + \Delta t\right) = \boldsymbol{\omega}_i\left(t + \Delta t/2\right) + \frac{\mathbf{t}_i(t + \Delta t)}{I_i}\frac{\Delta t}{2}.$$

As already mentioned in Section 3.1.5, the collisions may be described using the coefficients of normal and tangential restitution, relating the pre-collisional and post-collisional relative velocities. For the spring-dashpot model, the following relashionships between the coefficients of restitution, the spring constants and the damping coefficients hold [116]:

$$\gamma_n = \sqrt{\frac{4m_{ij}k_n\left(\log e_n\right)^2}{\pi^2 + \left(\log e_n\right)^2}}$$
$$\gamma_t = \sqrt{\frac{2}{7}\frac{4m_{ij}k_t\left(\log e_t\right)^2}{\pi^2 + \left(\log e_t\right)^2}}$$
$$k_t = \frac{2}{7}k_n\frac{\pi^2 + \left(\log e_t\right)^2}{\pi^2 + \left(\log e_n\right)^2}$$

with the reduced mass $m_{ij} = m_i m_j/(m_i + m_j)$ (for spheres of equal mass m, $m_{ij} = m/2$). Also, the collision time can be analytically obtained:

$$t_c = \frac{\pi}{\left[\dfrac{k_n}{m_{ij}} - \dfrac{1}{4}\dfrac{\gamma_n^2}{m_{ij}^2}\right]}^{1/2}.$$

The value of the spring constant k_n should be large enough to avoid particle interpenetration, yet not so large as to require an unreasonably small simulation time step Δt, since an accurate simulation typically requires $\Delta t \sim t_c/50$ [116].

SS-DEM simulations provide the complete microscopic description of the system at each time step, i.e., the position and the velocity of each particle, as well as the interparticle forces at contact. Macroscopic (continuum mechanical) variables, such as concentration, mean velocity, granular temperature, stresses, etc., can be determined by an appropriate averaging procedure [4], which consists of both spatial and temporal averaging. Here, the continuous concentration, ν, and velocity, $\mathbf{u}$, fields are computed using the definition by Serero et al. [113]

$$\nu(\mathbf{x}, t) = \sum_{i=1}^{N} \frac{\pi d_i^3}{6} k_i(\mathbf{x}_i(t) - \mathbf{x}),$$

$$\mathbf{u}(\mathbf{x}, t) = \frac{\displaystyle\sum_{i=1}^{N} m_i \mathbf{v}_i k_i(\mathbf{x}_i(t) - \mathbf{x})}{\displaystyle\sum_{j=1}^{N} m_j k_j(\mathbf{x}_j(t) - \mathbf{x})},$$

being $\mathbf{x} = (x, y, z)$ the position at which to compute the average field, $\mathbf{x}_i$ the position of the center of grain i, and N the total number of grains. k_i is a kernel that distributes the mass m_i of grain i over space. The uniform density kernel is adopted:

$$k_i(\mathbf{x}_i - \mathbf{x}) = \begin{cases} \rho_p & \text{when} \quad \|\mathbf{x}_i - \mathbf{x}\| < d_i/2 \quad \text{and} \quad \mathbf{x}_i \in V \\ 0 & \text{elsewhere,} \end{cases}$$

where $\|\cdot\|$ denotes the Euclidean norm of a vector and V is the averaging volume. In the case of Couette flows, the flows are uniform in x and z, and he averaging volume reduces to a slice having the same length and width of the whole domain (in the x and z directions), and assigned height Δs. Then, the condition $\mathbf{x}_i \in V$ is equivalent to require that the center of particle i is located within the averaging slice of thickness Δs centered at y_i: $y - \Delta s/2 < y_i < y + \Delta s/2$.
The fluctuating velocity of particle i is given by $\mathbf{V}_i(\mathbf{x}, t) = \mathbf{v}_i(t) - \mathbf{u}(\mathbf{x}, t)$. The granular temperature field is computed as

$$T(\mathbf{x}, t) = \frac{1}{3}\left(\frac{\displaystyle\sum_{i=1}^{N} m_i \left|\mathbf{v}_i\right|^2 k_i(\mathbf{x}_i - \mathbf{x})}{\displaystyle\sum_{j=1}^{N} m_j k_j(\mathbf{x}_j - \mathbf{x})} - |\mathbf{u}|^2\right).$$

Finally, the stress tensor is calculated as the sum of the "kinetic" (or streaming) and the "contact" contribution

$$\boldsymbol{\sigma} = \boldsymbol{\sigma}^k + \boldsymbol{\sigma}^c.$$

Usually, the kinetic and the contact parts of the stress tensor are computed as [79]:

$$\boldsymbol{\sigma}^k = \frac{1}{V}\sum_{i=1}^{N_v} m_i \mathbf{V}_i \otimes \mathbf{V}_i,$$
$$\boldsymbol{\sigma}^c = \frac{1}{V}\sum_{i=1}^{N_v}\sum_{j\neq i} \mathbf{F}_{ij} \otimes \mathbf{x}_{ij},$$

where $\otimes$ denotes the outer produc and N_v is the number of particles in the averaging volume. In these expressions, the kernel is implicitly a uniform density on a cube of fixed volume V. In the code, the stresses are computed using the same kernel implemented for the mean velocity and the temperature (which assigns uniform density over each grain volume), as proposed by Babic [5]. Then, the contact part of the stress tensor is more complicated to express and involves an integral over the branch vector. The adopted expressions for $\boldsymbol{\sigma}^s$ and $\boldsymbol{\sigma}^c$ read [4, 5]:

$$\boldsymbol{\sigma}^k = \sum_{i=1}^{N} m_i \mathbf{V}_i \otimes \mathbf{V}_i k_i(\mathbf{x}_i - \mathbf{x}),$$
$$\boldsymbol{\sigma}^c = \sum_{i=1}^{N}\sum_{i=1+1}^{N} \mathbf{F}_{ij} \otimes \mathbf{x}_{ij} \int_0^1 k_i(\mathbf{x} - \mathbf{x}_i + s\mathbf{x}_j)ds.$$

6.2.2. SS-DEM simulations of Couette granular flows

The SS-DEM code is employed to simulate the Couette flows of frictionless, inelastic, identical spheres of diameter d and density ρ_p. The flow configuration adopted is the same described in the previous Section and depicted in Fig. 6.1. Here, the granular material is bounded between two parallel, bumpy planes, one at rest and the other moving at constant velocity V. As already mentioned, the numerical results are given in nondimensional units: distances, times, velocities, forces, elastic constants and viscoelastic constants are, respectively, measured in units of d, d/V, V, $\rho_p d^2V^2$, $\rho_p dV^2$ and $\rho_p d^2V$.
All the simulations have been performed in a rectangular box of length $L_x = 20$, width $L_z = 10$ and height $L_y = 20$ - so that the flow gap is $H = L_y - 2 = 18$ - with $N = 3132$. The bumpiness has been generated by gluing, in a regular hexagonal array, a total of 340 particles at the two walls in the case of $\psi = \pi/5$, and 154 in the case $\psi = \pi/3$. Hence, taking into account the extra-space accessible to any flow particle in between the wall-spheres, $\bar{\nu} = 0.45$ when $\psi = \pi/5$ and $\bar{\nu} = 0.44$ when $\psi = \pi/3$. Periodic boundary conditions are employed in the x and z directions and the horizontal flat walls are located at $y = -1$ and $y = H+1$, the latter moving at constant horizontal velocity V. Those walls are treated as spheres of infinite size and density and the grains glued on their surface to create the bumpiness are treated like spheres of diameter 1 and infinite density. The particle stiffness of the linear spring model has been set as $k_n = 2 \cdot 10^5$ and the value of the damping coefficient γ_n is adjusted to obtain the chosen normal restitution coefficient. The non-dimensional ratio of the particle stiffness over the normal stress is greater than 10^5 in all the simulations. This ensures that the contact time during a collision is much less than the flight time in between two successive collisions, the latter can be considered instantaneous [16, 96] (as shown in Section 5.2.2), and the function f_r is equal to one.
Simulations have been performed by changing the coefficient of restitution ($e = 0.2$, 0.50, 0.60, 0.70, 0.80, 0.92, 0.98) and the bumpiness of the walls ($\psi = \pi/5$ and $\pi/3$).
This work focuses on the steady state of sheared granular flows, that is considered achieved

when the space-averaged granular temperature $\bar{T}$ becomes approximately constant (fluctuations around the time-averaged value less than 10%). The space-averaged granular temperature is computed as

$$\bar{T} = \frac{1}{3N}\left[\sum_{i=1}^{N}\|\mathbf{v}_i\|^2 - \left(\sum_{i=1}^{N}\|\mathbf{v}_i\|\right)^2\right].$$

We have checked that the steady state does not depend on the initial configuration, by preparing two different initial states, consisting of N spheres uniformly distributed in the volume. In the first case the spheres are initially at rest; in the second case, a linear distribution (from 0 to 1) of the x-velocity of the spheres is assigned. This second configuration corresponds to a higher value of the initial energy, i.e., of the initial space-averaged granular temperature. In both cases, the same steady state is achieved, i.e., with the same value of space-averaged granular temperature and the same distributions of the field variables.

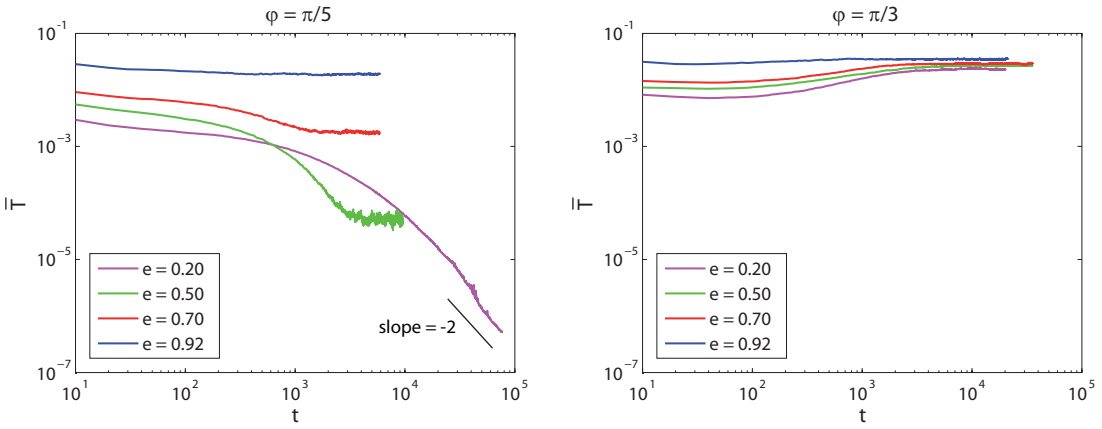

Figure 6.3.: Time evolution of the mean granular temperature for different values of the coefficient of restitution when $N = 3132$ and (a) $\psi = \pi/5$ ($\bar{\nu} = 0.45$); (b) $\psi = \pi/3$ ($\bar{\nu} = 0.44$).

The time at which the steady state is reached increases when the coefficient of restitution decreases (e.g., see Fig. 6.3(a) for the case $\psi = \pi/5$). Depending on the bumpiness, the mean granular temperature changes drastically its time dependence. For $\psi = \pi/3$ (Fig. 6.3(b)) $\bar{T}$ increases with time and reaches the steady state for each value of the coefficient of restitution. For $\psi = \pi/5$ (Fig. 6.3(a)), $\bar{T}$ is a decreasing function of t. Also, as the coefficient of restitution decreases, the mean granular temperature decreases faster in time. For sufficiently small coefficients of restitution (case $e = 0.2$ in Fig. 6.3(a)), the mean granular temperature continues to decrease, without reaching a steady state. The slope of the curve approaches the value -2 that characterizes the Homogeneous Cooling State (HCS) [45], where the rate of change of the granular temperature in the balance of fluctuating energy is only due to the collisional dissipation and the granular temperature obeys the Haff's law, $T \propto (1+t)^{-2}$ [48]. This finding will be discussed in the following Section.

Once the steady state is reached, measurements are averaged in time, over at least 2000 time steps, and over the lengths of the domain along the x and z directions, using 20

horizontal slices. Given that the averaging is sensitive to the amplitude of the spatial discretization [126], we checked that the number of slices is sufficiently large not to affect the results. Example of profiles of ν, u, T and u' are plotted in Fig. 6.4 for $\psi = \pi/5$ and $e = 0.80$, when 20 or 40 horizontal slices are employed. The velocity profile has a characteristic S-shape, in agreement with recent physical experiments performed on disks [85]. Also, the profile of the shear rate very much resembles the experimental findings. The concentration increases and the granular temperature decreases with distance from the walls. The core of the flow is dense, i.e., the concentration is larger than 0.49, and there the molecular chaos assumption breaks down.

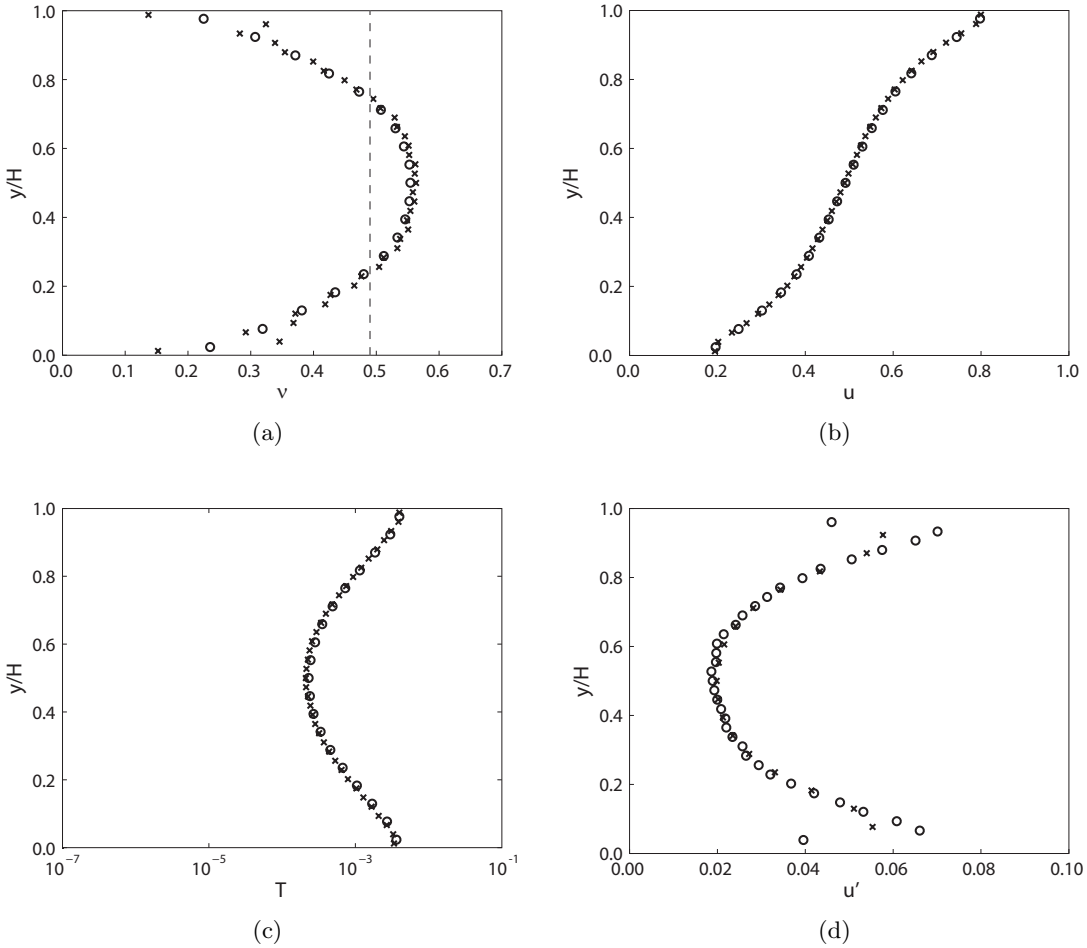

Figure 6.4.: Profiles of ν, u, T and u' obtained from SS-DEM simulations when $H = 18$, $\bar{\nu} = 0.45$, $\psi = \pi/5$ and $e = 0.80$, when the domain along the y-direction is divided into 20 (open circles) and 40 (crosses) slices to perform the averaging. The dashed line in (a) is the value of the concentration at the freezing point, $\nu = 0.49$.

In order to quantitatively test the code, we compare the SS-DEM results obtained on the Couette configuration with other numerical data taken from the literature. According to the kinetic theory, in the plane shear flows of frictionless and hard particles, the constitutive relations for the normal and the shear stress are given by Eqs. (6.2)-(6.3). Those are the same for both the cases of homogeneous and non homogeneous flows. Once σ, τ, T

and u' are measured, f_1 and f_2 can be computed as

$$f_1 = \frac{\sigma}{T}, \tag{6.26}$$

$$f_2 = \frac{\tau}{T^{1/2}u'}, \tag{6.27}$$

as functions of the concentration. Figs. 6.5(a) and 6.5(b) depict, respectively, the quantities σ/T and $\tau/\left(T^{1/2}u'\right)$ as functions of the concentration, where σ, T, τ and u' are those measured on the SS-DEM simulations on steady, non homogeneous plane shear flows when using $e = 0.70$ and $\psi = \pi/5$ (squares) and $\psi = \pi/3$ (diamonds). Also, the data obtained from the numerical simulations on steady, homogeneous plane shear flows of Mitarai and Nakanishi [88] (Event-Driven simulations, crosses) and Chialvo and Sundaresan [27] (SS-DEM simulations, circles) are plotted. Finally, the theoretical expressions of f_1 and f_2, Eqs. (4.46)-(4.47), with the radial distribution function given by Eq. (4.28), are also shown (lines).

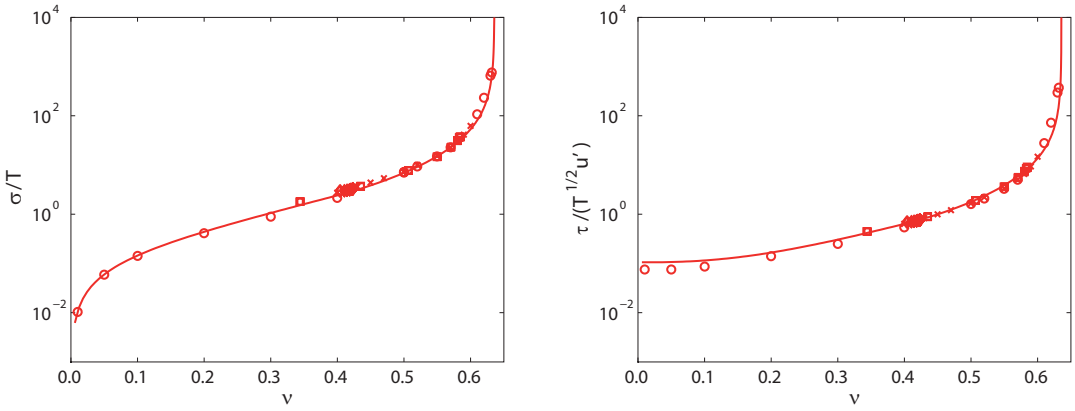

(a) (b)

Figure 6.5.: Numerical quantities σ/T (a) and $\tau/\left(T^{1/2}u'\right)$ (b) as functions of the concentration for $e = 0.7$. The numerical measurements obtained with the present SS-DEM simulations of non homogeneous flows when $\psi = \pi/5$ (squares) and $\psi = \pi/3$ (diamonds) are compared with the data obtained by Mitarai and Nakanishi [88] (crosses) and Chialvo and Sundaresan [27] (circles) on homogeneous flows. The lines represent the theoretical expressions of f_1 (4.46) and f_2 (4.47) with g_0 given by Eq. (4.28).

All the numerical data collapse, independently of the simulation method and the flow configuration, and are in very good agreement with the theoretical curves. Similar agreement is obtained for other values of the coefficient of restitution.

6.3. Results and comparisons

In this Section, we compare the results of the numerical integration of Eqs. (6.7)-(6.10), with the SS-DEM simulations in terms of profiles of concentration, velocity and granular temperature, distinguishing between small and large bumpiness.

6.3.1. Small bumpiness

Figs. 6.6(a), 6.6(b) and 6.6(c) show, respectively, the distribution of concentration, velocity and granular temperature obtained from the present SS-DEM simulations when using $\psi = \pi/5$, $\bar{\nu} = 0.45$ and various coefficients of restitution. The lines in Fig. 6.6 represent the solution of the numerical integration of Eqs. (6.7)-(6.10) when using $\bar{\nu} = 0.45$, as in the simulations, and the boundary conditions developed by Richman [105].

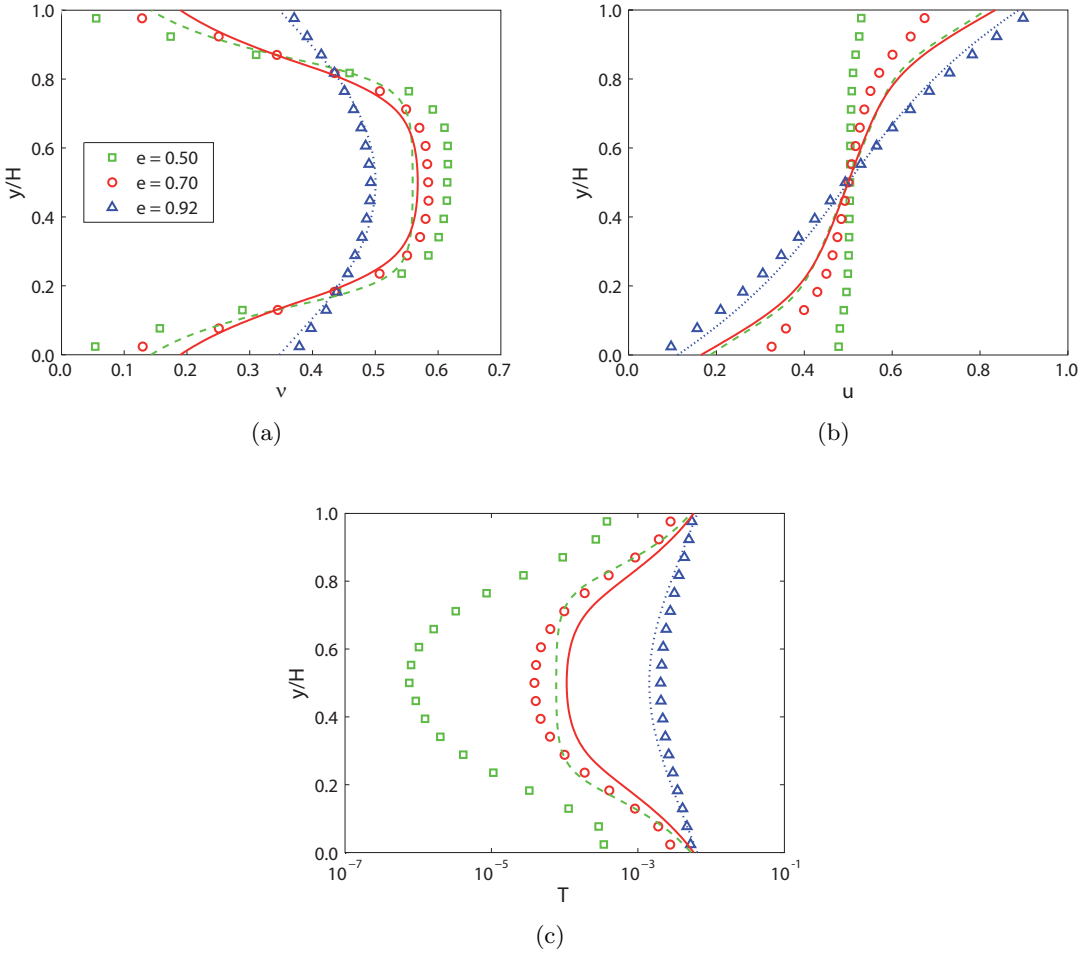

Figure 6.6.: Distribution of concentration (a), velocity (b) and granular temperature (c) obtained from the present SS-DEM simulations (symbols) for $\psi = \pi/5$, $\bar{\nu} = 0.45$ and various coefficients of restitution. The data are compared with the numerical integration of Eqs. (6.7)-(6.10) for $e = 0.50$ (dashed line), $e = 0.70$ (solid line) and $e = 0.92$ (dot-dashed line) when the boundary condition on the slip velocity is Eq. (6.15).

The SS-DEM simulations reveal that the concentration increases with the distance from the wall (Fig. 6.6(a)), and the maximum concentration decreases with the coefficient of restitution. The velocity profiles are not linear (Fig. 6.6(b)), and the slip velocity increases as the coefficient of restitution decreases. Also, the walls are always "hotter" than the interior (Fig. 6.6(c)), i.e., the granular temperature is lower in the core of the flow. The boundaries are said to be "energetic", i.e., the fluctuating energy flux is directed towards the interior of the flow. For very inelastic particles ($e = 0.5$), the granular material roughly moves as a plug and a dense core surrounded by two more dilute layers appear.

Figs. 6.6(a), 6.6(b) and 6.6(c) show that, at small bumpiness ($\psi = \pi/5$), and using the boundary conditions of Richman [105], the modified kinetic theory only qualitatively reproduces the SS-DEM results. Those boundary conditions were developed for nearly elastic particles. Actually, the slip velocity and the concentration are underestimated, and the granular temperature is strongly overestimated when the coefficient of restitution is far from unity. On the other hand, the profiles are very well predicted when using nearly elastic particles ($e = 0.92$).
Fig. 6.7(a) depicts the value of the measured slip velocity u_w as a function of the coefficient of restitution. For $e = 0.5$, the slip velocity approaches the value 0.5, for which

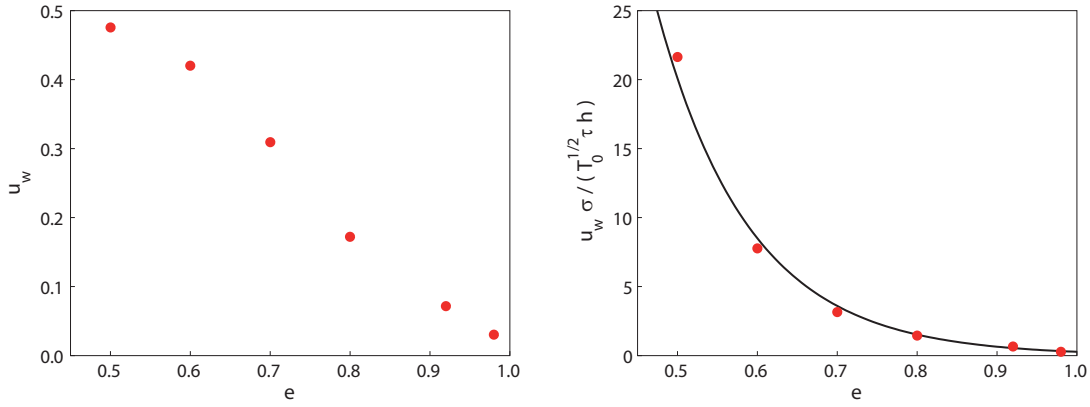

(a) (b)

Figure 6.7.: (a) Slip velocity as a function of the coefficient of restitution obtained from the present SS-DEM simulations when $\psi = \pi/5$. (b) Correction for the theoretical expression of the coefficient h given in Eq. (6.16) obtained from the present SS-DEM simulations. The solid line represents Eq. (6.29).

there is a condition of perfect slip at the walls: in that case, the particles do not touch the walls, so that no exchange of energy with the boundaries is possible. This is the reason why, for e lower than 0.5, the energy initially put into the system is entirely dissipated in collisions and the evolution of the mean granular temperature obeys the Haff's law (Fig. 6.3(a)). The boundary condition proposed by Richman [105] for the slip velocity is given by Eq. (6.15), and can be rewritten as

$$\frac{u_w \sigma}{T_0^{1/2} \tau} = \sqrt{\frac{\pi}{2}} h. \tag{6.28}$$

There, h is defined by Eq. (6.16) as a function of the concentration, the coefficient of restitution and the bumpiness. The quantity on the left-hand-side of Eq. (6.28) can be inferred by the numerical simulations once u_w, σ, T_0 and τ are measured. Fig. 6.7(b) shows the ratio of the quantity $u_w \sigma / \left(T_0^{1/2} \tau \right)$ obtained from the SS-DEM simulations to the coefficient h obtained from Eq. (6.16) using $\psi = \pi/5$ and the numerical values of the concentration at the walls. The boundary condition on the slip velocity of Richman [105] must be corrected in order to reproduce the measurements. On the basis of best fitting, we propose to use

$$\frac{u_w \sigma}{T_0^{1/2} \tau} = h \exp(7.3 - 8.6e), \tag{6.29}$$

which represents the solid line in Fig. 6.7(b).
If we employ Eq. (6.29) instead of Eq. (6.15) as a boundary condition, when numerically integrating the equations of kinetic theory, the agreement with the numerical simulations is remarkable even in the case of very inelastic particles, as can be seen in Figs. 6.8(a), 6.8(b) and 6.8(c). We expect the numerical coefficients in Eq. (6.29) to depend on the bumpiness and, perhaps, the particle stiffness. We postpone to future works a systematic investigation on the role of those quantities in determining the correction to the slip velocity.

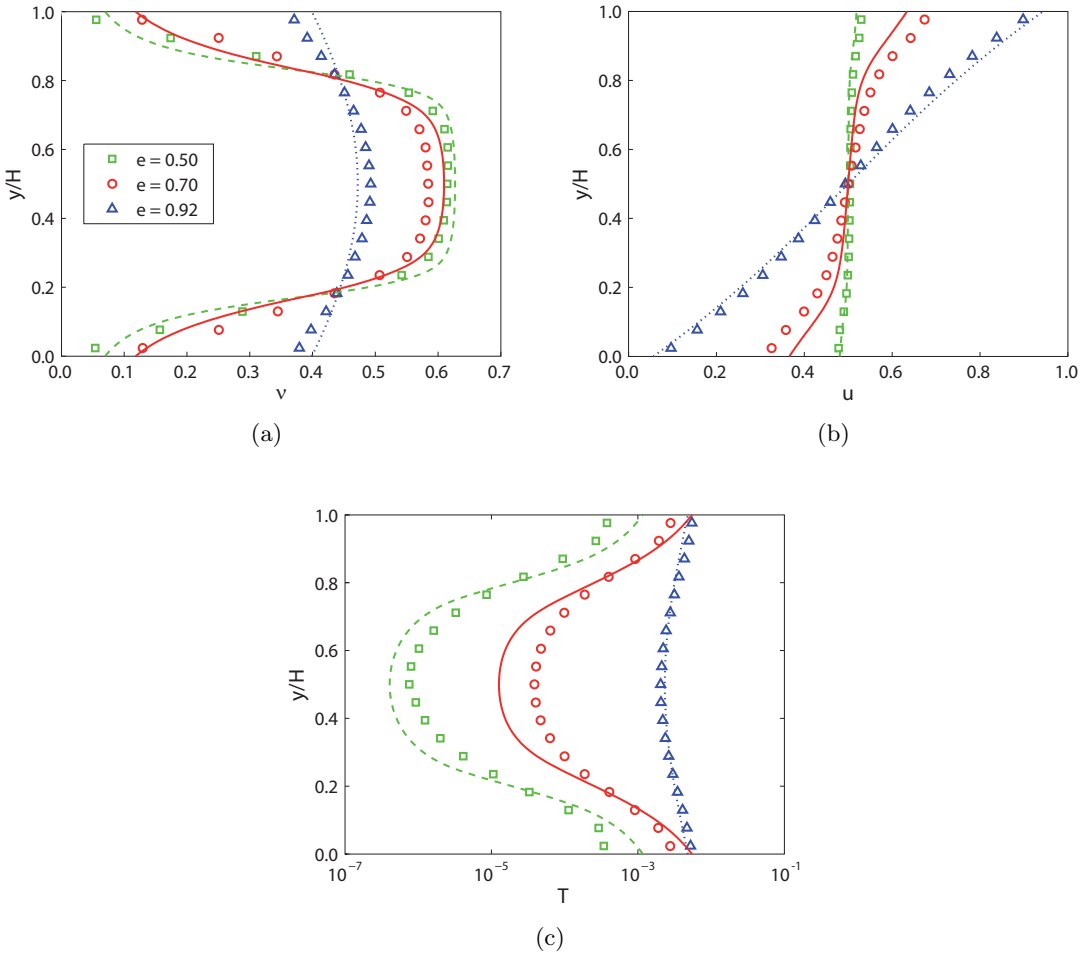

Figure 6.8.: Comparison of the SS-DEM results for $\psi = \pi/5$ and $\bar{\nu} = 0.45$ with the new profiles of concentration (a), velocity (b) and granular temperature (c) obtained by numerically integrating Eqs. (6.7)-(6.10) using Eq. (6.29) as the boundary condition for the slip velocity.

6.3.2. Large bumpiness

Figs. 6.9 shows the variable's profiles obtained from the present SS-DEM simulations when using $\psi = \pi/3$, $\bar{\nu} = 0.44$ and various coefficients of restitution, together with the solution of the numerical integration of Eqs. (6.7)-(6.10) when the boundary conditions of Richman [105] are employed.
The SS-DEM simulations indicate that, at large bumpiness ($\psi = \pi/3$), the concentration

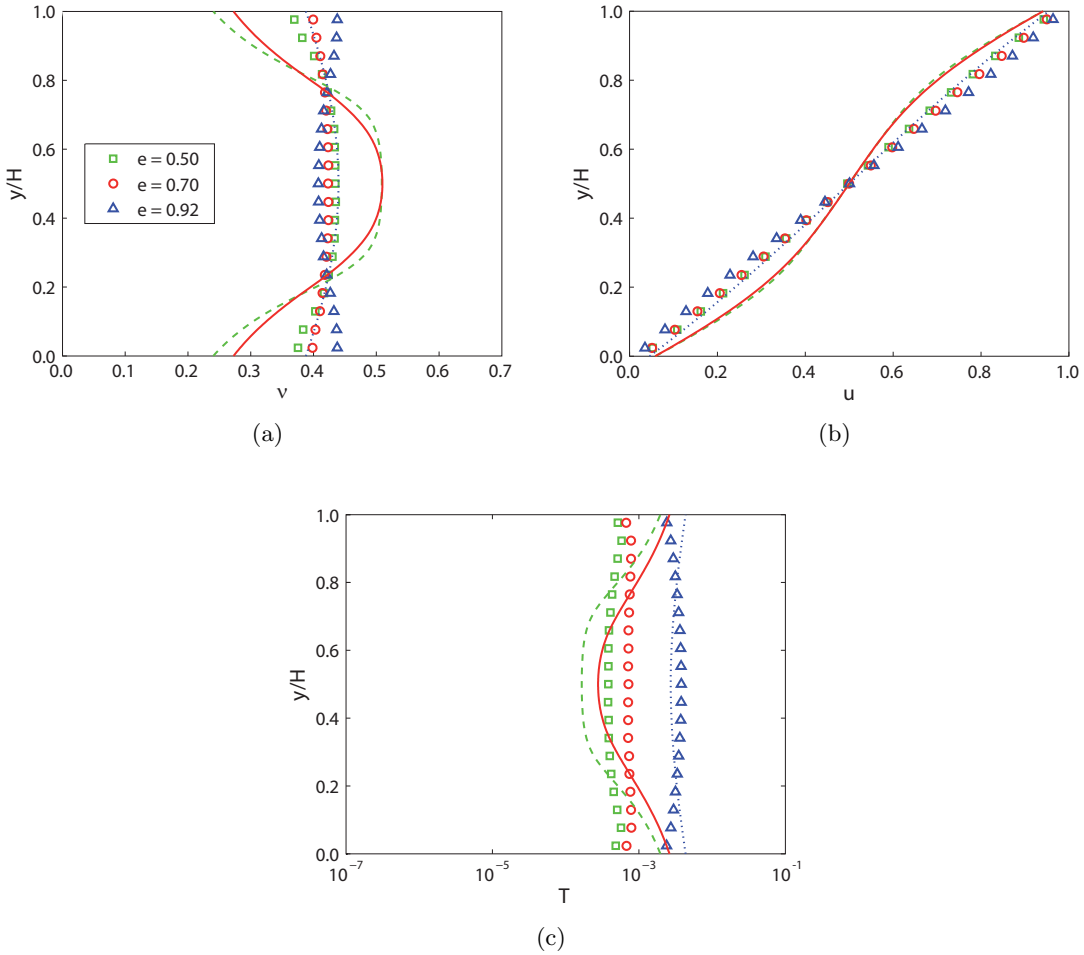

Figure 6.9.: Distribution of concentration (a), velocity (b) and granular temperature (c) obtained from the present SS-DEM simulations (symbols) for $\psi = \pi/3$, $\bar{\nu} = 0.44$ and various coefficients of restitution. The data are compared with the numerical integration of Eqs. (6.7)-(6.10) for $e = 0.50$ (dashed line), $e = 0.70$ (solid line) and $e = 0.92$ (dot-dashed line) when the boundary conditions are Eqs. (6.15) and (6.19).

and the granular temperature are rather uniform (Figs. 6.6(a) and 6.6(c), respectively), and the velocity profile is linearly distributed with zero slip velocity (Fig. 6.9(b)), for all the values of the coefficient of restitution. Then, the flows resemble (homogeneous) simple shear flows. Predictions of the modified kinetic theory in the case $\psi = \pi/3$ when the boundary conditions Eqs. (6.15) and (6.19) are employed strongly disagree with the SS-DEM results. Visual observation of the particle motion suggests that, for large enough bumpiness, some of the flowing particles get stuck in the gaps between the particles glued at the walls; those trapped particles contribute then to create a "disordered" bumpy wall, similar to that employed in the numerical simulations of Silbert et al. [116], which is far less energetic than the "ordered" bumpy wall of Richman [105]. In the case $e = 0.70$ and 0.92, the walls are even slightly colder than the interior (Fig. 6.9(c)), i.e., the boundaries are dissipative (the fluctuating energy flux is directed towards the walls).
If we use $u_w = Q_w = 0$ instead of Eqs. (6.15) and (6.19), i.e., we assume that the boundaries are neutral (they do not furnish nor subtract fluctuating energy), and the mean

concentration obtained by averaging the SS-DEM profiles as boundary conditions, the numerical integration of the modified kinetic theory, which coincides with the analytical solution of simple shear flows, provides a fairly good agreement with the SS-DEM simulations, as shown in Figs. 6.10(a), 6.10(b) and 6.10(c).

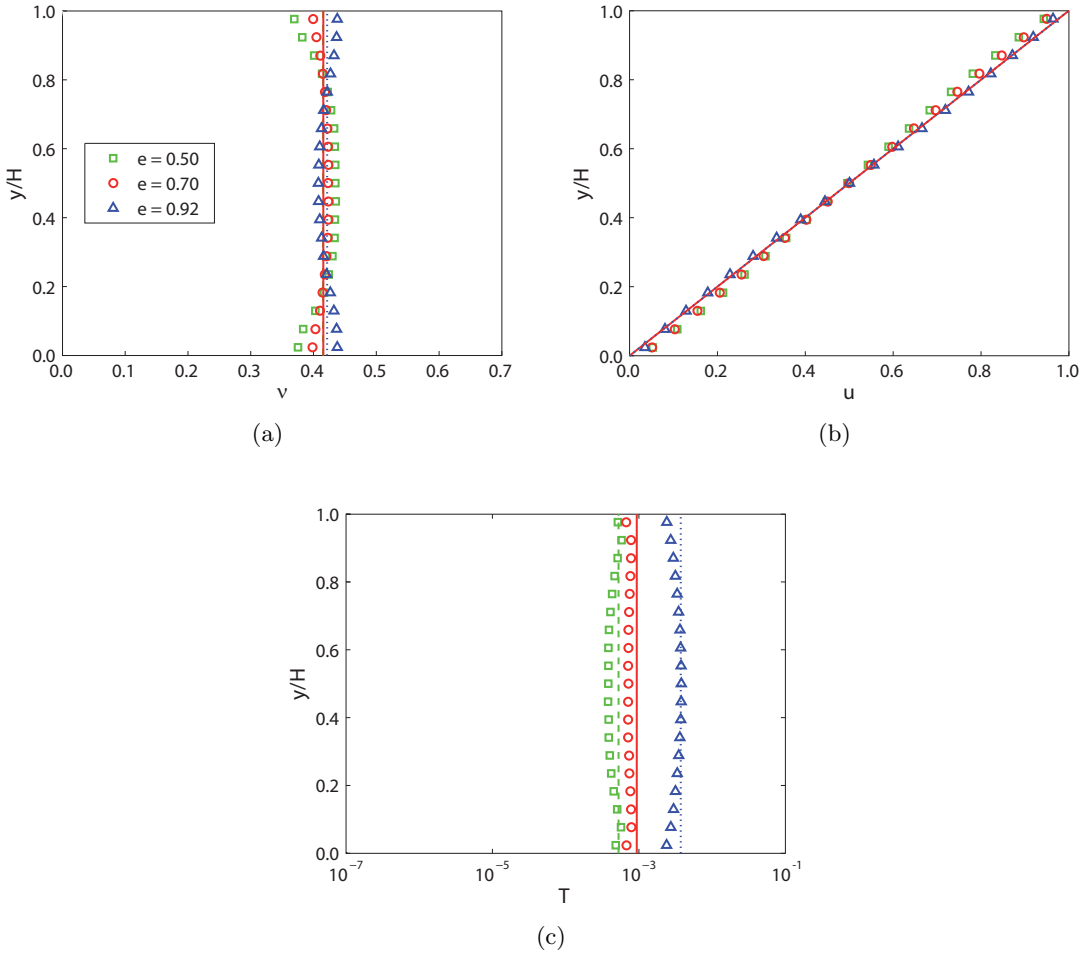

Figure 6.10.: Comparison of the SS-DEM results for $\psi = \pi/3$ and $\bar{\nu} = 0.44$ with the new profiles of concentration (a), velocity (b) and granular temperature (c) obtained by numerically integrating Eqs. (6.7)-(6.10) using $u_w = Q_w = 0$ as boundary conditions.

To check our intuition about the particles being trapped at the walls, we have also performed SS-DEM simulations, with $e = 0.7$, when random conformations of particles are glued at the walls (the details for the generation of this kind of boundaries are given in Silbert et al. [116]). The distributions of the concentration, velocity and granular temperature are very similar to the case $\psi = \pi/3$, as illustrated in Figs. 6.11(a), 6.11(b) and 6.11(c). The mean concentration is different in the two cases, because the space accessible to the flowing particles, whose number is constant and equal to 3132, is different. Also, the fact that the mean concentration measured in the SS-DEM simulatons $\bar{\nu}_{\mathrm{DEM}}$ is, in general, less than the theoretical value 0.44, that would characaterize the $\psi = \pi/3$ case when $N = 3132$, is an indication of particle trapping. Indeed, a rough estimate of the

thickness Δ of this trapped particle layer is

$$\Delta = \frac{N}{2L_xL_z}\left(1 - \frac{\bar{\nu}_{\mathrm{DEM}}}{0.44}\right). \tag{6.30}$$

Fig. 6.11(d) shows that Δ goes to zero as e approaches one. Also, the thickness Δ saturates to a constant value for coefficients of restitution lower than 0.7. Once again, we postpone to future works the generalization of these findings to other values of the bumpiness and the particle stiffness.

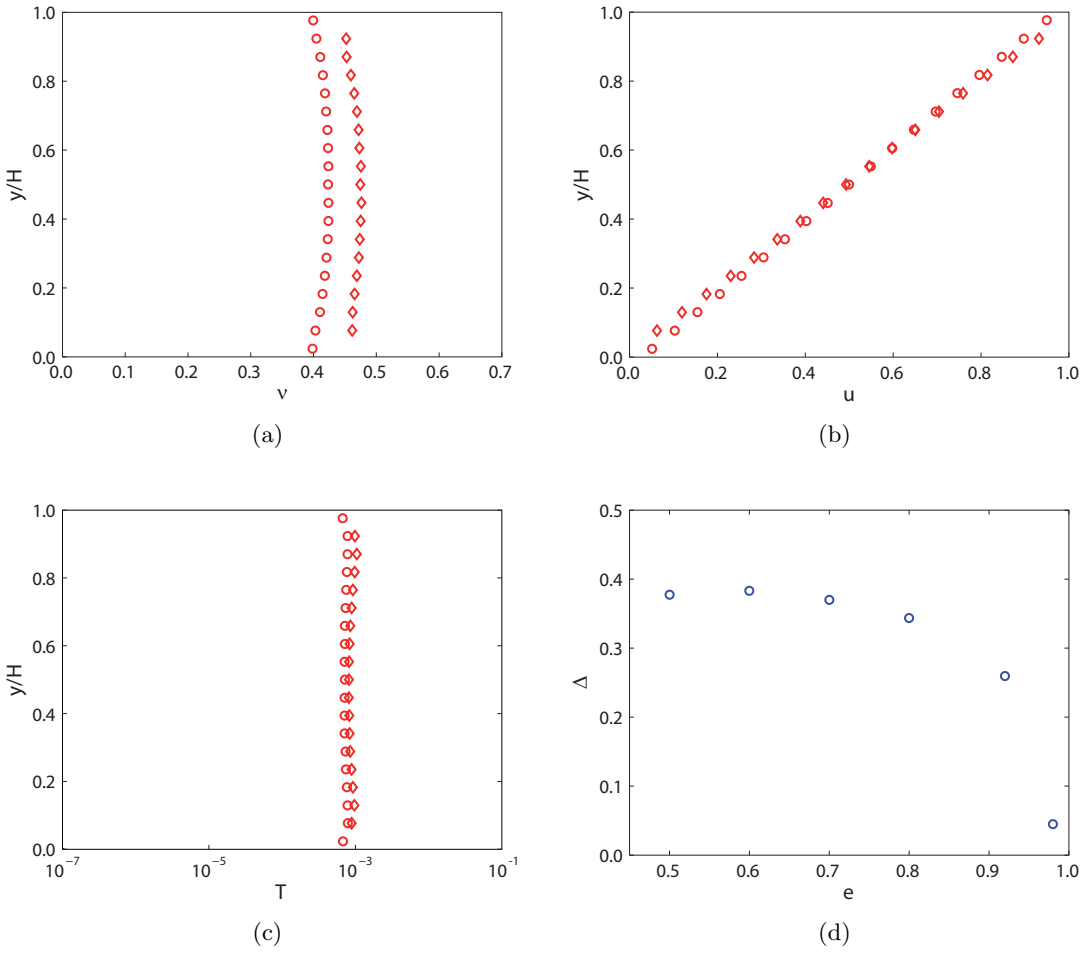

Figure 6.11.: Distribution of concentration (a), velocity (b) and granular temperature (c) obtained from the present SS-DEM simulations with ordered ($\psi = \pi/3$, circles) and disordered (diamonds) bumpy walls, when $e = 0.7$. (d) Thickness of the trapped particle layer as a function of the coefficient of restitution when $\psi = \pi/3$.

Finally, Fig. 6.12 shows the influence of the coefficient of restitution on the stress ratio, s/p, for both the cases of small and large bumpiness. Contrary to results reported for 2D plane shear flows of frictional grains submitted to imposed pressure [30], the coefficient of restitution strongly affects the stress ratio. In the range $0.50 \leq e \leq 0.98$, the stress ratio obtained from the present SS-DEM simulations is a decreasing function of the coefficient of restitution for large bumpiness ($\psi = \pi/3$, open circles); while s/p has a maximum around $e = 0.80$ for small bumpiness ($\psi = \pi/5$, filled circles). The predictions of kinetic

theory when Eqs. (6.29) and (6.19) are employed as boundary conditions for $\psi = \pi/5$, and $u_w = Q_w = 0$ for $\psi = \pi/3$ are, once again, in a fairly good agreement with the simulations (filled and open squares, respectively). The drop in the stress ratio for small bumpiness and coefficients of restitution less than 0.8 is due to the already mentioned increasing of the slip velocity, with the corresponding approaching to the Homogeneous Cooling State, in which the shear stress, and consequently the stress ratio, vanishes.

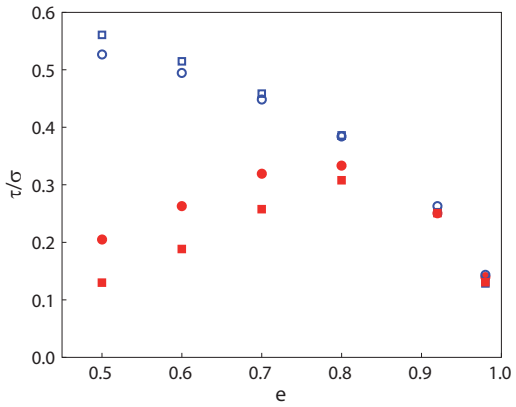

Figure 6.12.: Stress ratio τ/σ as a function of the coefficient of restitution obtained from the SS-DEM simulations when $\psi = \pi/5$ (filled circles) and $\psi = \pi/3$ (open circles), and from the numerical integration of Eqs. (6.7)-(6.10) with the proposed modifications of the boundary conditions ($\psi = \pi/5$, filled squares; $\psi = \pi/3$, open squares).

6.4. Conclusions

In this Chapter, the theoretical model is numerically solved for the shear flows of identical, frictionless particles bounded between two parallel, bumpy planes, at constant volume (Couette flow). According to the model, when the particles are frictionless, the force chains can not develop and the steady flow is always in the collisional regime. Then, the model reduces to the modified kinetic theory. The bumpiness is due to spheres identical to those of the flow, glued at the walls in a regularly spaced, hexagonal array. 3D SS-DEM simulations have been performed in the same flow configuration in order to test the theory and to investigate the role of the coefficient of restitution and the bumpiness of the boundaries.

At small bumpiness, the SS-DEM simulations show that the concentration increases with the distance from the wall, for every value of the coefficient of restitution, and the wall is always "hotter" than the interior. The slip velocity at the boundaries decreases with the elasticity of the particles, and, for coefficients of restitution less than 0.5, the slip is perfect: the boundaries do not touch the flowing particles, so that the system evolves accordingly to the Homogeneous Cooling State (it is not possible to obtain a steady shear flow). Also, the measured stress ratio is a non-monotonic function of the coefficient of restitution, and reaches a maximum for $e = 0.80$. The results of the numerical integration of the theory agree well with the simulations if a correction to the expression of the slip velocity depending on the coefficient of restitution is introduced in the boundary conditions derived for nearly elastic particles by Richman [105].

At large bumpiness, the SS-DEM simulations show nearly uniform profiles of concentration and granular temperature, and linear distributions of the velocity field, as for simple

shear flows. This is due to the fact that, when the gaps between the spheres glued at the walls is large enough, some of the soft flowing particles get stuck, making the bumpy wall more "disordered", and, then, more dissipative than expected. Even in the case of large bumpiness, the model is able to reproduce the simulation results, if both the slip velocity and the fluctuating energy flux at the walls are taken to be zero.
Summarizing, we have shown that the modified kinetic theory has the capability of quantitatively reproducing the flow of frictionless spheres in the entire range of concentration for which the collisions can be considered nearly instantaneous and random (i.e., the entire collisional regime of granular flows). Numerical simulations dealing with friction, non-instantaneous collisions and enduring contacts will be the subject of future works.

7. Conclusions

The fundamental characteristic of granular flows is that the interactions between grains are intrinsically dissipative. The energy of the system is dissipated through two mechanisms: nearly instantaneous collisions and enduring contacts among grains, which are involved in force chains. When only one of the two mechanisms is present, the granular material behaves like a gas (only collisions) or like a solid (only force chains).
This thesis is focused on the development of a constitutive model for granular flows able to reproduce the phase transition between the two extreme regimes, where both enduring contacts and collisions are considered. In this perspective, the present research lies between soil mechanics and fluid dynamics, and aims to incorporate and connect the approaches coming from those two (very) different points of view.
The critical state theory of soil mechanics and the kinetic theory of granular gases have been merged to provide a theoretical description of steady granular flows under shear conditions. The energy and the stress tensor are assumed to be the linear sum of a quasi-static and a collisional contribution, independently modeled by using the aforementioned theories, and accounting, separately, for the two dissipative mechanisms (enduring contacts involved in force chains and collisions, respectively). The interpretation of the constitutive relationship in the light of standard viscoplasticity is the first step towards an evolving constitutive model capable of describing the mechanical behavior of granular material under both solid-like and fluid-like conditions.
The first part of this thesis concerns the application of the constitutive model to the homogeneous shear flows of frictionless and frictional spheres. A critical discussion of the main features of the model has been presented and numerical data taken from the literature have been used to test the theory in this configuration. Several conclusions can be drawn from the analysis. First, dimensional analysis suggests that simple shear flows are governed by four dimensionless variables: the concentration, the stress ratio, the inertial number (ratio of the time scales associated with the motion perpendicular and parallel to the flow) and the ratio of the normal stress to the particle stiffness. The latter does not play any role only if the particles are very hard. On the other hand, when the ratio of the normal stress to the particle stiffness is not negligible, a non-monotonic behavior of the normal stress occurs in pressure-imposed flows when force chains are presents. Second, the model is able to qualitatively reproduce the characteristic features of concentration-imposed flows, shown by the numerical simulations, in the whole range of flow regimes. In particular:

- when the particles are rigid and the the flow is in the collisional regime (i.e., force chains are not present), kinetic theory successfully reproduces all the variables governing the system if the expression of the radial distribution function proposed in this work is adopted; a perfect quantitative agreement between the numerical results and the theory has been shown for various values of the coefficient of restitution and using both frictionless and slightly frictional particles.

- The presence of the quasi-static contribution allows the theory to predict the asymptotic behavior of the normal stress at vanishingly small shear rates and concen-

trations larger than the random loose packing. A purely collisional model cannot reproduce such a rate-independent response.

- The introduction of the function f_r, which accounts for the role of non-instantaneous collisions (i.e., particle stiffness) in the collisional contribution, allows to capture the change of slope in the normal stress which happens at large values of the shear rate.

The second part of this thesis is dedicated to the study of inhomogeneous shear flows of frictionless spheres. The dynamics of an assembly of hard and frictionless spheres sheared between two bumpy walls has been investigated by performing numerical Soft-Sphere Discrete Element Method simulations. The influence of the inelasticity of the particles (i.e., the coefficient of restitution) and the boundary conditions (i.e., bumpiness of the walls) have been investigated. We have used the information obtained from the numerical simulations to propose appropriate boundary conditions, distinguishing between small and large bumpiness. Those boundary conditions have been employed to numerically integrate the differential equations of the theory, which, for frictionless particles, reduces to the collisional contribution. Finally, the numerical results have been compared with the predictions of the theoretical model. The main conclusions of this study are:

- at small bumpiness, the boundaries are energetic: the flux of energy is directed towards the interior of the flow. As a result, the walls are always hotter than the interior and the concentration increases with the distance from the wall. The slip velocity increases with the inelasticity of the particles, and for very inelastic particles, the granular material roughly moves as a plug. When the slip velocity approaches the value 0.5, for which there is a condition of perfect slip at the walls, the particles do not touch the walls, so that no exchange of energy with the boundaries is possible. In that case, the energy initially put into the system is entirely dissipated in collisions and the steady state is never reached.

- At large bumpiness, we have observed that some flowing particles get stuck in the gaps between the wall spheres. The bumpy walls become "disordered", and, then, more dissipative (or less energetic) than expected. The concentration and the granular temperature exhibit a rather uniform profile, resembling homogeneous flows.

- The coefficient of restitution strongly affects the stress ratio, as well as the distributions of concentration and granular temperature, in both cases of small and large bumpiness.

- We have proved that the kinetic theory has the capability of quantitatively reproducing the flow of frictionless spheres in the entire range of concentration for which the collisions can be considered nearly instantaneous.

7.1. Recommendations and future works

This work is a first step towards a complete and accurate description of the rheology of granular flows. There are several limitations and many aspects that can be improved in future research.

Even though the collisional contribution (i.e., modified kinetic theory) has been demostrated to predict extremely well the flows of hard, frictionless and slightly frictional particles, it quantitatively disagrees with the numerical simulations when very frictional and/or soft

particles are considered.
The role of the friction into the collisional term has been modeled using an effective coefficient of restitution whose expression has been derived for slightly frictional particles. In order to correctly account for the friction, a rigorous approach would be to include the balance equations for the mean spin and the rotational fluctuation energy in the set of hydrodynamic equations. Alternatively, a new expression for the effective coefficient of restitution must be inferred from the numerical simulations.
The particle stiffness has been introduced into the collisional contribution in order to account for the non-instantaneous duration of the collisions. When the particles are soft, not only the time duration of a collision increases, but also multiple collisions occur. In the present model, the collisions are assumed to be binary. This assumption leads to the underprediction of the normal stress at large shear rate in the concentration-imposed simple shear flows. Therefore, a possible direction of future research is the generalization of the model to include the role of multiple collisions.

The simple approach based on linearly adding the quasi-static and collisional contribution qualitatively reproduces simple shear flows but, up to now, is unable to simulate flows at concentrations larger than the shear rigidity. According to the model, this limit concentration represents densest disordered configuration of identical spheres attainable under steady, shearing conditions. The numerical results have shown that this threshold can be overcome by the flows, and ordered configurations can be reached. As a consequence, the theory must be extended to the denser flows of ordered configurations.

The unexpected non-monotonic trend of the stress ratio with the shear stress (or, equivalently, with the inertial number) in the regime where both collisions and force chains coexist, must be further investigated. Numerical simulations on homogeneous pressure-imposed shear flows of frictional and soft particles could be performed in order to confirm (or refute) this peculiarity of the model.

Finally, in inhomogeneous shear flows, the numerical simulations performed in this work have shown that the granular material response changes drastically when using small or large bumpiness. Future research can focus on a systematic investigation on the role of the bumpiness. In particular, on the basis of numerical measurements of the slip velocity and the energy flux at the walls, a generalization of the theoretical boundary conditions here proposed can be drawn. The study could be also extended to the influence of the particle stiffness and the friction.

Last but not least, the development of a 3D continuum mechanics based numerical code for the solution of the set of hydrodynamics equations provided by the theory is probably the most ambitious challenge.

A. Kinetic theory auxiliary functions

In this Appendix the auxiliary functions estimated by [40] for the revised kinetic theory are reported. The coefficients η^*, κ^*, μ^* and γ^* appearing in the expressions of the shear viscosity, η, the thermal conductivity, κ, the coefficient of the density gradient, μ and the bulk viscosity, γ, are:

$$\begin{aligned}
\eta^* &= \eta^{\kappa*}\left[1+\frac{4}{5}\nu g_0(1+e_n)\right]+\frac{3}{5}\gamma^* \\
\kappa^* &= \kappa^{\kappa*}\left[1+\frac{6}{5}\nu g_0(1+e_n)\right]+\left(\frac{16}{5}\right)^2\frac{\nu^2 g_0}{\pi}(1+e_n)\left(1+\frac{7}{32}c^*\right) \\
\mu^* &= \mu^{\kappa*}\left[1+\frac{6}{5}\nu g_0(1+e_n)\right] \\
\gamma^* &= \frac{128}{5\pi}\nu^2 g_0(1+e_n)\left(1-\frac{1}{32}c^*\right)
\end{aligned}$$

with

$$\begin{aligned}
\eta^{\kappa*} &= \left(\nu_\eta^*-\frac{1}{2}\zeta^{0*}\right)^{-1}\left[1-\frac{2}{5}(1+e_n)(1-3e_n)\nu g_0\right] \\
\kappa^{\kappa*} &= \frac{2}{3}\left(\nu_\kappa^*-2\zeta^{0*}\right)^{-1}\left(1+\frac{1}{2}(1+p^*)c^*+\frac{3}{5}\nu g_0\left(1+e_n\right)^2\left\{2e_n-1+\left[\frac{1+e_n}{2}-\frac{5}{3(1+e_n)}\right]c^*\right\}\right) \\
\mu^{\kappa*} &= 2\left(2\nu_\kappa^*-3\zeta^{0*}\right)^{-1}\left\{\left(1+\nu\frac{g_0'}{g_0}\right)\zeta^{0*}\kappa^{\kappa*}+\frac{p^*}{3}\left(1+\nu\frac{p^{*\prime}}{p^*}\right)c^*+\right. \\
&\quad \left.-\frac{4}{5}\nu g_0\left(1+\frac{\nu}{2}\frac{g_0'}{g_0}\right)(1+e_n)\left\{e_n(1-e_n)+\frac{1}{4}\left[\frac{4}{3}+e_n(1-e_n)\right]c^*\right\}\right\} \\
c^* &= 32(1-e_n)\left(1-2e_n^2\right)\left[81-17e_n+30e_n^2(1-e_n)\right]^{-1} \\
p^* &= 1+2(1+e_n)\nu g_0 \\
\nu_\eta^* &= g_0\left[1-\frac{1}{4}\left(1-e_n\right)^2\right]\left[1-\frac{1}{64}c^*\right] \\
\nu_\kappa^* &= \frac{1}{3}(1+e_n)g_0\left[1+\frac{33}{16}(1-e_n)+\frac{19-3e_n}{1024}c^*\right] \\
\zeta^{0*} &= \frac{5}{12}g_0\left(1-e_n^2\right)\left(1+\frac{3}{32}c^*\right)
\end{aligned}$$

where $g_0'=\dfrac{dg_0}{d\nu}$ and $p^{*\prime}=\dfrac{dp^*}{d\nu}=2(1+e_n)\left(g_0+\nu g_0'\right)$.
The coefficient ζ^* appearing in the expression of the collisional rate of dissipation of fluctuating energy, Γ, reads:

$$\zeta^*=\zeta^{0*}+\zeta^{1*}$$

where

$$\zeta^{1*} = \left[-\frac{5}{96}\frac{d}{\nu}\sqrt{\frac{\pi}{T}}(1-e_n)(p^*-1) + \frac{5}{32}\left(1-e_n^2\right)\left(1+\frac{3}{64}c^*\right)g_0 C_d \right] \nabla \cdot \mathbf{u}$$

$$C_d = \frac{5}{96}\frac{d}{\nu}\sqrt{\frac{\pi}{T}}\left[\frac{1}{2}\zeta^{0*} + \nu_\gamma^* + \frac{5}{64}c^*\left(1+\frac{3}{64}c^*\right)g_0\left(1-e_n^2\right)\right]^{-1}\left[\frac{4}{15}\lambda\nu g_0 + (p^*-1)\left(\frac{2}{3}-e_n\right)c^*\right]$$

$$\nu_\gamma^* = \frac{1+e_n}{48}g_0\left[128 - 96e_n + 15e_n^2 - 15e_n^3 + \frac{c^*}{64}(15e_n^3 - 15e_n^2 + 498e_n - 434)\right]$$

$$\lambda = \frac{3}{8}\left[(1-e_n)\left(5e_n^2+4e_n-1\right) + \frac{c^*}{12}\left(159e_n + 3e_n^2 - 19e_n - 15e_n^3\right)\right].$$

B. Comparison of the collisional contribution with numerical results

From the constitutive relation for the collisional normal stress and shear stress, for plane shear flows,

$$f_1 = \frac{\sigma_{\mathrm{col}}}{\rho_p T}, \tag{B.1}$$

$$f_2 = \frac{\tau_{\mathrm{col}}}{\rho_p d T^{1/2} \dot{\gamma}}, \tag{B.2}$$

so that the functions f_1 and f_2 can be obtained from the numerical (measured) values of σ_{col}, τ_{col}, T and $\dot{\gamma} = u'$. In this Appendix, we show the comparison of the theoretical expressions of f_1 and f_2, Eqs. (4.46) and (4.47), with the measured quantities $\sigma / (\rho_p T)$ and $\tau / \left(\rho_p d T^{1/2} \dot{\gamma}\right)$ obtained, in the collisional regime, from the numerical simulations of Mitarai and Nakanishi [88] and Chialvo and Sundaresan [27] on homogeneous plane shear flows and the present SS-DEM simulations of inhomogeneous plane shear flows, using different values of the normal coefficient of restitution and of the interparticle friction coefficient.

Frictionless spheres ($\mu = 0$)

In the case of nearly elastic particles ($e = 0.98$ and 0.99), f_1 is slightly underpredicted if the proposed radial distribution function is adopted (Figs. B.6(a) and B.7(a)). Replacing Eq. (4.28) with Eq. (4.27) into Eq. (4.46) would allow a good fitting also for the case of nearly elastic particles ($e > 0.95$).

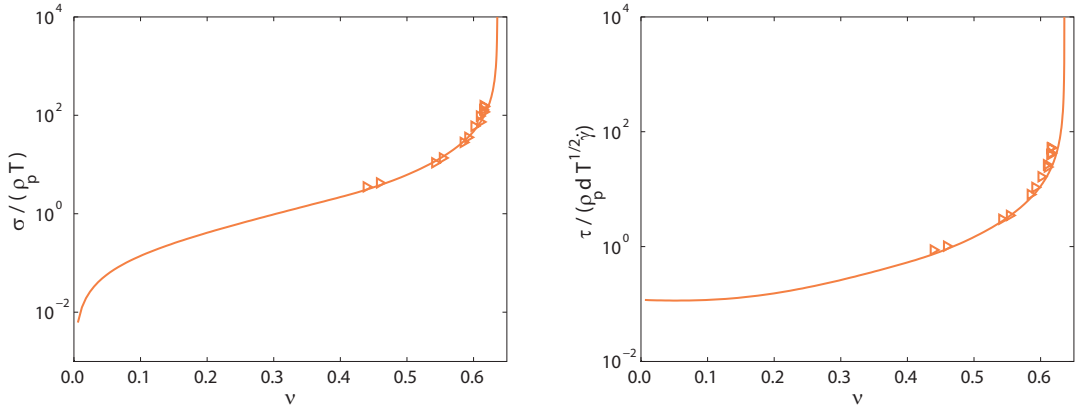

Figure B.1.: Theoretical f_1 (a) and f_2 (b) (solid lines, Eqs. 4.46 and (4.47)), compared with the numerical $\sigma / (\rho_p T)$ and $\tau / \left(\rho_p d T^{1/2} \dot{\gamma}\right)$ obtained from numerical simulations when $\mu = 0$ ($\nu_{\mathrm{s}} = \nu_{\mathrm{rcp}} = 0.636$) and $e = 0.5$ (symbols).

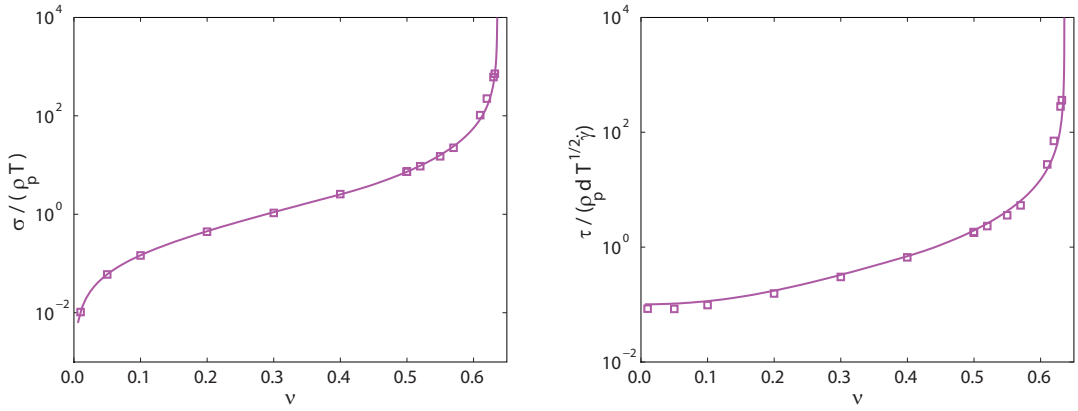

Figure B.2.: Same as in Fig. B.1 but for $e = 0.8$.

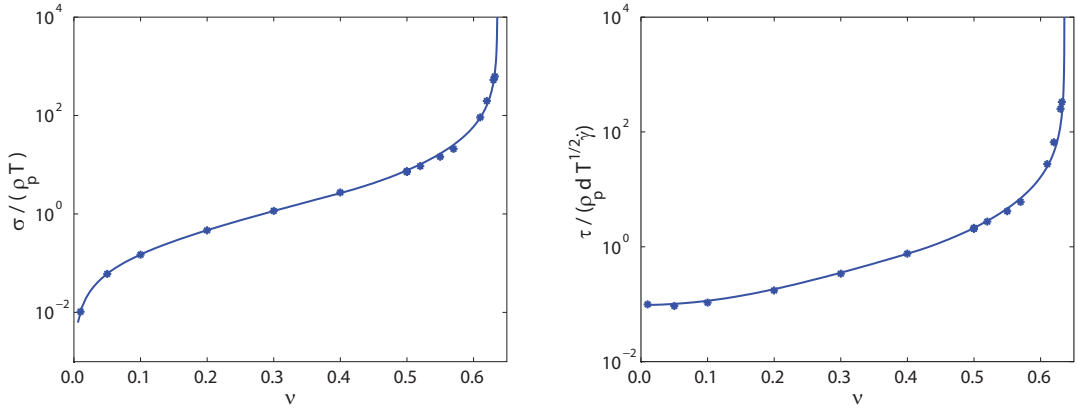

Figure B.3.: Same as in Fig. B.1 but for $e = 0.9$.

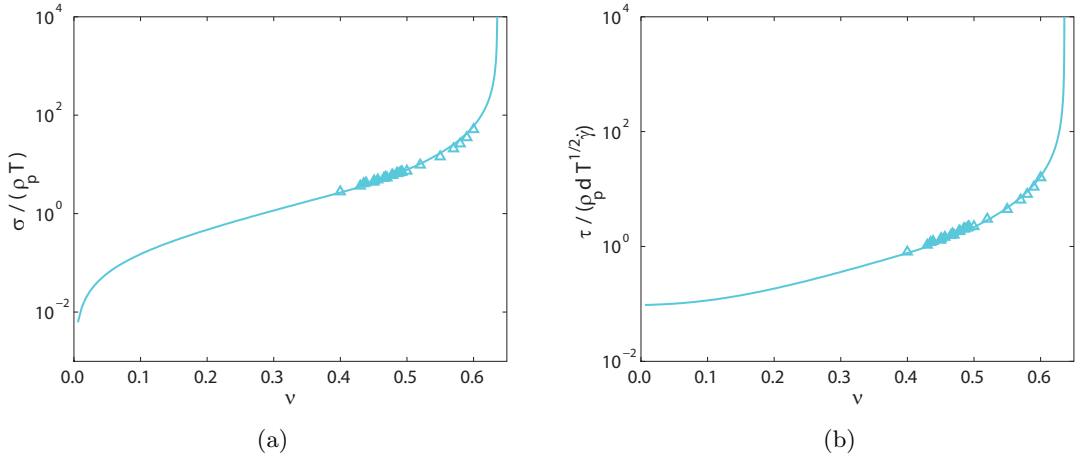

Figure B.4.: Same as in Fig. B.1 but for $e = 0.92$.

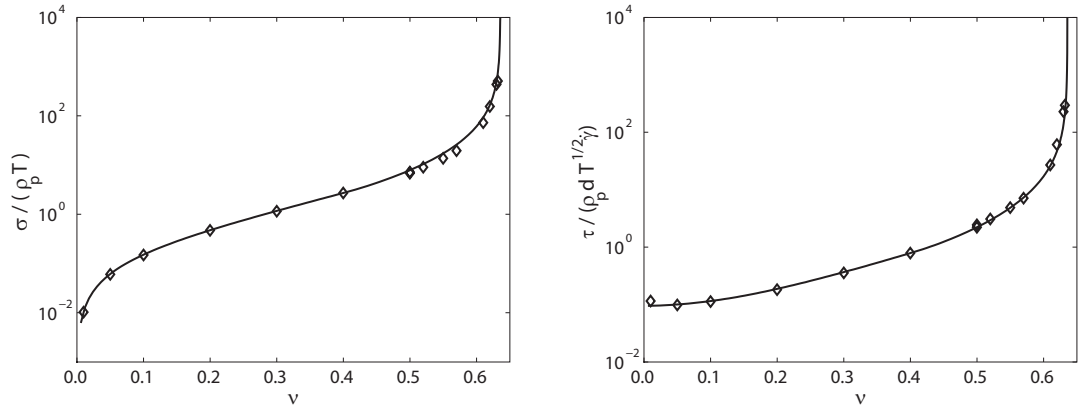

Figure B.5.: Same as in Fig. B.1 but for $e = 0.95$.

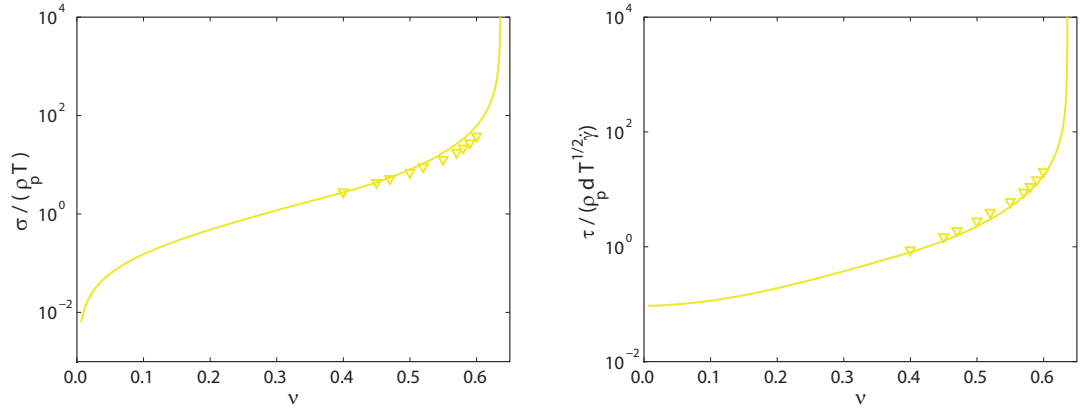

Figure B.6.: Same as in Fig. B.1 but for $e = 0.98$.

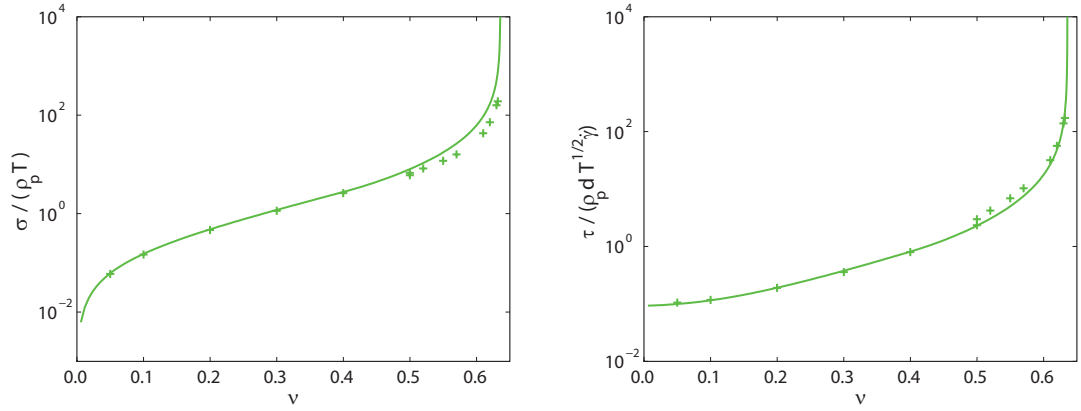

Figure B.7.: Same as in Fig. B.1 but for $e = 0.99$.

Slightly frictional spheres ($\mu = 0.1$)

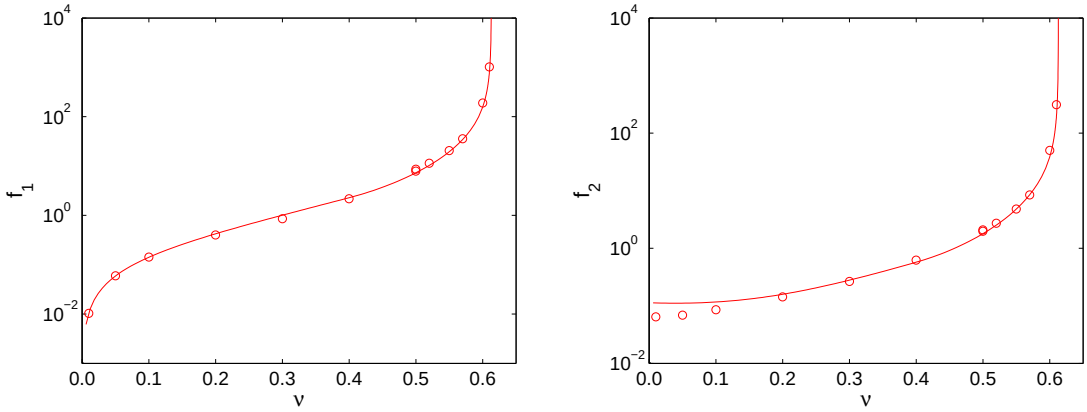

Figure B.8.: Theoretical f_1 (a) and f_2 (b) (solid lines, Eqs. 4.46 and (4.47)), compared with the numerical $\sigma/\left(\rho_p T\right)$ and $\tau/\left(\rho_p d T^{1/2}\dot{\gamma}\right)$ obtained by Chialvo and Sundaresan [27] when $\mu = 0.1$ ($\nu_s = 0.613$), $e_t = 1$ and $e_n = 0.7$ (symbols).

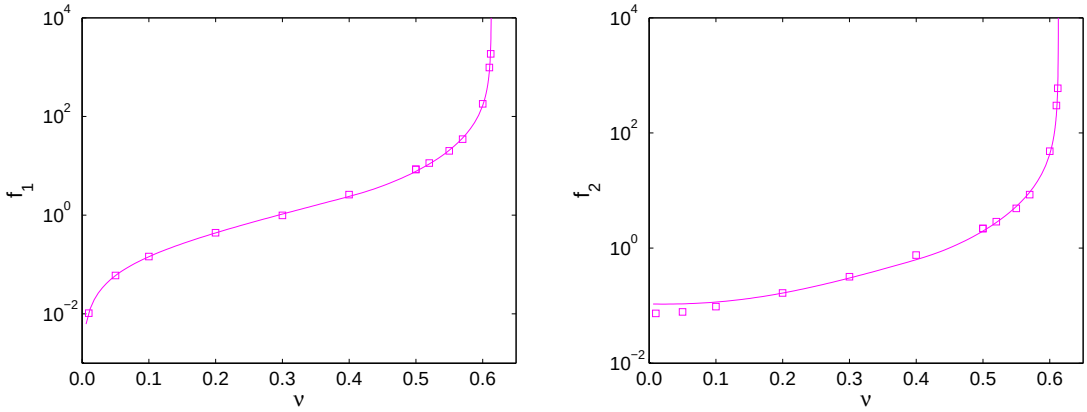

Figure B.9.: Same as in Fig. B.8 but for $e_n = 0.8$.

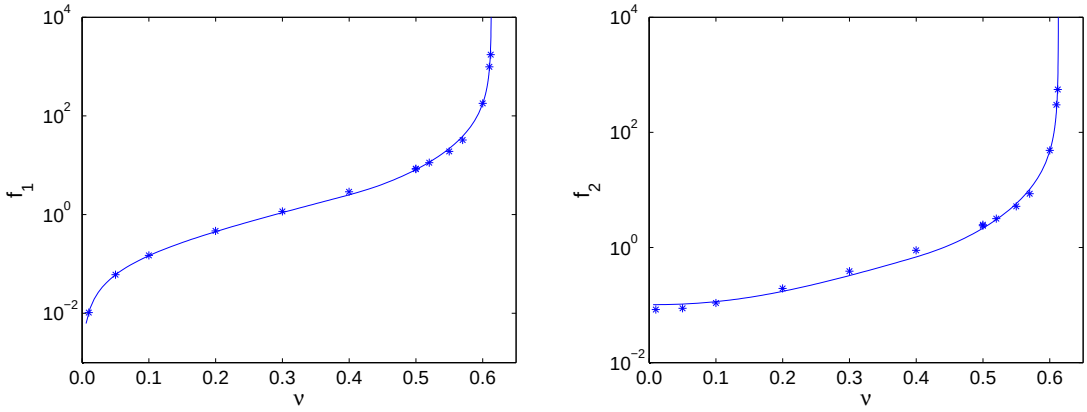

(a) (b)

Figure B.10.: Same as in Fig. B.8 but for $e_n = 0.9$.

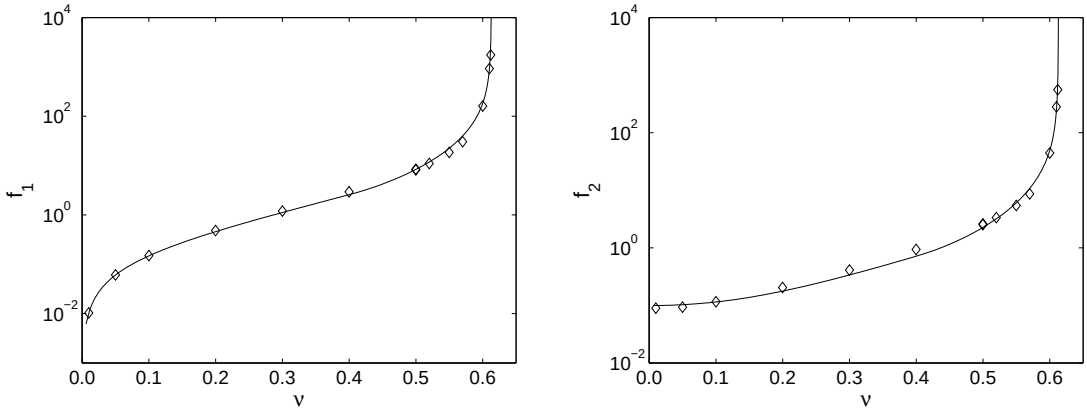

(a) (b)

Figure B.11.: Same as in Fig. B.8 but for $e_n = 0.95$.

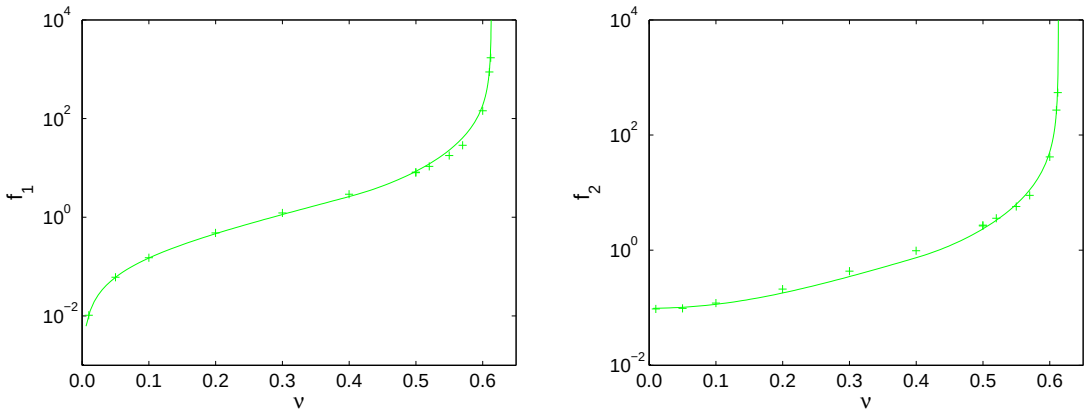

(a) (b)

Figure B.12.: Same as in Fig. B.8 but for $e_n = 0.99$.

Bibliography

[1] M. Alam, J.T. Willits, B.O. Arnarson, and S. Luding. Kinetic theory of a binary mixture of nearly elastic disks with size and mass-disparity. *Physics of Fluids*, 14: 4085–4087, 2002.

[2] I. Aranson and L. Tsimring. Patterns and collective behavior in granular media: Theoretical concepts. *Reviews of Modern Physics*, 78:641–692, 2006.

[3] B.O. Arnarson and J.T. Willits. Thermal diffusion in binary mixtures of smooth, nearly elastic spheres with and without gravity. *Physics of Fluids*, 10:1324–1328, 1998.

[4] M. Babic. Unsteady Couette granular flows. *Physics of Fluids*, 9:2486–2505, 1997.

[5] M. Babic. Average balance equations for granular materials. *International Journal of Engineering Science*, 35:523–548, 1997.

[6] M. Babic, H.H. Shen, and H.T. Shen. The stress tensor in granular shear flows of uniform, deformable disks at high solids concentrations. *Journal of Fluid Mechanics*, 219:81–118, 1999.

[7] R.A. Bagnold. Experiments on a gravity-free dispersion of large solid spheres in a newtonian fluid under shear. *Proceedings of the Royal Society A*, 255(1160):49–63, 1954.

[8] J.P. Bardet and I. Vardoulakis. The asymmetry of stress in granular media. *International Journal of Solids and Structures*, 38:353–367, 2001.

[9] V. Becker, T. Schwager, and T. Pöeschel. Coefficient of tangential restitution for the linear dashpot model. *Physical Review E*, 77:011304, 2007.

[10] K. Been and M.G. Jefferies. Discussion: a state parameter for sands. *Géotechnique*, 36:123–132, 1986.

[11] D. Berzi. Extended kinetic theory applied to dense, granular, simple shear flows. *Acta Mechanica*, 2013, submitted.

[12] D. Berzi and J.T. Jenkins. A theoretical analysis of free-surface flows of saturated granular-liquid mixtures. *Journal of Fluid Mechanics*, 608:393–410, 2008.

[13] D. Berzi and J.T. Jenkins. Approximate analytical solutions in a model for highly concentrated granular flows. *Physical Review E*, 78:011304, 2008.

[14] D. Berzi and J.T. Jenkins. Steady inclined flows of granular fluid mixtures. *Journal of Fluid Mechanics*, 641:359–387, 2009.

[15] D. Berzi and J.T. Jenkins. Surface flows of inelastic spheres. *Physics of Fluids*, 23: 013303, 2011.

[16] D. Berzi, C. di Prisco, and D. Vescovi. Constitutive relations for steady, dense granular flows. *Physical Review E*, 84:031301, 2011.

[17] J.J. Brey, J.W. Dufty, and A. Santos. Dissipative dynamics for hard-spheres. *Journal of Statistical Physics*, 87:1051–1066, 1997.

[18] J.J. Brey, J.W. Dufty, C.S. Kim, and A. Santos. Hydrodynamics for granular flow at low density. *Physical Review E*, 58:4638–4653, 1998.

[19] N. Brilliantov and T. Pöschel. Granular gases with impact-velocity-dependent restitution coefficient. In T. Pöschel and S. Luding, editors, *Granular Gases*, volume 564 of *Lecture Notes in Physics*, pages 100–124. Springer Berlin Heidelberg, 2001.

[20] N.V. Brilliantov and T. Pöschel. *Kinetic Theory of Granular Gases*. Oxford University Press, Oxford, U.K., 2004.

[21] N. Brodu, P. Richard, and R. Delannay. Shallow granular flows down flat frictional channels: Steady flows and longitudinal vortices. *Physical Review E*, 87:022202, 2013.

[22] L. Bureau, T. Baumberger, and C. Caroli. Rheological aging and rejuvenation in solid friction contacts. *European Physical Journal E*, 8:331–337, 2002.

[23] C.S. Campbell. Rapid granular flows. *Annual Review of Fluid Mechanics*, 22:57–92, 1990.

[24] C.S. Campbell. Granular shear flows at the elastic limit. *Journal of Fluid Mechanics*, 465:261–291, 2002.

[25] N.F. Carnahan and K.E. Starling. Equation of state for nonattracting rigid spheres. *Journal of Chemical Physics*, 51:635–636, 1969.

[26] S. Chapman and T.G. Cowling. *The mathematical theory of non-uniform gases*. Cambridge University Press, Cambridge, U.K., 1970.

[27] S. Chialvo and S. Sundaresan. A modified kinetic theory for frictional granular flows in dense and dilute regimes. *Physics of Fluids*, 25:070603, 2013.

[28] S. Chialvo, J. Sun, and S. Sundaresan. Bridging the rheology of granular flows in three regimes. *Physical Review E*, 85:021305, 2012.

[29] P.A. Cundall and O.D.L. Strack. A discrete numerical model for granular assemblies. *Géotechnique*, 29:47–65, 1979.

[30] F. da Cruz, S. Emam, M. Prochnow, J. Roux, and F. Chevoir. Rheophysics of dense granular materials: Discrete simulation of plane shear flows. *Physical Review E*, 72: 021309, 2005.

[31] R.C. Daniel, A.P. Poloski, and A.E. Saez. A continuum constitutive model for cohesionless granular flows. *Chemical Engineering Science*, 62:1343–1350, 2007.

[32] R. Delannay, M. Louge, P. Richard, N. Taberlet, and A. Valance. Towards a theoretical picture of dense granular flows down inclines. *Nature Materials*, 6:99–108, 2007.

[33] C. di Prisco and S. Imposimato. Experimental analysis and theoretical interpretation of triaxial load controlled loose sand specimen collapses. *Mechanics of Cohesive-Frictional Materials*, 2:93–120, 1997.

[34] C. di Prisco and F. Pisanó. An exercise on slope stability and perfect elasto-plasticity. *Géotechnique*, 61:923–934, 2011.

[35] N. Estrada, A. Taboada, and F. Radjaï. Shear strength and force transmission in granular media with rolling resistance. *Physical Review E*, 78:021301, 2008.

[36] G.R. Farrell, K.M. Martini, and N. Menon. Loose packings of frictional spheres. *Soft Matter*, 6:2925–2930, 2010.

[37] S.F. Foerster, M.Y. Louge, H. Chang, and K. Allia. Measurements of the collision properties of small spheres. *Physics of Fluids*, 6:1108–1115, 1994.

[38] Y. Forterre and O. Pouliquen. Flows of dense granular media. *Annual Review of Fluid Mechanics*, 40:1–24, 2008.

[39] A. Gajo and D. Muir Wood. Severn-Trent sand: a kinematic hardening constitutive model for sands: the $q - p$ formulation. *Géotechnique*, 49:595–614, 1999.

[40] V. Garzó and J.W. Dufty. Dense fluid transport for inelastic hard spheres. *Physical Review E*, 59:5895–5911, 1999.

[41] V. Garzó and J.W. Dufty. Hydrodynamics for a granular binary mixture at low density. *Physics of Fluids*, 14:1476–1490, 2002.

[42] V. Garzó, J.W. Dufty, and C.M. Hrenya. Enskog theory for polydisperse granular mixtures. I. Navier-Stokes order transport. *Physical Review E*, 76:031303, 2007.

[43] V. Garzó, C.M. Hrenya, and J.W. Dufty. Enskog theory for polydisperse granular mixtures. II. Sonine polynomial approximation. *Physical Review E*, 76:031303, 2007.

[44] GDR-MiDi. On dense granular flows. *European Physical Journal E*, 14:341–365, 2004.

[45] I. Goldhirsch. Rapid granular flows. *Annual Review of Fluid Mechanics*, 35:267–293, 2003.

[46] I. Goldhirsch. Introduction to granular temperature. *Powder Technology*, 182:130–136, 2008.

[47] A. Goldstein and M. Shapiro. Mechanics of collisional motion of granular materials. Part 1. General hydrodynamic equations. *Journal of Fluid Mechanics*, 282:75–114, 1995.

[48] P.K. Haff. Grain flow as a fluid-mechanical phenomenon. *Journal of Fluid Mechanics*, 134:401–430, 1983.

[49] H. Hwang and K. Hutter. A new kinetic model for rapid granular flow. *Continuum Mechanics and Thermodynamics*, 7:357–384, 1995.

[50] H.M Jaeger, S.R. Nagel, and R.P. Behringer. Granular solids, liquids, and gases. *Reviews of Modern Physics*, 68:1259–1273, 1996.

[51] M. Jean. Contact dynamics method. In F. Radjaï and F. Dubois, editors, *Discrete-element modeling of granular materials*. Wiley, 2001.

[52] J.T. Jenkins. Dense shearing flows of inelastic disks. *Physics of Fluids*, 18:103307, 2006.

[53] J.T. Jenkins. Dense inclined flows of inelastic spheres. *Granular Matter*, 10:47–52, 2007.

[54] J.T. Jenkins and D. Berzi. Dense inclined flows of inelastic spheres: tests of an extension of kinetic theory. *Granular Matter*, 12:151–158, 2010.

[55] J.T. Jenkins and F. Mancini. Balance laws and constitutive relations for plane flows of a dense, binary mixture of smooth, nearly elastic, circular disks. *Journal of Applied Mechanics*, 54:27–34, 1987.

[56] J.T. Jenkins and F. Mancini. Kinetic theory for binary mixtures of smooth, nearly elastic spheres. *Physics of Fluids A: Fluid Dynamics (1989-1993)*, 1:2050–2057, 1989.

[57] J.T. Jenkins and M.W. Richman. Grad's 13-moment system for a dense gas of inelastic spheres. *Archive for Rational Mechanics and Analysis*, 87:355–377, 1985.

[58] J.T. Jenkins and M.W. Richman. Plane simple shear of smooth inelastic circular disks: the anisotropy of the second moment in the dilute and dense limits. *Journal of Fluid Mechanics*, 192:313–328, 1988.

[59] J.T. Jenkins and S.B. Savage. A theory for the rapid flow of identical, smooth, nearly elastic, spherical particles. *Journal of Fluid Mechanics*, 130:187–202, 1983.

[60] J.T. Jenkins and C. Zhang. Kinetic theory for identical, frictional, nearly elastic spheres. *Physics of Fluids*, 14:1228–1235, 2002.

[61] S. Ji and H.H. Shen. Characteristics of temporalspatial parameters in quasisolid-fluid phase transition of granular materials. *Chinese Science Bulletin*, 51:646–654, 2006.

[62] S. Ji and H.H. Shen. Internal parameters and regime map for soft polydispersed granular materials. *Journal of Rheology*, 52:87–103, 2008.

[63] P.C. Johnson and R. Jackson. Frictional-collisional constitutive relations for granular materials, with application to plane shearing. *Journal of Fluid Mechanics*, 176:67–93, 1987.

[64] P.C. Johnson and R. Jackson. Frictional-collisional equations of motion for particulate flows and their application to chutes. *Journal of Fluid Mechanics*, 210:501–535, 1990.

[65] P. Jop. Hydrodynamic modeling of granular flows in a modified Couette cell. *Physical Review E*, 77:032301, 2008.

[66] P. Jop, Y. Forterre, and O. Pouliquen. Crucial role of sidewalls in granular surface flows: consequences for the rheology. *Journal of Fluid Mechanics*, 541:167–192, 2005.

[67] P. Jop, Y. Forterre, and O. Pouliquen. A constitutive law for dense granular flows. *Nature*, 441:727–730, 2006.

[68] A. Karion and M.L. Hunt. Wall stresses in granular Couette flows of mono-sized particles and binary mixtures. *Powder Technology*, 109:145–163, 2000.

[69] D. Kolymbas. *Constitutive modelling of granular materials*. Springer, Berlin, Germany, 2000.

[70] V. Kumaran. Dense granular flow down an inclined plane: from kinetic theory to granular dynamics. *Journal of Fluid Mechanics*, 599:121–168, 2008.

[71] V. Kumaran. Dynamic of dense sheared granular flows. Part 1. Structure and diffusion. *Journal of Fluid Mechanics*, 632:109–144, 2009.

[72] C.H. Lee and C.J. Huang. Model of sheared granular material and application to surface-driven granular flows under gravity. *Physics of Fluids*, 22:043307, 2010.

[73] A.W. Lees and S. F. Edwards. The computer study of transport processes under extreme conditions. *Journal of Physics C: Solid State Physics*, 5:1921–1929, 1972.

[74] J. Liu and A.D. Rosato. General features of granular Couette flow and intruder dynamics. *Journal of Physics: Condensed Matter*, 17:S2609–S2622, 2005.

[75] G. Lois, J. Carlson, and A. Lemaitre. Numerical tests of constitutive laws for dense granular fows. *Physical Review E*, 72:051303, 2005.

[76] G. Lois, A. Lemaitre, and J. Carlson. Emergence of multi-contact interactions in contact dynamics simulations. *Europhysics Letters*, 76:318, 2006.

[77] A. Lorenz, C. Tuozzolo, and M.Y. Louge. Measurements of impact properties of small, nearly spherical particles. *Experimental Mechanics*, 37:292–298, 1997.

[78] M.Y. Louge. Model for dense granular flows down bumpy inclines. *Physical Review E*, 67:061303, 2003.

[79] S. Luding. Introduction to discrete element methods: Basics of contact force models and how to perform the micro-macro transition to continuum theory. *European Journal of Environmental and Civil Engineering - EJECE 12*, 12(7-8):785–826, 2008.

[80] C.K.K. Lun. Kinetic theory for granular flow of dense, slightly inelastic, slightly rough spheres. *Journal of Fluid Mechanics*, 223:539–559, 1991.

[81] C.K.K. Lun and S.B. Savage. A simple kinetic theory for granular flow of rough, inelastic, spherical particles. *Journal of Applied Mechanics*, 54:47–53, 1987.

[82] T.S. Majmudar and R.P. Behringer. Contact force measurements and stress-induced anisotropy in granular materials. *Nature*, 435:1079–1082, 2005.

[83] S. McNamara. Molecular dynamics method. In F. Radjaï and F. Dubois, editors, *Discrete-element modeling of granular materials*. Wiley, 2001.

[84] S. McNamara. Event-driven method. In F. Radjaï and F. Dubois, editors, *Discrete-element modeling of granular materials*. Wiley, 2001.

[85] T. Miller, P. Rognon, B. Metzger, and I. Einav. Eddy viscosity in dense granular flows. *Physical Review Letters*, 2013 in press.

[86] P. Mills, P.G. Rognon, and F. Chevoir. Rheology and structure of granular materials near the jamming transition. *Europhysics Letters*, 81:64005, 2008.

[87] N. Mitarai and H. Nakanishi. Bagnold scaling, density plateau, and kinetic theory analysis of dense granular flow. *Physical Review Letters*, 94:128001, 2005.

[88] N. Mitarai and H. Nakanishi. Velocity correlations in the dense granular shear flows: Effects on energy dissipation and normal stress. *Physical Review E*, 75:031305, 2007.

[89] N. Mitarai, H. Hayakawa, and H. Nakanishi. Collisional granular flow as a micropolar fluid. *Physical Review Letters*, 88:174301, 2002.

[90] L.S. Mohan, K.K. Rao, and P.R. Nott. A frictional cosserat model for the slow shearing of granular materials. *Journal of Fluid Mechanics*, 457:377–409, 2002.

[91] J.M. Montanero and A. Santos. Monte Carlo simulation method for the Enskog equation. *Physical Review E*, 54:438–444, 1996.

[92] D. Muir Wood. *Soil behaviour and critical state soil mechanics*. Cambridge University Press, Cambridge, U.K., 1990.

[93] D. Muir Wood. *Geotechnical modelling*. Spon Press, New York, 2004.

[94] D. Muir Wood. The magic of sands. *Canadian Geotechnical Journal*, 44:1329–1350, 2007.

[95] A.D. Orlando and H.H. Shen. Effect of particle size and boundary conditions on the shear stress in an annular shear cell. *Granular Matter*, 14:423–431, 2012.

[96] M. Otsuki, H. Hayakawa, and S. Luding. Behavior of pressure and viscosity at high densities for two-dimensional hard and soft granular materials. 184:110–133, 2010.

[97] M. Pailha and O. Pouliquen. A two-phase flow description of the initiation of underwater granular avalanches. *Journal of Fluid Mechanics*, 633:115–135, 2009.

[98] P. Perzyna. Fundamental problems in viscoplasticity. *Advances in Applied Mechanics*, 9:243–377, 1966.

[99] T. Pöschel and V. Buchholtz. Molecular dynamics of arbitrarily shaped granular particles. *Journal de Physique I*, 5:1431–1455, 1995.

[100] T. Pöschel and S. Luding. *Granular Gases*. Springer, Berlin, Germany, 2001.

[101] T. Pöschel, N.V. Brilliantov, A. Formella, M. Heckler, C. Krülle, P. Müller, C. Salue na, and T. Schwager. Contact of granular particles and the simulation of rapid flows using event-driven molecular dynamics. *European Journal of Environmental and Civil Engineering - EJECE 12*, 12(7-8):827–870, 2008.

[102] O. Pouliquen. Scaling laws in granular flows down rough inclined planes. *Physics of Fluids*, 11:542–548, 1999.

[103] F. Radjaï. Contact dynamics method. *European Journal of Environmental and Civil Engineering - EJECE 12*, 12(7-8):871–900, 2008.

[104] M.F. Rahaman, J. Naser, and P.J. Witt. An unequal granular temperature kinetic theory: description of granular flow with multiple particle classes. *Powder Technology*, 138:82–92, 2003.

[105] M.W. Richman. Boundary conditions based on a modified maxwellian velocity distribution function for flows of identical, smooth, nearly elastic spheres. *Acta Mechanica*, 75:227–240, 1988.

[106] K.H. Roscoe, A.N. Schofield, and C.P. Wroth. On the yielding of soils. *Géotechnique*, 8:22–53, 1958.

[107] J.-N. Roux and G. Combes. Quasistatic rheology and the origin of strain. *Comptes Rendus Physique*, 3:131–140, 2002.

[108] S.B. Savage. The mechanics of rapid granular flows. *Advances in Applied Mechanics*, 24:289, 1984.

[109] S.B. Savage. Analyses of slow high-concentration flows of granulars. *Journal of Fluid Mechanics*, 377:1–26, 1998.

[110] A.N. Schofield and C.P. Wroth. *Critical state soil mechanics*. McGraw-Hill, London, U.K., 1968.

[111] N. Sela and I. Goldhirsch. Hydrodynamic equations for rapid flows of smooth inelastic spheres. *Journal of Fluid Mechanics*, 361:41–74, 1998.

[112] D. Serero, I. Goldhirsch, S.H. Noskowicz, and M.L. Tan. Hydrodynamics of granular gases and granular gas mixtures. *Journal of Fluid Mechanics*, 554:237–258, 2006.

[113] D. Serero, C. Goldenberg, S.H. Noskowicz, and I. Goldhirsch. The classical granular temperature and slightly beyond. *Powder Technology*, 182:257, 2008.

[114] Z. Shojaaee, J.N. Roux, F. Chevoir, and D. Wolf. Shear flow of dense granular materials near smooth walls. I. Shear localization and constitutive laws in the boundary region. *Physical Review E*, 86:011301, 2012.

[115] L.E. Silbert. Jamming of frictional spheres and random loose packing. *Soft Matter*, 6:2918–2924, 2010.

[116] L.E. Silbert, D. Ertas, G.S. Grest, T.C. Halsey, D. Levine, and S.J. Plimpton. Granular flow down an inclined plane: Bagnold scaling and rheology. *Physical Review E*, 64:051302, 2001.

[117] C. Song, P. Wang, and H.A. Makse. A phase diagram for jammed matter. *Nature*, 453:629–632, 2008.

[118] S. Torquato. Nearest-neighbor statistics for packing of hard spheres and disks. *Physical Review E*, 51:3170–3182, 1995.

[119] H. van Beijeren and M.H. Ernst. The modified Enskog equation. *Physica*, 68:437–456, 1973.

[120] H. van Beijeren and M.H. Ernst. The modified Enskog equation. *Physica*, 70:225–242, 1973.

[121] I.G. Vardoulakis and J. Sulem. *Bifurcation Analysis in Geomechanics*. Blackie Academic and Professional, Glasgow, U.K., 1995.

[122] D. Vescovi, C. di Prisco, and D. Berzi. From solid to granular gases: the steady state for granular materials. *International Journal for Numerical and Analytical Methods in Geomechanics*, 37:2937–2951, 2013.

[123] D. Vescovi, D. Berzi, P. Richard, and N. Brodu. Plane shear flows of frictionless spheres: kinetic theory and 3D Soft-Sphere DEM simulations. *Physics of Fluids*, 2014, submitted.

[124] O.R. Walton. Granular solids flow project. Technical report, 1988.

[125] Y. Wang and K. Hutter. Granular material theories revisited. In N.J. Balmforth and A. Provenzale, editors, *Geomorphological Fluid Mechanics*, volume 582 of *Lecture Notes in Physics*, pages 79–107. Springer Berlin Heidelberg, 2001.

[126] T. Weinhart, R. Hartkamp, A. Thornton, and S. Luding. Coarse-grained local and objective continuum description of 3D granular flows down an inclined surface. *Physics of Fluids*, 25:070605, 2013.

[127] J.T. Willits and B.O. Arnarson. Kinetic theory of a binary mixture of nearly elastic disks. *Physics of Fluids*, 11:3116–3122, 1999.

[128] M.J. Woodhouse and A.J. Hogg. Rapid granular flows down inclined planar chutes. Part 1. Steady flows, multiple solutions and existence domains. *Journal of Fluid Mechanics*, 652:427–460, 2010.

[129] C.P. Wroth. Soil behaviour during shear - existence of critical void ratios. *Engineering*, 186:409–413, 1958.

[130] H. Xu, M. Louge, and A. Reeves. Solutions of the kinetic theory for bounded collisional granular flows. *Continuum Mechanics and Thermodynamics*, 15:321–349, 2003.

[131] P. Zamankhan. Kinetic theory of multicomponent dense mixtures of slightly inelastic spherical particles. *Physical Review E*, 52:4877–4891, 1995.